ATOMKI

ANNUAL REPORT

2005

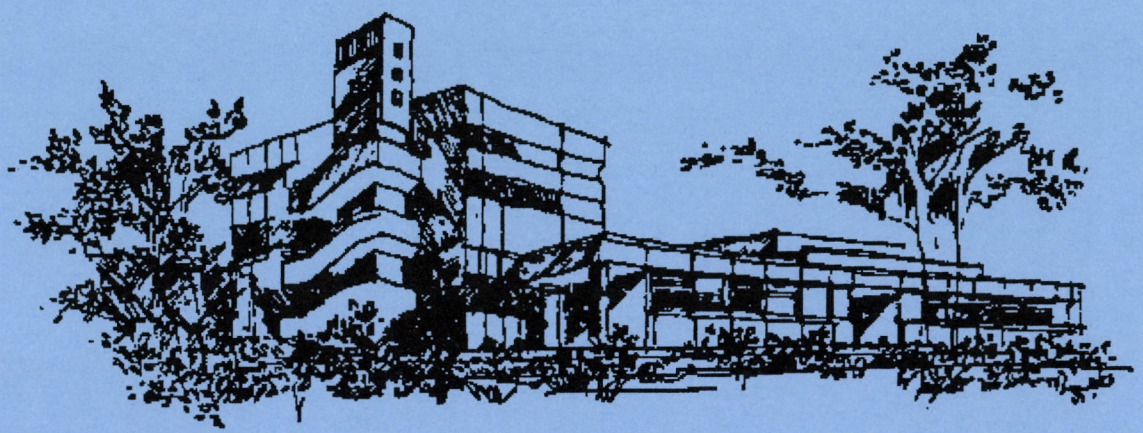

INSTITUTE OF NUCLEAR RESEARCH
OF THE HUNGARIAN ACADEMY OF SCIENCES
DEBRECEN, HUNGARY

INSTITUTE OF NUCLEAR RESEARCH
OF THE HUNGARIAN ACADEMY OF SCIENCES
DEBRECEN, HUNGARY

ANNUAL REPORT
2005

ATOMKI

Postal address:
P.O. Box 51
H-4001 Debrecen,
Hungary

Editor:
I. Rajta

HU ISSN0 0231-3596

Preface

The Preface is utterly different from the rest of the Annual Report. It is subjective, incomplete, and it contains what is never reported on anywhere else. It is not about anything particular, and it is not addressed to anybody; it is meant for any reader, that is all readers.

2005 was the World Year of Physics, and we celebrated it, first of all, with an extremely attractive program for the Physics Days, which is the physics feast for the general public every year. This time the main events focussed on the aftermath of Einstein's great papers. The Brownian motion was covered by Prof. Dezső Beke (Debrecen University) in his talk on *Random Walk of Atoms – Mixing by Diffusion.* The transition to the photoelectric effect was paved by Prof. Gyula Faigel (Research Institute for Solid State Physics and Optics, Budapest). The title of his talk was *How to Measure the Distance between Two Atoms?* This was followed by a talk on *Photoelectrons and their Companions – 100 years of the Photoeffect* by Dr. László Kövér (Atomki), and the summit of events was, of course, a talk on special relativity. We invited Prof. Frigyes Károlyházy (Eötvös University, Budapest) for this occasion, and he took the audience for a highly enjoyable *Excursion to Space-Time.* The program was rounded off by a show of famous experiments at the School Museum of Debrecen's four-and-a-half-century-old famous school, the 'Reformed College'. Following the Physics Days, we also held a Particle Physics Day for the first time this year. Prof. Zoltán Trócsányi held what we called a 'master class' to secondary school pupils. He introduced them to the basic facts of particle physics, and analysed an actual particle-physics experiment with their participation.

2005 was also a year of nuclear physics conferences in Debrecen. In May we had the 20th International Nuclear Physics Divisional Conference of the European Physical Society, the second such meeting in Atomki on nuclear physics in astrophysics (and is referred to as NPA–2 as well). A month later we had the third International ENS Symposium, where this time ENS stood for Exotic Nuclear Systems. At the end of the latter meeting, the Nuclear Physics European Collaboration Committee (NuPECC) also held its session here.

In preparation for the EPS conference the idea of a lecture to the general public was raised, to pay tribute to the World Year of Physics. The occasion we have found was the commemoration of an event that took place half-way between Einstein's year and the current year. This was a research result, perhaps the most significant one ever published from this Institute: the detection of the repulsive effect of the neutrino emitted in β-decay, by A. Szalay and J. Csikai. Julius Csikai, *Professor Emeritus Instituti,* is among us, and he made a deep impression with his talk on their experiment. They had photographed the β-decay of ^{6}He in a cloud chamber. In a few snap-shots it was clearly seen that the tracks of the electron and the repelled nucleus do not form a straight angle, which provides an evidence for momentum non-conservation unless the antineutrino is assumed to exist. This became a celebrated confirmation of the existence of the (anti)neutrino, and, later, a textbook example. The experiment was a typical small-science adventure, but still had an impact on the frontiers of knowledge both in nuclear and in particle physics. This talk commemorated another half-way event as well: Professor Csikai was born half-way between Einstein's year and the year of his famous experiment.

There were three important lectures held at the Academy by our members. In winter there were the inaugural addresses given by Professor József Pálinkás *(Atoms and their Debris in Exotic Events)* and by myself *(Identity and Non-identity: the Pauli Principle in Nuclei)*, and there was a talk by Prof. Attila Krasznahorkay at a session associated with the General Assembly held in May *(Indications for a New Elementary Particle in Nuclear Transitions).* In

autumn Prof. Csikai was awarded the Wigner Prize of the Academy and Paks Nuclear Power Plant.

In the 'Honours List', I should mention first that in October Prof. Dénes Berényi, our Director from 1976 to 1989, was conferred an Honorary Degree at the University of Ungvár (Uzh-horod, Ukraine). The Szalay Prize was awarded to Dr. József Molnár for his exceptionally broad scope of development work in nuclear electronics. Dr. Tamás Vertse, member of our Section for Theoretical Physics, has been appointed full professor at the Faculty of Informatics, University of Debrecen. Young scientists' awards were granted to Dr. György Gyürky (again!) and to Dr. Bertalan Juhász.

I should mention not only the awards given to us but also an award given by one of us. I have learned from the year-book of the famous Grammar School of the Reformed Church at Pápa, Western Hungary, that their former pupil, our distinguished colleague, Professor Emeritus Tibor Fényes has given a substantial private gift to the school, to equip it with a whole range of modern physical instruments. His generosity brings honour to his Institute as well.

We commemorated the 75th birthday of Professor Ede Koltay by a session of talks entitled 'From the Van de Graaff Accelerators to Saharan Sand Storms'.

Dr. Zoltán Gácsi has brought honour to us in a completely different way. He is not only a nuclear physicist but a hobby painter as well, and we had seen a few pictures painted by him after the great nineteenth-century painter, Mihály Munkácsy. In 2005 he had an exhibition. He has earned unanimous acclaim not only by the replicas, but also by original paintings. I am proud and glad to rest my eyes on his beautiful landscape of Poroszlay Road, with the old-style brick-and-iron fence of the Institute on the right, hanging in my office since then.

To crown an age-old intensive collaboration, a formal Cooperation Agreement has been signed with one of the most important research centres of Japan, the RIKEN Institute. It was a coincidence that the former Director of RIKEN, Professor Akito Arima visited the Institute and gave a seminar talk here. At the same time a group of Debrecen nuclear physicists were doing an experiment at RIKEN. Professor Arima came to Hungary as Director of the Tokyo Science Museum and Chairman of the Japan Science Foundation to take part in the World Science Forum held in Budapest in November.

In our laboratories our major development is a reconstruction of the beam lines of the electrostatic accelerator VdG–5. The vacuum and the beam quality are expected to become much better, which will improve the performance of the accelerator, especially for the scanning ion microprobe. This work has been made possible by a grant from the Operative Program for Economic Competitiveness (GVOP). It was started in autumn, 2005, and the work is expected to be completed by the summer coming.

Another GVOP project has made it possible to create a spin-off firm as a joint venture of the Academy and of the Institute with some members of the Institute. The name of the firm is Vacuum Tightness and Measurement Techniques (VTMT), Ltd. They are to use their expertise in mass spectrometry, vacuum techniques and cryotechniques to improve industrial production procedures by reducing environmental pollution and increasing the reliabilty of products.

In summer the PET Centre of the Medical Faculty has moved from Atomki to its new site at the Teaching Hospital of the University, but the radiochemical laboratory (and, occasionally, our cyclotron as well) is still used to produce radiopharmaceuticals for them.

Finally, I should mention a few research results that seem to have set the lines for the future.

The Section of Experimental Nuclear Physics have been working hard with their Dutch colleagues to verify the observation, in nuclear transitions, of a new particle beyond the Standard

Model. It is tentatively identified with the 'U-boson', which is the particle whose decay seems to be responsible for an abundance of electron–positron pairs in the Universe. These U-bosons help us to find the dark matter since they are supposed to be emitted by dark-matter particles. Experiments performed at the Atomki cyclotron and repeated several times at our VdG–5 accelerator make the indication stronger and stronger. A $0^- \longrightarrow 0^+$ electromagnetic transition is studied, which is strictly forbidden both via direct γ-ray transition and internal pair creation, and yet electron–positron pairs have been observed from this transition. The angular correlation between the pairs suggests that a boson of 8.4 MeV mass has been created in an intermediate step, and the pair comes from its decay. The boson seems to be of axial vector (1^+) nature. The evidence is still not strong enough because of poor statistics, but no alternative explanation seems to emerge.

Last year we published a comprehensive study of the nucleus ^{16}C, which is based on our experiments performed at RIKEN. The behaviour of ^{16}C can be explained by assuming that its neutron skin can be excited almost independently of the ^{12}C core. More recently, ^{17}C has been found to behave similarly. Moreover, the hypothetical halo neutron of ^{19}C has been found to be on an s-orbit, which confirms that this neutron does indeed form a well-developed single-neutron halo.

A significant step has been made towards understanding the behaviour of high-transition-temperature superconductors of perovskite type. It has been shown that the phase transition between the two-dimensional and three-dimensional arrangements that brings about the superconductive phase, is a phase transition for the magnetic vortices as well. In this temperature range the motions of the vortex fibres become parallel. The phenomenon has been understood in terms of renormalisation-group considerations.

A three-year project for the construction of a PET camera for the examination of small animals has been completed. It is to be used in tests of the effects of prospective drugs for pharmaceutical industry. It contains very original solutions of electronics, and is hoped to be a step towards the leading edge in medical tomography.

Our financial conditions have been gradually worsening, but, at the same time, a substantial increase of support is expected through the National Development Plan mostly from EU sources under the new seven-year budget. For this hope to come true, we have to turn towards lucrative industrial innovation rapidly. We are willing to turn, but we would like to preserve research at the same time. Reports on the degree of our success in this matter will be given in the next issues of the Annual Report. That is a good point to finish with.

The financial and personnel conditions in 2005 are given in the pie charts to follow this Preface.

This Report, prepared in LaTeX, is available on the web at www.atomki.hu in PDF format.

Debrecen, 25 May 2006

Rezső G. Lovas
Director

Organizational structure of ATOMKI

Director:	R.G. Lovas, corresponding member of the HAS
Deputy directors:	Zs. Fülöp, Ph.D.
	S. Mészáros, C.Sc.
Finance director:	Dr. M. Pálinkás

- Secretariat (Scientific Secretary: Z. Máté, C.Sc.)
- Library (Librarian: Mrs. M. Nagy)
- Accounting (Head: Mrs. J. Sass)
- Basic Services and Maintenance (Head: Mr. I. Katona)
- Mechanical Workshop (Head: Mr. I. Gál)

Scientific Sections

Division of Nuclear Physics (Head: J. Cseh, D.Sc.)

- Section of Experimental Nuclear Physics (Head: A. Krasznahorkay, D.Sc.)
- Section of Electrostatic Accelerators (Head: I. Rajta, Ph.D.)
    - Nuclear Astrophysics Group
    - Ion Beam Analysis Group
- Section of Theoretical Physics (Head: A. Kruppa, D.Sc.)

Division of Atomic Physics (Head: Á. Kövér, D.Sc.)

- Section of Atomic Collisions (Head: B. Sulik, D.Sc.)
- Section of Electron Spectroscopy (Head: L. Kövér, Ph.D.)

- Section of Environmental and Earth Sciences (Head: Á.Z. Kiss, D.Sc.)
    - Laboratory of Environmental Studies
    - Radon Group
    - K-Ar Laboratory
    - Radiation- and Environmental Protection Group
    - QMS Laboratory
- DE TTK - ATOMKI Department of Environmental Physics (Head: S. Sudár, C.Sc.)
- Cyclotron Section (Head: F. Tárkányi, C.Sc.)
- Section of Electronics (Head: J. Gál, C.Sc.)

Data on ATOMKI

At present the Institute employs 196 persons. The affiliation of personnel to units of organization and the composition of personnel are given below.

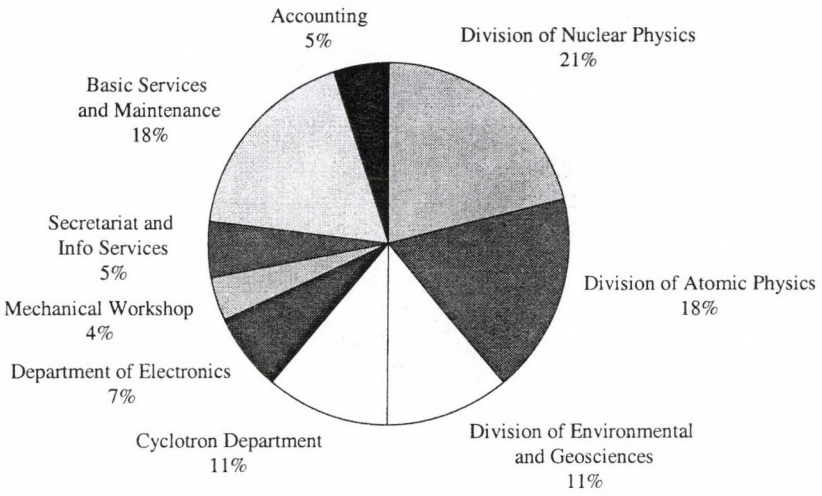

Figure 1. Affiliation of personnel to units of organization

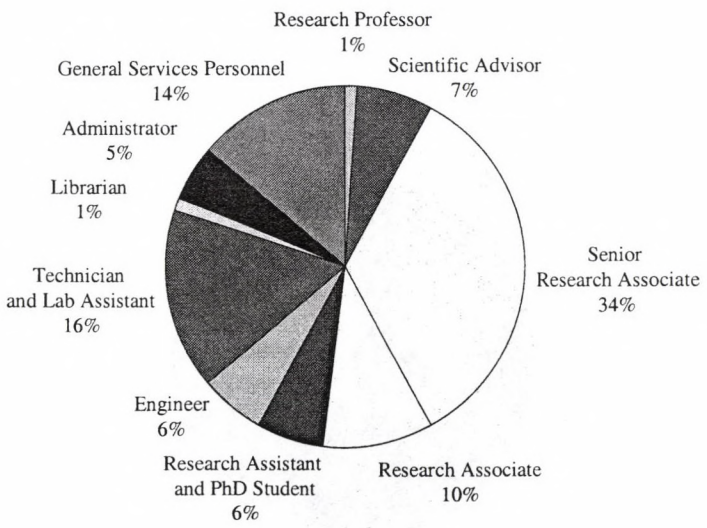

Figure 2. Composition of personnel

Finance

The total budget of the Institute for the year 2005 was 1235 million Hungarian Forints. The composition of the budget and the share of personnel expenditure within the budget are shown below.

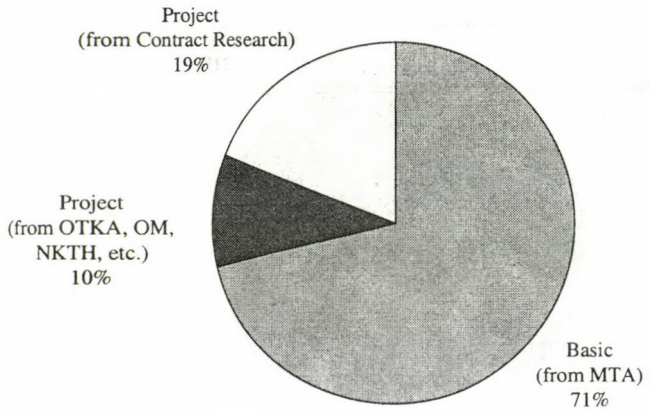

Figure 3. Composition of the budget of the Institute
MTA: Hungarian Academy of Sciences
OTKA: National Fund for Scientific Research
OM: Ministry of Education
NKTH: National Office for Research and Technology

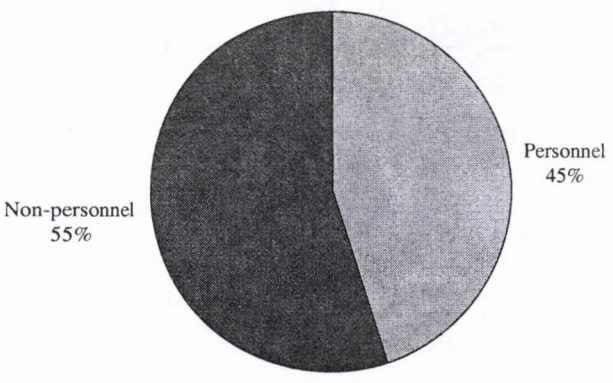

Figure 4. Breakdown of expenditure into personnel and non-personnel expenditures

Table of contents

1.1 On the pseudo-norm in some $\mathcal{PT}$-symmetric potentials

G. Lévai

$\mathcal{PT}$-symmetric quantum mechanical systems possess non-hermitian Hamiltonian, still they have some characteristics similar to hermitian problems. The most notable of these is their discrete energy spectrum, which can be partly or completely real. These systems are invariant under the *simultaneous* action of the $\mathcal{P}$ space and $\mathcal{T}$ time inversion operations. Perhaps the simplest $\mathcal{PT}$-symmetric Hamiltonian contains a one-dimensional Schrödinger operator with a complex potential satisfying the $V^*(-x) = V(x)$ relation. Another typical feature $\mathcal{PT}$-symmetric systems have in common with hermitian problems is that their basis states form an orthogonal set provided that the inner product is redefined as $\langle\psi|\phi\rangle_{\mathcal{PT}} \equiv \langle\psi|\mathcal{P}\phi\rangle$. However, the norm defined by this inner product, the pseudo-norm turned out to possess indefinite sign, and this raised the question of the probabilistic interpretation of $\mathcal{PT}$-symmetric systems. This problem was later put into a more general context when it was found that $\mathcal{PT}$ symmetry is a special case of pseudo-hermiticity, and this explains most of the peculiar features of $\mathcal{PT}$-symmetric systems. There have been several attempts to link $\mathcal{PT}$-symmetric, and in general, pseudo-hermitian systems with equivalent hermitian ones, and the sign of the pseudo-norm was found to play an important role in this respect.

It is thus essential to evaluate the pseudo-norm for various potentials, especially considering the fact that there are some inconsistencies in the available results. Numerical studies indicated that the sign of the pseudo-norm typically alternates according to the n principal quantum number as $(-1)^n$, and this was later proven for a class of potentials that are written in a polynomial form of ix. However, some potentials of other type did not fit into this line: this was the case for the Scarf II potential, the most well-known exactly solvable $\mathcal{PT}$-symmetric potential [1]. In contrast with the other examples, this potential is finite at the boundaries ($x = \pm\infty$) and it has finite number of discrete levels. Considering these circumstances it seemed worthwhile to study the Scarf I potential,

$$V(x) = \left(\frac{\alpha^2+\beta^2}{2} - \frac{1}{4}\right)\frac{1}{\cos^2 x} + \frac{\alpha^2-\beta^2}{2}\frac{\sin x}{\cos^2 x}$$

($x \in [-\frac{\pi}{2}, \frac{\pi}{2}]$), which is $\mathcal{PT}$-symmetric and has real energy eigenvalues if $\alpha^* = \beta$ holds. The Scarf II potential has similar structure, except for some constant factors and that it contains hyperbolic, rather than trigonometric functions.

We found a closed expression for the pseudo-norm of the Scarf I potential and it turned out that it varies as $(-1)^n$ similarly to other potentials that are infinite at the boundaries and have infinite number of discrete levels [2]. This potential has some further remarkable features. First, it contains the infinite square well as a special case, together with a specific $\mathcal{PT}$-symmetric extension. Some other $\mathcal{PT}$-symmetric extensions of the infinite square well have been analysed in terms of (semi-)numerical methods, so comparison with these is certainly an interesting task. Second, since the Scarf I potential is singular at the boundaries, the boundary conditions play an especially important role in this case. It turned out that the solutions are regular at the boundaries if $\mathrm{Re}(\alpha) < \frac{1}{2}$ holds, however, $\mathcal{PT}$-normalizability has a less strict condition: $\mathrm{Re}(\alpha) < 1$. This is especially interesting considering the fact that similarly to other $\mathcal{PT}$-symmetric potentials a second set of solutions is also possible with opposite quasi-parity, and these solutions are obtained from the $(\alpha, \beta) \to (-\alpha, -\beta)$ transformation (which, of course, leaves the potential invariant). A novel feature of the Scarf I potential is that although states with the same quasi-parity form an orthogonal set, there is non-orthogonality between states with opposite quasi-parity [2].

[1] G. Lévai, F. Cannata, A. Ventura, Phys. Lett. A **300** (2002) 271.

[2] G. Lévai, in preparation.

1.2 Perturbative treatment of possible failures in the adiabatic theorem

T. Vértesi and R. Englman [a)]

The adiabatic theorem (AT) is one of the oldest and basic results in quantum physics [1], and has been in widespread use ever since. The theorem concerns the evolution of systems subject to slowly varying Hamiltonians. Roughly, its content is that a system prepared in an instantaneous eigenstate of a time-dependent Hamiltonian $H(t)$ will remain close to an instantaneous eigenstate at later times, provided the Hamiltonian changes sufficiently slowly. The role of the AT in the study of slowly varying quantum mechanical systems spans a vast array of fields and applications. In a recent application the adiabatic geometric phases [2] have been proposed to perform various quantum computational tasks on a naturally fault-tolerant way [3].

Additional interest has arisen in adiabatic processes in connection with the concept of adiabatic quantum computing [4], where the solution to a problem is encoded in the (unknown) ground state of a (known) Hamiltonian. The evolution of the quantum state is governed by a time-dependent Hamiltonian $H(t)$, starting with an initial Hamiltonian H_i with a known ground state and slowly (adiabatically) evolving to the final Hamiltonian H_f with the unknown ground state, e.g.,

$$H(t) = (1 - t/T)\, H_i + (t/T)\, H_f \,, \qquad (1)$$

where $0 \leq t/T \leq 1$ and T controls the rate at which $H(t)$ varies. Since the ground state of the system is very robust against external perturbations and decoherence, this scheme offers many advantages compared to the conventional quantum circuit model of quantum computation.

The achievable speed-up of adiabatic quantum algorithms (compared to classical methods) depends on the value of the run-time T. The standard AT yields a general criterion to estimate the necessary run-time T, however recently Marzlin and Sanders [5] have claimed that an inconsistency does exist for a particular class of Hamiltonians, so that the condition for the estimate of T may do not hold. Marzlin and Sanders start with a time-dependent Hamiltonian $H^a(t)$ for which it is presumed that the AT is satisfied and from this Hamiltonian they construct a dual Hamiltonian,

$$H^b(t) = -U^{a\dagger}(t) H^a(t) U^{a\dagger}(t) \,, \qquad (2)$$

where $U^a(t)$ is the time evolution operator for the original Hamiltonian, $H^a(t)$. Then it is demonstrated that the AT can be very inaccurate for the dual Hamiltonian $H^b(t)$.

We argue in a perturbational analysis [6], that in the dual b-system the breakdown of the application of the AT can be traced to the appearance of some nonzero terms and is related to two time scales in the Hamiltonian $H^b(t)$. The Hamiltonian $H(t)$ in equation (1) depends only on one time scale (t/T), then from our analytical investigations follows that AT implies a good estimate for the required run-time T of quantum adiabatic algorithms regardless of the existing inconsistency in the AT. On the other hand, in the case of resonance, when some frequency in the Hamiltonian is nearly equal to one of the transition frequencies of the system, the Hamiltonian has intrinsically two time scales giving rise to possible failure in the application of the adiabatic theorem.

a) Soreq NRC, Yavne 81800, Israel

[1] Max Born and Vladimir Fock, Z. Phys. **51**, 165 (1928).

[2] Michael V. Berry, Proc. R. Soc. A,**392**, 45 (1984).

[3] Artur Ekert et al., J. Mod. Opt. **47**, 2501 (2000).

[4] Edward Farhi et al., Science **292** 472 (2001).

[5] Karl-Peter Marzlin and Barry C. Sanders, Phys. Rev. Lett. **93** 160408 (2004).

[6] Tamás Vértesi and Robert Englman, Phys. Lett. A (in press).

1.3 Spreading of technological developments in socio-economic systems

F. Kun[a)] *and K.F. Pál*

Recently, it has been recognized that various aspects of the time evolution of modern socio-economic systems show strong analogies to complex systems extensively studied by physical sciences. During the last decade the application of methods and models of statistical physics provided a novel insight into social and economical problems and led to the emergence of new branches of physical research.

In the framework of the present project we proposed a simple cellular automata model of the spreading of new technological developments in socio-economic systems. In our model the socio-economic system is defined in a general sense: the elements/members of the system are called agents, which may be firms or simply individuals. Depending on the meaning of agents, the system under consideration can be a macro-economic system where firms compete with each other, or it can be a society where individuals purchase products of different technological level. Technological development occurs such that agents adopt more advanced technologies of their social environment in order to minimize their costs. Technological development due to innovation can be captured in the model as a random external driving.

As a first step, we analyzed the basic setup of the model where agents have random technological levels uniformly distributed between 0 and 1 and interact solely with their nearest neighbors in a square lattice without considering external driving. Computer simulations revealed that even under these simplifying assumptions a rather complex behavior of the system emerges: when the most advanced technologies do not provide enough improvement (enough cost reduction) in the system, the agents tend to form clusters of different technological levels where even low level technologies may survive for a long time. At intermediate values of the advantage provided by the new technologies, the global technological level of the society improves, however, it does not reach the optimum. That implies that there are agents in the system which had to reduce their technological level to improve the efficiency of their communication. The optimal (maximum) technological development is achieved by the society if advances offered surpass a well-defined threshold value. The threshold value depends on the extension of the social environment of agents [1].

a) Department of Theoretical Physics, University of Debrecen

[1] F. Kun, K.F. Pál, K. Inoue, and S. Yamazaki, preprint.

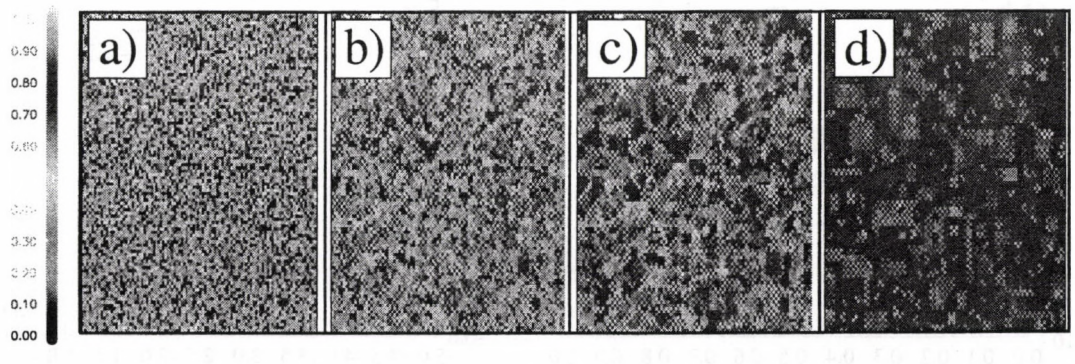

Figure 1. *a)* A square lattice of agents with random technological levels uniformly distributed between 0 and 1. *b, c, d)* Time evolution of the system into a steady state with a high technological level.

2.1 Radiative corrections to three-jet event-shapes in lepton-proton scattering

Z. Trócsányi

The analysis of event-shape observables in e^+e^--annihilations and in deeply-inelastic lepton-proton scattering (DIS) proved to be a powerful method to study Quantum Chromodynamics (QCD). The standard QCD analysis of event-shapes consists of matching the next-to-leading order (NLO) and resummed next-to-leading logarithmic (NLL) predictions. Recently, much progress has been achieved in computing resummed predictions at the NLL accuracy for three-jet event shapes [1]. In Ref. [2] we computed predictions to the same three-jet event shapes at the NLO accuracy in order to facilitate the matching. Here, we report results of such computations for the three-jet event-shape observable $K_{\rm out}$ that measures the out-of-event-plane QCD radiation; its precise definition can be found in Ref. [1]. For the numerical computations we used the NLOJET++ program [3].

We computed the distributions for fixed values of the DIS kinematic variables Q^2 and $x_{\rm B}$ and used the same selection cuts as in the resummation computation [1]. Figure 1. shows the differential distributions for $K_{\rm out}$. The shaded bands correspond to the range of scales $Q^2/2 \le \mu^2 \le 2Q^2$, where μ is the renormalization-scale (the factorization-scale is chosen to be the same). The radiative corrections are in general large and increase with increasing value of $K_{\rm out}$ because the phase space for events with large out-of-plane radiation with three partons in the final state (at LO) is much smaller than that with four partons in the final state (real corrections). The cross sections decrease rapidly with increasing $K_{\rm out}$, leaving the small and medium $K_{\rm out}$-region for experimental analysis.

In the small $K_{\rm out}$-region, the logarithmic contributions of the type $\ln K_{\rm out}/Q$ are dominant as can be seen on the plot in the right panel. The fixed-order predictions diverge with $K_{\rm out} \to 0$ with alternating signs, which makes the resummation of these large logarithmic contributions mandatory. Reliable theoretical predictions can be obtained by matching the cross sections valid at the NLO and NLL accuracy.

[1] A. Banfi, G. P. Salam and G. Zanderighi, CAESAR homepage: qcd-caesar.org.

[2] Z. Nagy and Z. Trócsányi, [arXiv:hep-ph/0511328].

[3] Z. Nagy, NLOJET++ homepage: www.cpt.dur.ac.uk/~nagyz/nlo++/.

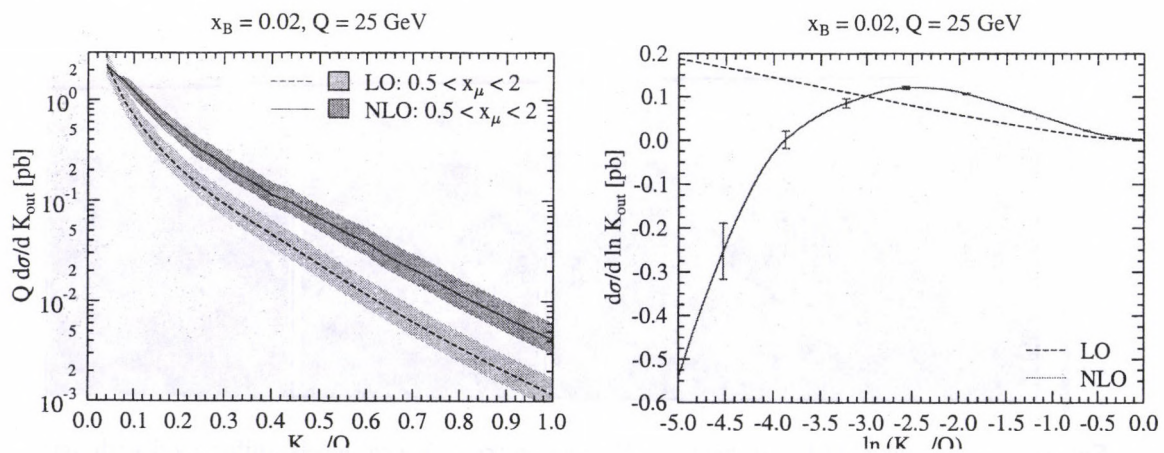

Figure 1: Differential distribution of $K_{\rm out}$ as a function of $K_{\rm out}/Q$ (left panel) $\ln K_{\rm out}/Q$ (right panel).

2.2 Coulomb suppression in the proton-proton elastic scatterings studied via the Trojan Horse Method applied to the ^{2}H(p,pp)n three-body reaction

C. Spitaleri[a)], A. Tumino[a)], S. Cherubini[a)], V. Crucillá[a)], Z. Elekes, Zs. Fülöp, M. Gulino[a)], Gy. Gyürky, G.G. Kiss, M. La Cognata[a)], L. Lamia[a)], F. Mudó[a)], R.G. Pizzone[a)], G. Rapisarda[a)], S. Romano[a)], E. Somorjai

The Trojan Horse Method is an indirect tool to study charged particle two-body reactions at sub-Coulomb energies. The method selects the quasi-free contribution of an appropriate three-body reaction performed at energies well above the Coulomb barrier in a way that the two-body interaction can be investigated at ultra-low energies. Moreover, since the quasi-free two-body reaction can be considered as taking place inside the nuclear field, no Coulomb suppression is expected. The Trojan Horse Method has successfully been applied to reactions connected with fundamental astrophysical problems [1-6]. Here we report on a recent application of this method to investigate the proton-proton scattering, the simplest case where the Coulomb suppression can be observed. The proton-proton cross section was extensively studied in the past. Its energy trend is well known and appears to be very similar to that of n-n or p-n systems (1/v behaviour) except at low proton energies where a deep minimum shows up ($E_{lab} = 382.43$ keV, $\theta_{cm} = 90°$). This minimum is described as being the signature of the interference between the nuclear and the Coulomb scattering amplitudes. Therefore, if one extracts the proton-proton cross section under the Trojan Horse prescriptions Coulomb effects are expected to be suppressed, i.e. the Trojan Horse cross section should not exhibit the minimum. The proton-proton scattering was investigated by means of the ^{2}H(p,pp)n three-body reaction performed at ATOMKI. A 5 MeV proton beam from the cyclotron was delivered onto a deuterated polyethylene target, 250 μg/cm^2 thick. Proton-proton coincidences were measured by four Position Sensitive Detectors (PSD), 5x1 cm^2, 500 μm thick detectors, placed two of them at symmetrical angles (14°) with respect to the beam direction, and the other two centered at 29° and 59°, all of them covering about 18°. The trigger to the acquisition system was given by the coincidence between the PSD at 14°, placed alone on one side, and the logic *or* of the other three PSD's, all placed on the same side with respect to the beam direction.

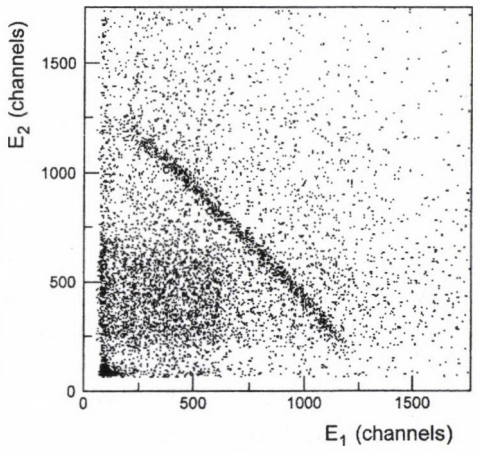

Figure 1. Locus of events in the E_p vs. E_p plane from coincidences between the most forward PSD's.

In Fig. 1, an example of locus of events is shown in the E_p vs. E_p plane for coincidences between the most forward PSD's. The angular ranges were chosen in order to cover momentum values of the undetected neutron *spectator* ranging from -100 MeV/c to 100 MeV/c. This will allow also to cross check the method inside and outside the phase-space regions where the quasi-free contribution is expected. The analyses of the experimental results are in progress.

a) DMFCI, Universitá di Catania and Laboratori Nazionali del Sud, INFN, Catania, Italy

[1] C. Spitaleri *et al.*, Phys. Rev. C60 (1999) 055802.
[2] M. Lattuada *et al.*, Ap. J. 562 (2001) 1076.
[3] C. Spitaleri *et al.*, Phys. Rev. C63 (2001) 005801.
[4] A. Tumino *et al.*, Phys. Rev. C67 (2003) 065803.
[5] C. Spitaleri *et al.*, Phys. Rev. C69 (2004) 055806.
[6] M. La Cognata *et al.*, Phys. Rev. C72 (2005) 065802.

2.3 ^{3}He(α,γ)^{7}Be cross section measurement at low energies

Gy. Gyürky, Z. Elekes, Zs. Fülöp, E. Somorjai, for the LUNA collaboration

The ^{3}He(α,γ)^{7}Be reaction is the key process for the production of ^{7}Be and ^{8}B neutrinos in the sun. The solar neutrino flux resulting from the ^{7}Be(p,γ)^{8}B reaction followed by the ^{8}B β-decay depends on nuclear physics and astrophysics inputs. The ^{3}He(α,γ)^{7}Be reaction is one of the major source of uncertainty in determining the B solar neutrino flux and dominates over the present observational accuracy of 7 %.

In the last twenty years the ^{3}He(α,γ)^{7}Be reaction has been measured using two techniques. In the first method direct α-capture γ rays are detected (on-line method), while in the second the γ-radiation following the ^{7}Be β-decay is measured (activation method). The lowest energy where the cross section has been measured is $E_{c.m} \approx 100$ keV far above the astrophysically relevant energy window (10 keV $\leq E_{c.m} \leq$ 35 keV). Moreover, the average extrapolated S(0)-factors, obtained with the two techniques, show a discrepancy of the order of 11 %.

The LUNA underground accelerator facility in Gran Sasso National Laboratory, Italy provides a unique possibility of measuring extremely low cross sections [1,2]. The combination of the high current LUNA2 400 keV accelerator and a well-shielded gas target setup in this low-background facility allows the measurement of the ^{3}He(α,γ)^{7}Be cross section down to $E_{c.m} = 70$ keV with a precision better than 5%.

The aim of the LUNA collaboration is to measure the ^{3}He(α,γ)^{7}Be cross section with both techniques [1]. In the on-line method a differentially pumped windowless ^{3}He recirculated gas target is bombarded by an α-beam of 200 μA intensity. The prompt γ-radiation is detected with an ultra low background high volume HPGe detector equipped with lead shielding and radon box. In the activation method the same gas target setup is used and the produced ^{7}Be nuclei are implanted in the beam-stop. After the irradiation the beam-stop is transported to the low background counting laboratory of Gran Sasso where the γ-radiation following the β-decay of the produced ^{7}Be is measured with two well shielded HPGe detectors.

Different experiments have been carried out at ATOMKI in connection with the ^{3}He(α,γ)^{7}Be activation measurement. Parasitic reactions such as ^{6}Li(d,n)^{7}Be and ^{10}B(p,α)^{7}Be induced by the d or p impurities of the beam on the Li or B impurities of the beam stop can lead to the undesired production of ^{7}Be. In order to investigate the impurities of the beam stop, the same material (oxygen-free copper) was irradiated with 700 keV protons and deuterons at ATOMKI. The samples were then measured with the low background HPGe detector at Gran Sasso. No induced ^{7}Be activity was found and upper limits were calculated for the possible impurities.

Low activity ^{7}Be sources have been prepared at ATOMKI and their absolute activities have been measured with three different HPGe detectors of the ATOMKI. These calibrated sources have been used to measure the absolute efficiency of the two detectors at LNGS which were used for the activation measurements.

The experiments in Gran Sasso have been started with the activation method. Data taking and analysis are in progress.

[1] A. Formicola *et al.* (LUNA Collaboration) Phys. Lett. B 591 (2004) 61.

[2] D. Bemmerer *et al.* (LUNA Collaboration) Eur. Phys. J. A 24 (2005) 313.

[3] H. Costantini *et al.* (LUNA Collaboration) Eur. Phys. J. A (in press)

2.4 A light $J^\pi = 1^+$ isoscalar neutral boson in nuclear transitions

A. Krasznahorkay, F.W.N. de Boer[a], J. Gulyás, A. Vitéz, Z. Gácsi, T.J. Ketel[b], M. Csatlós, M. Hunyadi, J. van Klinken[c], A. Krasznahorkay Jr, L. Csige

Last year we could observe e^+e^- pairs from the 10.95 MeV $0^- \rightarrow 0^+$ forbidden transition in ^{16}O [1]. The angular correlation of the e^+e^- pairs was measured with standard Multi-wire Proportional Counters (MWPC), which were inserted between the ΔE and E detectors of the telescopes [2]. The angular correlation of the pairs showed an unusual structure. Instead of the monotonically decreasing feature predicted by the IPC theory it shows a maximum at 103°. This behavior could be described by assuming the creation and the subsequent decay of a predicted [3]light neutral boson with a mass of m = 8.5 MeV/c^2, which value agrees well with the previously suggested value of 9 MeV/c^2 [4].

The experimental value of the boson creation probability compared to the γ-decay probability ($P_b \approx 5 \times 10^{-5}$) turned out to be much smaller then the previously published value, which was observed in an M1 transition [4]. If the boson has a J^π of 1^+ as predicted by Fayet [3], then we had to have an L=1 emission in the 10.95 MeV $0^- \rightarrow 0^+$ transition, which explains the smaller creation probability. L=1 emission of the $J^\pi = 1^+$ particle should then also happen in a M2 $2^- \rightarrow 0^+$ transition. That was the reason we started to study the 8.87 MeV M2 transition in ^{16}O.

To get large cross-section for populating the 8.87 MeV 2^- state we chose the $^{19}F(p,\alpha\gamma)^{16}O$ reaction for the experiment. The γ and e^+e^- measurements have been performed et $E_p = 5.8$ MeV. The proton beam has been obtained from a 20-MeV isochronous cyclotron of the institute. The results are shown in Fig. 1.

We could observe a peak at about $\theta = 139°$, which nicely confirms our expectations. As the mass of the boson is only slightly smaller then the energy of the transition, their velocity is much smaller then in the 10.95 MeV transition. That is the reason of the larger correlation angle.

With an average value of the mass of the boson (m = 8.4(2) MeV/c^2) both twobody-decay pattern of the e^+e^- pair correlations can be explained. Moreover, the observation of the e^+e^- decay in both an M0 and in M2 transition supports the predicted $J^\pi = 1^+$ nature of the particle.

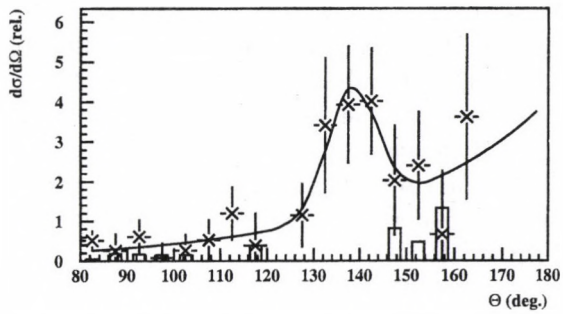

Figure 1. Angular correlation of the e^+e^- pairs obtained from the decay of the 8.87 MeV M2 transition.

a) NIKHEF, Amsterdam, The Netherlands.

b) Free Univ. Amsterdam, The Netherlands.

c) KVI, Groningen, The Netherlands.

[1] A. Krasznahorkay *et al.*, Atomki Ann. Rep. (2004) 3.; AIP proceedings **802** (2005) 236; Acta Phys. Pol.**B37** (2006) 239.

[2] A. Vitéz *et al.*, Atomki Ann. Rep. (2005)

[3] P. Fayet, Nucl. Phys. **B187** (1981) 184.; C. Boehm and P. Fayet, Nucl. Phys.**B683** (2004) 219.

[4] F.W.N. de Boer *et al.*, J. Phys. **G27** (2001) L29.

2.5 Electron screening in ^{7}Li(p,α)α and ^{6}Li(p,α)^{3}He for different environments

Zs. Fülöp, Gy. Gyürky, E. Somorjai, for the LUNA collaboration

We continued our systematic study on the anomalous enhancement of electron screening potential (U_e) for metallic environments [1,2]. Here, we report on studies aiming at the determination of the U_e dependence at the 100 kV accelerator of the Dynamitron-Tandem-Laboratorium at the Ruhr University Bochum, Germany in (p,α) reactions on two Li isotopes in various forms [3].

The electron screening in the ^{7}Li(p,α)α reaction has been studied between $E_p = 30$ to 100 keV for different environments: Li_2WO_4 insulator, Li metal, and PdLi alloy. The results are summarized in Fig. 1. For the insulator a screening potential energy of $U_e = 185 \pm 150$ eV was observed, consistent with the atomic adiabatic limit. However, for the Li metal and the PdLi alloy we found large values of $U_e = 1280 \pm 60$ and 3790 ± 330 eV, respectively: the values can be explained by the plasma model of Debye applied to the quasi-free metallic electrons in these samples. As it is shown in Fig. 2 similar results have been found for the ^{6}Li(p,α)^{3}He reaction.

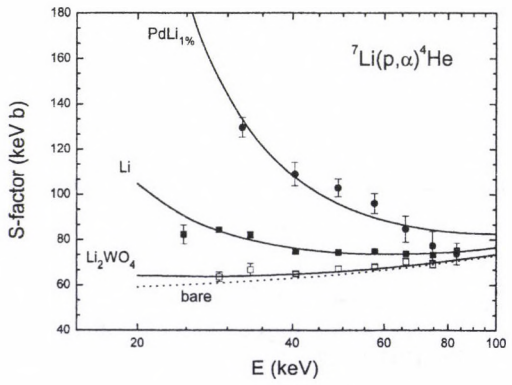

Figure 1. Astrophysical S-factor of ^{7}Li(p,α)α reaction for different environments: Li_2WO_4 insulator, Li metal, and PdLi alloy. The solid curves include the bare S-factors denoted by dotted curve, and used to determine the U_e screening potential.

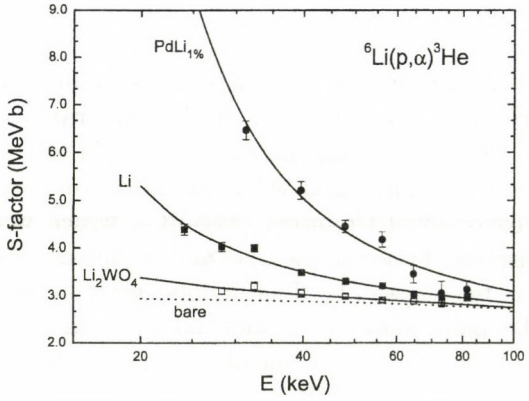

Figure 1. Astrophysical S-factor of ^{6}Li(p,α)^{3}He reaction for different environments: Li_2WO_4 insulator ($U_e = 320 \pm 110$ eV), Li metal ($U_e = 1320 \pm 70$ eV), and PdLi alloy ($U_e = 3760 \pm 260$ eV).

The present data for the electron screening in the ^{7}Li(p,α)α and ^{6}Li(p,α)^{3}He reactions for different environments give a consistent picture: (i) the present data proves the isotopic independence of the electron screening effect [4], i.e., the same U_e value for ^{7}Li and ^{6}Li nuclides, (ii) for the Li_2WO_4 insulator the atomic electron cloud leads to one acceleration mechanism, while the Li metal and the PdLi alloy exhibit an additional acceleration mechanism due to the quasi-free metallic electrons at the Debye radius. In comparison to the data in the d(d,p)t reaction for metals [1,2], the screening potential energy scales with the charge of the target nucleus, as expected from the Debye model.

[1] F. Raiola *et al.*, Phys. Lett. B547 (2002) 193.

[2] F. Raiola *et al.*, Eur. Phys. J. A19 (2004) 283.

[3] J. Cruz *et al.*, Phys. Lett. B624 (2005) 181.

[4] S. Engstler *et al.*, Z. Phys. A342 (1992) 471.

2.6 Decay of ^{7}Be in metallic environment at room temperature

Zs. Fülöp, Gy. Gyürky, E. Somorjai,
D. Schürmann[a], F. Raiola[a], F. Strieder[a], C. Rolfs[a],
B.N. Limata[b], L. Gialanella[b], G. Imbriani[b], V. Roca[b], M. Romano[b],
N. De Cesare[c], A. D'Onofrio[c], D. Rogalla[c], F. Terrasi[c]

The ^{7}Be produced in the ^{3}He(α,γ)^{7}Be reaction of the pp-chain is essential for predicting the ^{8}B solar neutrino flux. The termination of the pp-II chain can proceed via two different paths: the reaction ^{7}Be(p,γ)^{8}B, which indeed produces the high energy solar neutrinos, and in competition, the ^{7}Be decay to ^{7}Li. The half-life of radioactive nuclei decaying only by electron capture depends on the electron density at the nucleus. Therefore, these isotopes are expected to have a different half-life in a stellar plasma. The recently observed enhanced electron screening in metals [1,2] might connect the stellar plasma to metals, because in both environments free electrons play the dominant role.

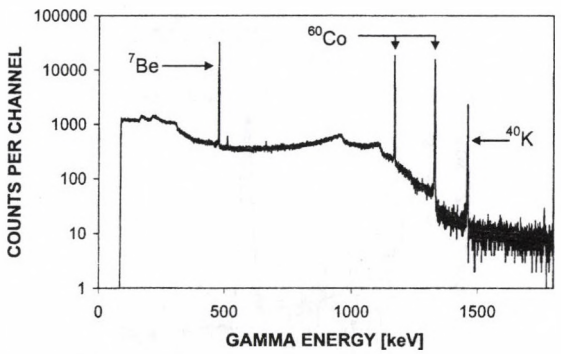

Figure 1. Gamma spectrum of the ^{7}Be implanted W sample taken for 12 hours. The peaks of ^{7}Be, ^{60}Co and ^{40}K are indicated.

We started to search for the changes in the half-life of ^{7}Be implanted into various metals at room temperature. The implanted samples are prepared for the first time using a high purity radioactive ^{7}Be ion beam. The ^{7}Be was produced by the ^{7}Li(p,n)^{7}Be reaction on ^{7}Li metallic targets at the ATOMKI cyclotron, Debrecen, with a 11.4 MeV proton beam of typically 20 μA intensity. The radiochemical separation of the ^{7}Be from the carrier material and the preparation for the use of the sample in a sputter source were carried out by the isotopic laboratory of the Ruhr-Universität Bochum. Finally, the high purity ^{7}Be radioactive beam was accelerated at the Naples tandem accelerator and the ^{7}Be nuclei were implanted into different metals such as Pd, Zr, W and Ta, resulting in activities between 3.6 and 36 kBq.

The decay curve of the implanted sources was measured by well shielded HPGe detectors. To reduce the systematic errors, the half-life of ^{7}Be was determined relative to that of well known sources. Directly at the back of the ^{7}Be sample, a ^{60}Co source is mounted. Any possible movement of the ^{7}Be source during the counting can easily be seen by the change of the measured ^{60}Co intensity. Additionally, an extended ^{40}K source is fixed inside the lead cage allowing for the control of the long term stability of the system. Fig. 1 shows a γ-spectrum measured on the implanted tungsten sample for 12 hours. The 478 keV ^{7}Be peak as well as the peaks of the reference sources can clearly be seen.

The preliminary results [3,4] show no change in the half-life within the experimental errors achieved (0.3-0.4%). This is compatible with the predictions of the Debye model applied to the free electrons in metals [4].

a) Ruhr-Universität Bochum, Germany
b) Universitá 'Federico II', Napoli, Italy
c) Seconda Universitá di Napoli, Caserta, Italy

[1] F. Raiola *et al.*, Phys. Lett. B547 (2002) 193.
[2] F. Raiola *et al.*, Eur. Phys. J. A19 (2004) 283.
[3] Zs. Fülöp *et al.*, Nucl. Phys. A758 (2005) 697c.
[4] B.N. Limata *et al.*, Eur. Phys. J. A27 (2006)

2.7 Decoupling of valence neutrons from the core in ^{17}B

Zs. Dombrádi, Z. Elekes, R. Kanungo[a], H. Baba[b], Zs. Fülöp, J. Gibelin[c], Á. Horváth[d], E. Ideguchi[e], Y. Ichikawa[e], N. Iwasa[f], H. Iwasaki[e], S. Kanno[b], S. Kawai[b], Y. Kondo[b], T. Motobayashi[a], M. Notani[e], T. Ohnishi[e], A. Ozawa[a], H. Sakurai[e], S. Shimoura[e], E. Takeshita[b], S. Takeuchi[a], I. Tanihata[g], Y. Togano[b], C. Wu[a], Y. Yamaguchi[a], Y. Yanagisawa[a], A. Yoshida[a], K. Yoshida[a]

Recently, an extremely large $M_n/M_p \sim 4N/Z$ ratio was observed in ^{16}C. In this nucleus, the neutron effective charge of $e_n = 0.15$ was deduced and can be considered as a clear indication of the decoupling of the valence neutrons from the ^{14}C core. ^{17}B is another nucleus where a significant decoupling may take place since an anomalous electric quadrupole moment of its ground state was measured at Q=38.6 $\pm$ 1.5 mb [2]. In order to check this idea by deducing the neutron deformation, we studied the inelastic scattering of ^{17}B in inverse kinematics. The experiment was done at the RIPS beamline of the RIKEN accelerator research facility (for details see ref. [3].) Fig. 1 shows the Doppler corrected spectra of γ rays with and without the secondary liquid hydrogen target. A single peak at 1089(15) keV can be seen in the bottom panel, which corresponds to the transition between the first excited and the ground state. To derive the quadrupole deformation parameter ($\beta_2^{pp'}$), a distorted wave calculation was performed. In this way, we got $\beta_2^{pp'}$=0.57 $\pm$ 0.05 value. From a comparison with the previously determined electric quadrupole moment, we deduced the deformation parameter of the neutron and proton distributions to be $\beta_n \sim 0.6$ and $\beta_p = 0.36$. Exploiting this information on the neutron and proton deformations of ^{17}B, an upper limit on the neutron effective charge of $e_n < 0.12$ has been deduced. This value is in a good agreement with the one deduced in [2] of $e_n \approx 0.1$ and 4 times smaller than the one characteristic for nuclei close to the stability in this mass region.

a) RIKEN
b) Rikkyo University
c) Institut de Physique Nucléaire
d) Eötvös Loránd University
e) University of Tokyo
f) Tohoku University
g) Argonne National Laboratory

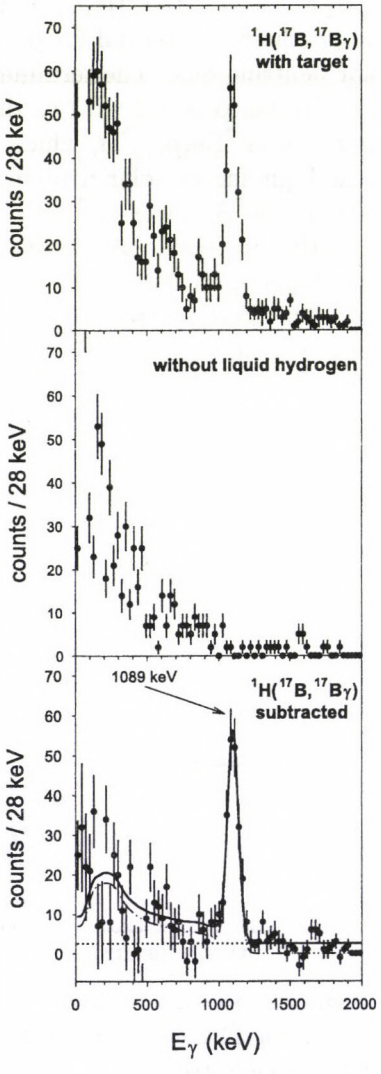

Figure 1. Doppler-corrected spectra of γ rays emerging from ^{1}H(^{17}B,^{17}B) reaction can be seen at the top of the figure. The middle spectrum is taken without the liquid hydrogen, while the spectrum in the bottom panel is produced by subtracting the two spectra.

[1] Z. Elekes *et al.*, Phys. Lett. B586 (2004) 34.
[2] H. Ogawa *et al.*, Phys. Rev. C67 (2003) 064308.
[3] Zs. Dombrádi *et al.*, Phys. Lett. B621 (2005) 81.

2.8 N=14 shell closure studied via ^{22}O(d,d'γ) reaction

Z. Elekes, Zs. Dombrádi, S. Bishop[a], Zs. Fülöp, J. Gibelin[b], T. Gomi[a], Y. Hashimoto[c], N. Imai[a], N. Iwasa[d], H. Iwasaki[e], G. Kalinka, Y. Kondo[c], A.A. Korsheninnikov[a,f], K. Kurita[g], M. Kurokawa[a], N. Matsui[c], T. Motobayashi[a], T. Nakamura[c], T. Nakao[e], E.Yu. Nikolskii[a,f], T.K. Ohnishi[a], T. Okumura[c], S. Ota[h], A. Perera[a], A. Saito[e], H. Sakurai[e], Y. Satou[c], D. Sohler, T. Sumikama[a], D. Suzuki[g], M. Suzuki[g], H. Takeda[e], S. Takeuchi[a], Y. Togano[g], Y. Yanagisawa[a]

The experiment was performed in RIKEN where a 94 A·MeV energy primary beam of ^{40}Ar with 60 pnA intensity hit a ^{9}Be production target of 0.3 cm thickness. The reaction products were momentum- and mass–analyzed by the RIPS fragment separator. The total intensity was approximately 1500 cps having an average ^{22}O intensity of 600 cps. The identification of incident beam species was performed by energy loss and time-of-flight. The secondary beam was transmitted to a secondary CD_2 target of 30 mg/cm^2 at the final focus of RIPS. The reaction occurred at an energy of 34 A·MeV. The position of the incident particles was determined by two PPACs placed at F3 upstream of the target. The scattered particles were detected and identified by a 2x2 matrix silicon telescope placed 96 cm downstream of the target. 80 NaI(Tl) scintillator detectors surrounded the target to detect de–exciting γ rays emitted by the inelastically scattered nuclei.

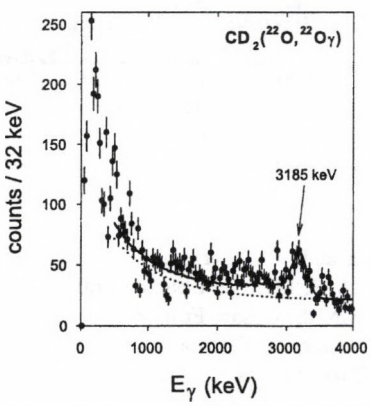

Figure 1. Doppler-corrected spectra of γ rays emerging from ^{22}O+CD_2 reaction. The solid line is the final fit including the spectrum curve from GEANT4 simulation and an additional smooth polynomial background plotted as a separate dotted line.

In Fig. 1. the Doppler–corrected γ ray spectra for ^{22}O nucleus is presented. The position of the single peak was determined at 3185(15) keV. The above energy for ^{22}O is in a good agreement with the value 3199(8) keV determined earlier [1]. After the peak position has been determined, we calculated the cross section for ^{22}O+^{2}H reaction to be $\sigma(0_1^+ \rightarrow 2_1^+)$=19±3 mb. From a distorted wave analysis, we derived the "matter" deformation length to be δ_M=0.77±0.07 fm which corresponds to a moderate mass deformation of β_M=0.23±0.02. We can compare this result with the data from ^{22}O+^{197}Au reaction [3] where the proton deformation (β_p) was derived to be between 0.2 and 0.24. This means that the neutron deformation of ^{22}O is very close to that of the proton one taking into account the mass deformation determined in the present study. This result is in contrast with the expectations that the increasing neutron number may lead to a stronger neutron decoupling. In reality, the $M_n/M_p \sim \beta_n/\beta_p$ ratios are 2, 3 and 1 for ^{18}O, ^{20}O and ^{22}O, respectively. The increasing trend is stopped by the N=14 subshell closure which makes both the proton and neutron distributions nearly spherical in ^{22}O.

a) RIKEN
b) Institut de Physique Nucléaire
c) Tokyo Institute of Technology
d) Tohoku University
e) University of Tokyo
f) Kurchatov Institute
g) Rikkyo University
h) Kyoto University

[1] M. Stanoiu *et al.*, Phys. Rev. C69 (2004) 034312.
[2] S. Agostinelli *et al.*, NIM A506 (2003) 250.
[3] P.G. Thirolf *et al.*, Phys. Lett. B485 (2000) 16.

2.9 ^{36}Ca: The mirror nucleus of the doubly magic ^{36}S

A. Bürger[a,b], M. Stanoiu[c,d], F. Azaiez[c], Zs. Dombrádi, D. Sohler, A. Algora, A. Al-Khatib[a], B. Bastin[e], G. Benzoni[f], R. Borcea[g], C. Bourgeois[c], P. Bringel[a], E. Clément[b], J.-C. Dalouzy[h], Z. Dlouhy[i], A. Drouart[b], C. Engelhardt[a], S. Franchoo[c], Zs. Fülöp, A. Görgen[b], S. Grévy[e], H. Hübel[a], F. Ibrahim[c], W. Korten[b], J. Mrázek[i], A. Navin[h], C. Timis[j], F. Rotaru[g], P. Roussel-Chomaz[h], M.-G. Saint-Laurent[h], G. Sletten[k], O. Sorlin[h], Ch. Theisen[b], D. Verney[c], S. Williams[j]

Isospin symmetry is a consequence of the approximate charge invariance of nucleon-nucleon forces. The strong interaction conserves the charge symmetry very well and the Coulomb energies are almost state-independent in a nucleus. The large bulk displacement energies produced by the monopole part of the Coulomb field are approximately cancelled in the excitation energy differences of the mirror nuclei. As a result, energy spectra are quite analogous between mirror nuclei. A small Coulomb effect may remain, due to differences in the radii of the single particle states. Especially, when the proton states are weakly bound, the wave function of the protons in the last shell becomes wider due to larger penetration to the classically forbidden region and consequently the Coulomb energy decreases.

In the neutron-deficient ^{36}Ca, the 2_1^+ state is expected to be unbound by about 500 keV, which may allow for a larger extension of the proton orbits. A measure of the increase of the proton radius may be the lowering of the energy of the 2_1^+ state in ^{36}Ca relative to the position of the same state in the mirror nucleus ^{36}S. To check if this happens, an experiment was performed at GANIL in Caen, France.

During the experiment the primary ^{40}Ca beam of around 95 A×MeV was fragmented in the SISSI target. The resulting beam cocktail was purified in the "α" spectrometer consisting of two dipole magnets and a degrader with the setting optimised for ^{37}Ca. The fragments were identified event by event through a time-of-flight measurement between the α spectrometer and the secondary ^{9}Be target of 1072 μm thickness, in which further nucleons were removed at an energy of around 61 A×MeV. After passing through the target, the produced fragments were identified using the spectrometer SPEG by time-of-flight and energy loss measurements. To detect the emitted gamma rays, the Chateau de Cristal array consisting of 74 BaF_2 scintillators was placed around the Be target. The Doppler-corrected gamma-ray spectrum obtained for ^{36}Ca is shown in fig. 1. Using Gaussian fits for the peaks, the energy of the 2^+ state in ^{36}Ca has been determined to be $E(2^+)$=3050(60) keV, 240 keV lower than the corresponding value in ^{36}S much larger than the usual mirror energy differences, indicating a drip line effect.

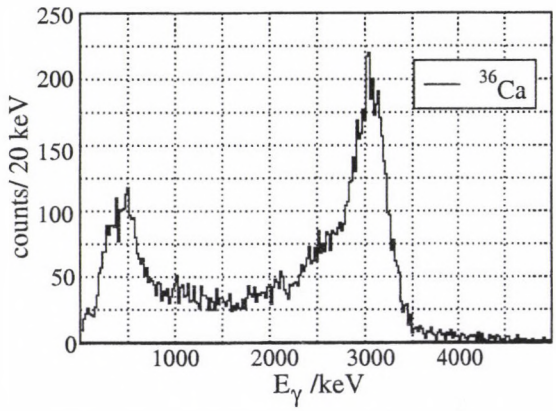

Figure 1. Gamma-ray spectrum obtained for ^{36}Ca.

a) Universität Bonn, Germany
b) DAPNIA/SPhN, CEA Saclay France
c) IN2P3-CNRS, Orsay, France
d) GSI, Darmstadt, Germany
e) LPC, Caen, France
f) INFN Milano, Italy
g) IFIN-HH, Bucharest-Magulere, Romania
h) GANIL, Caen, France
i) NPI, Rez, Czech Republic
j) University of Surrey, UK
k) NBI, Univ. Copenhagen, Denmark

2.10 First observation of the 2_1^+ excited state in the neutron-rich ^{42}Si

S. Grévy[a], B. Bastin[b], Zs. Dombrádi, D. Sohler, N.L. Achouri[b], J.C. Angélique[b], F. Azaiez[c], D. Baiborodin[d], R. Borcea[e], C. Bourgeois[c], A. Buta[e] A. Burger[f,g], R. Chapman[h], J.C. Dalouzy[a], A. Drouard[f], Z. Elekes, S. Franchoo[c], S. Iacob[e], B. Laurent[b], M. Lazar[e], X. Liang[h], E. Lienard[b], J. Mrázek[d], L. Nalpas[f], F. Negoita[e], N.A. Orr[b], Y. Penionskhevitch[i], Zs. Podolyák[j], F. Pougheon[c], P. Roussel-Chomaz[a], O. Sorlin[a], M. Stanoiu[c,k], I. Stefan[a], M.-G. Saint-Laurent[a], F. Nowacki[l], A. Poves[m]

The persistence of the N=28 shell closure at Z=14 was studied by in-beam γ-ray spectroscopy of the very neutron-rich ^{42}Si. Since ^{42}Si is next to the heaviest bound Si nucleus, the search for its excited states is an experimental challenge.

To determine the energy of the 2_1^+ state in ^{42}Si the method of two-step-fragmentation was used. The experiment was carried out at GANIL in Caen, France. A 4μA ^{48}Ca beam at 60 MeV/u was fragmented in the SISSI device. The primary reaction products were selected by the α spectrometer the magnets of which were optimised for ^{44}S. The beam particles were identified event by event using standard energy loss and time-of-flight method. The cocktail beam impinged onto a secondary ^{9}Be target of 185 mg/cm^2. The nuclei produced in the second fragmentation were transmitted through the SPEG spectrometer the Bρ value of which was adjusted to maximise the collection of ^{42}Si. The reaction products were unambiguously identified through their energy loss in an ionisation chamber and their mass over charge (A/Q) ratio deduced from time-of-flight and Bρ measurements. The ^{42}Si nuclei were produced exclusively from the ^{9}Be(^{44}S,^{42}Si) reaction. The total number of ^{42}Si nuclei observed is 132, which corresponds to a cross section of 102±26 μbarn.

To detect γ rays the secondary target was surrounded by the 4π array Chateau de Crystal consisting of 74 BaF_2 scintillators. The γ-ray spectra were obtained by selecting event-by-event the incoming nuclei and the ejectiles after the secondary target. Since the momentum of the reaction was measured directly with the SPEG spectrograph, a precise Doppler correction could be performed. As it can be seen in figure 1 a clear peak on a low background at 770±15 keV energy appears in the spectrum extracted in coincidence with ^{42}Si nuclei.

The low energy of the transition is a strong indication for the collapse of the N=28 spherical shell closure at Z=14 and the deformed nature of ^{42}Si. The small production cross section of ^{42}Si and the weak population of its excited states, on the other hand, can be interpreted as signatures of a closed proton shell. These findings together suggest that ^{42}Si is a deformed closed shell nucleus in agreement with the predictions of recent mean field calculations.

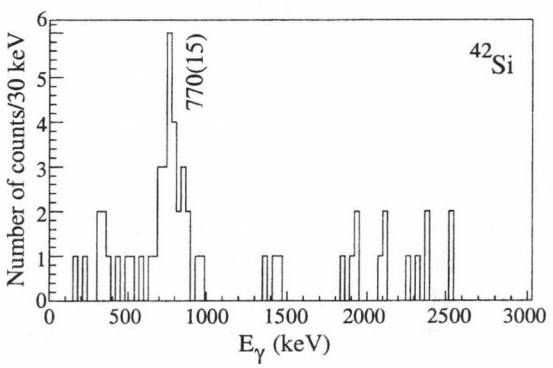

Figure 1. Addback energy spectrum of γ rays detected in coincidence with ^{42}Si nuclei.

a) GANIL, Caen, France
b) LPC, Caen, France
c) IN2P3-CNRS, Orsay, France
d) NPI, Rez, Czech Republic
e) IFIN-HH, Bucharest-Magulere, Romania
f) DAPNIA/SPhN, CEA Saclay France
g) Universität Bonn, Germany
h) University of Paisley, Scotland, UK
i) FLNR, JINR, Dubna, Russia
j) University of Surrey, UK
k) GSI, Darmstadt, Germany
l) IreS, Strasbourg, France
m) Universidad Autónoma de Madrid, Spain

2.11 Calculation of the response function of the NPI TAS spectrometer

A. Algora, J.L. Tain[a], B. Rubio[a], A.B. Perez[a], L. Caballero[a], J. Agramunt[a], E. Nácher[a], A. Krasznahorkay, M. Hunyadi, J. Gulyás, A. Vitéz, L. Batist[b], K. Burkard[c], W. Hüller[c], H. Penttilä[d], A. Nieminen[d], I. Moore[d], S. Rinta-Antila[d], P. Karvonen[d], A. Jokinen[d], A. Kankainen[d], T. Eronen[d], U. Hager[d], T. Sonoda[d], J. Äystö[d], J. Hakala[d], W. Gelletly[e], A. Garcia[f], I. Izosimov[g], A.L. Nichols[h]

The decay data of some of the important fission products are extremely complex and suffer from the inadequacies caused by the so called Pandemonium effect [1]. This effect has significant consequences in the decay-heat calculations because of levels missed in the experiment at high excitation energy; the result is an underestimation of the γ energy and an overestimation of the β energy released in the decay. The only way to avoid this problem is the application of total absorption techniques (TAS) to β-decay studies.

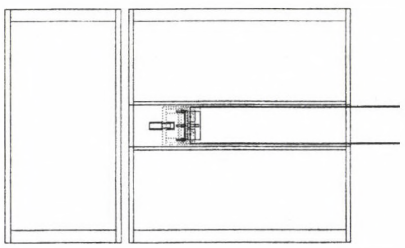

Figure 1. Geometry of the NPI TAS.

This has motivated our recent study of the decay of ^{104,105}Tc isotopes [2] at the Univ. of Jyväskylä IGISOL facility. The incomplete β-decay data on these isotopes were identified in [3] as the possible source of a substantial discrepancy between the calculations and the experiments in the γ-ray component of the reactor decay-heat in the cooling range from 300 to 3000 s after the fission event.

The first step in the analysis of the TAS data is the calculation of the response function of the spectrometer. The complexity of this problem requires the application of Monte Carlo techniques. First, we need to implement the geometry of the setup in full detail (see Fig. 1). Later, the response function to all possible gamma cascades are calculated. The quality of the Monte Carlo simulations can be checked by comparing simulations of radioactive sources with measurements. In Fig. 2, the results of the simulations of ^{22,24}Na sources using GEANT4 are compared with measurements. These sources were produced using a (p,2p) reaction on a Mg target during the experiment.

Preliminary results of the analysis of the ^{104}Tc decay, show that a large amount of β-strength is concentrated near the Q-value of the decay. Such pattern is required to understand the discrepancy in the calculations of the decay-heat.

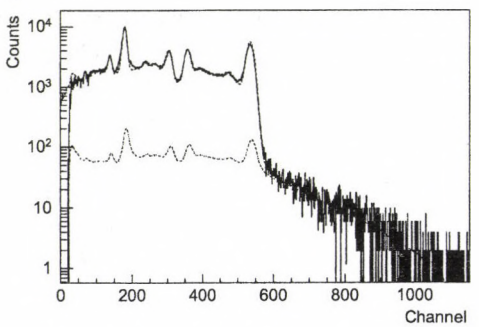

Figure 2. Comparison of the simulation (blue) with the measured sources of ^{22,24}Na (black). The lower spectrum (red) represents the contribution of the pulse pile-up.

Acknowledgements

A.A. recognizes support from the MERG-CT-2004-506849 contract, and the János Bolyai fellowship.

a) IFIC,CSIC-Univ. de Valencia, Valencia, Spain
b) NPI, St. Petersburg, Russia
c) GSI, Darmstadt, Germany
d) Univ. of Jyväskylä, Jyväskylä, Finland
e) Univ. of Surrey, Guildford, UK
f) Univ. of Washington, Seattle, USA
g) V. G. Khlopin Radium Inst., St. Petersburg, Russia
h) IAEA Nuclear Data Section, Vienna, Austria

[1] J.C. Hardy, *et al.*, Phys. Lett. 71B(1977)307
[2] A. Algora, *et al.*, ATOMKI Ann. Rep. 2004, p.16
[3] T. Yoshida, *et al.*, J. of Nucl. Sci. &Tech. 36(1999)135

2.12 Maximally aligned states in the proton drip line nucleus ^{106}Sb

D. Sohler, M. Palacz[a], Zs. Dombrádi, M. Hjorth-Jensen[b], C. Fahlander[c], L.-O. Norlin[d], J. Nyberg[e], T. Bäck[d], K. Lagergren[d,f], D. Rudolph[c], A. Algora, C. Andreoiu[c], G. de Angelis[g], A. Atac[h], D. Bazzacco[i], J. Cederkäll[c], B. Cederwall[d], B. Fant[j], E. Farnea[i], A. Gadea,[g], M. Górska[k], H. Grawe[k], N. Hashimito-Saitoh[k], A. Johnson[d], A. Kerek[d], W. Klamra[d], J. Kownacki[a], S. M. Lenzi[g], A. Likar[l], M. Lipoglavšek[l], M. Moszyński[m], D. R. Napoli[g], C. Rossi-Alvarez[i], H. A. Roth[n], T. Saitoh[k], D. Seweryniak[o], Ö. Skeppstedt[n], J. Timár M. Weiszflog[h], M. Wolińska[a]

High-spin states in ^{106}Sb were studied in the ^{54}Fe(^{58}Ni,1α1p1n) reaction by in-beam γ-spectroscopic methods using the EUROBALL detector array equipped with charged particle and neutron detectors. On the basis of measured $\gamma\gamma$-coincidence relations, angular distributions, and linear polarization ratios a significantly extended level scheme was constructed. The obtained level scheme is shown in fig. 1. The experimental results were interpreted within the framework of the *gdsh* shell model using a realistic effective nucleon-nucleon interaction. Candidates for states with fully aligned angular momenta in the $\pi(d_{5/2}, g_{7/2})^1 \nu(d_{5/2}, g_{7/2})^5$ valence space are identified at 4338 and 5203 keV, as well as in the $\pi(d_{5/2}, g_{7/2})^1\ \nu(d_{5/2}, g_{7/2})^4 h^1_{11/2}$ space at 6087, 6573 and 6783 keV marked with asterisks in fig. 1.

a) HIL, University of Warsaw, Warsaw, Poland
b) University of Oslo, Norway
c) Lund University, Lund, Sweden
d) Royal Inst. of Tech., Stockholm, Sweden
e) The Svedberg Laboratory, Uppsala, Sweden
f) Oak Ridge Nat. Lab., Oak Ridge, TN, USA
g) Laboratori Nazionali di Legnaro, Legnaro, Italy
h) Uppsala University, Uppsala, Sweden
i) Universitá di Padova, Padova, Italy
j) Helsinki University, Helsinki, Finland
k) GSI, Darmstadt, Germany
l) J. Stefan Institute, Ljubljana, Slovenia
m) Sołtan Inst. for Nucl. Studies, Świerk, Poland
n) Chalmers Univ. of Tech., Gothenburg, Sweden
o) Argonne National Laboratory, Chicago, USA

[1] D. Sohler *et al.*, Nucl. Phys. A 753 (2005) 251.

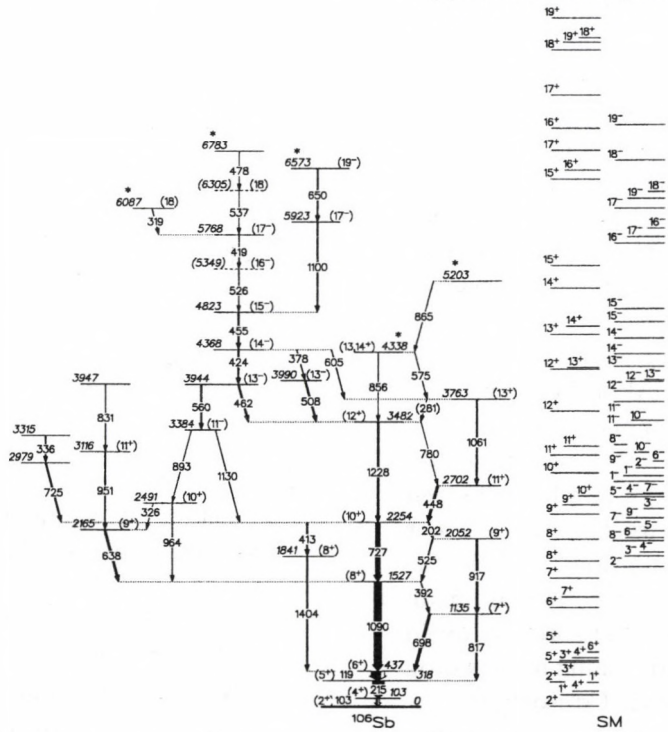

Figure 1. Proposed experimental level scheme of ^{106}Sb in comparison with results of shell model calculations.

2.13 ^{106,108}Cd(p,γ)^{107,109}In cross sections for the astrophysical p-process

Gy. Gyürky, G.G. Kiss, Z. Elekes, Zs. Fülöp, E. Somorjai

As a continuation of a systematic study of reactions relevant to the astrophysical p-process, the α-capture as well as the α-elastic scattering cross sections of the ^{106}Cd nucleus have been recently measured at ATOMKI [1,2]. In order to give a complete description of ^{106}Cd nucleus from the astrophysical p-process point of view, it is also necessary to measure the proton capture cross section of this isotope in the astrophysically relevant energy range and to compare the result with the predictions of statistical model calculations which are used in p-process modeling.

The proton capture cross section measurement has been carried out using the activation technique. In contrary to the case of the (α,γ) experiment, the proton capture of the other p-isotope of cadmium (^{108}Cd) also leads to a radioactive reaction product. Therefore it was possible to measure the (p,γ) cross section for both p-isotopes of cadmium: ^{106}Cd and ^{108}Cd.

The experiments have been carried out at the Van de Graaff and cyclotron accelerators of ATOMKI. The lower part of the investigated energy region between 2.4 and 3.6 MeV was measured at the Van de Graaf while the upper part between 3.6 and 4.8 MeV at the cyclotron. In order to find any possible systematic difference between the results obtained at the two accelerators, the E_p=3.6 MeV point has been measured with both accelerators, and perfect agreement was found.

Highly enriched ^{106}Cd as well as natural Cd evaporated onto thin Al backing was used for targets. The ^{108}Cd content in the enriched ^{106}Cd was still higher than the natural abundance thus the ^{108}Cd(p,γ) could be measured also with the enriched targets. In the lower part of the measured energy range, where the cross section of the studied reactions is small, the enriched targets were used in order to avoid the disturbing background coming from proton induced reactions on heavier Cd isotopes.

The γ-radiation from the decay of the produced ^{107}In and ^{109}In isotopes was measured with calibrated HPGe detector. For the analysis the recently measured precise half-life of ^{109}In has been used [3].

The resulting cross sections have been compared with the predictions of the statistical model calculations using the NON-SMOKER code [4]. For both measured reactions there is a good agreement between the measurements and the calculations. Fig. 1. shows the results in the form of astrophysical S-factor. The measured points obtained with enriched and natural targets are shown with different symbols. The results of the model calculations are also shown. The final analysis of the results is still in progress where the dependence of the model calculations on different input parameters will also be studied.

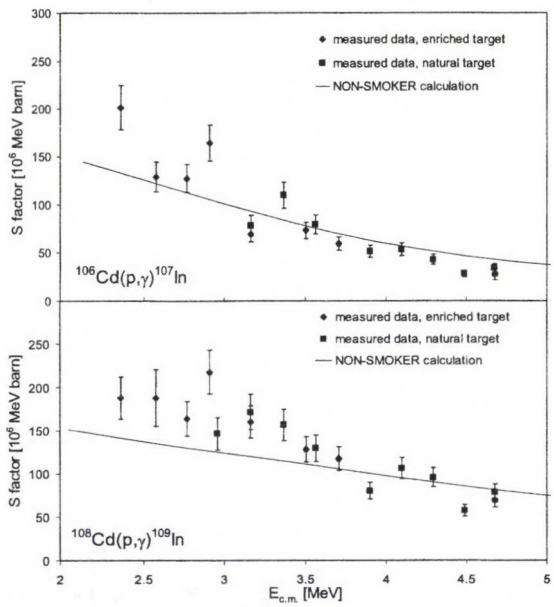

Figure 1. Astrophysical S-factor for the two studied reactions. The measured points as well as the model calculations are shown.

[1] Gy. Gyürky *et al.*, Phys. Rev. C *in press.*

[2] G.G. Kiss *et al.*, Eur. Phys. J. A *in press.*

[3] Gy. Gyürky *et al.*, Phys. Rev. C 71 (2005) 057302.

[4] T. Rauscher and F. K. Thielemann, At. Data Nucl. Data Tables 79 (2001) 47.

2.14 High-spin γ-ray spectroscopy of ^{121}Xe and ^{122}Xe

G. Berek, B.M. Nyakó, J. Timár and the HLHD collaboration[b)]

The balance and interplay between the two extreme facets of nuclear dynamics, collective rotation and single-particle alignment, is of fundamental importance in nuclear structure. A deformed nucleus can increase its spin by collective rotation about an axis perpendicular to its symmetry axis. In a rotational band, higher spin states are built by a gradual alignment of the spin vectors of all the available valence nucleons until, eventually, full alignment is reached. At this point, the rotational band has lost its collectivity and is said to terminate. The spectroscopy of band terminating states has been studied extensively by using the increased sensitivity of the escape suppressed spectrometers.

The neutron-deficient nuclei around mass number 120 are very well suited to study the interplay between single-particle and collective excitation modes. These nuclei with a few nucleons outside a closed-shell core are soft to γ-deformation and shape driving effects of nucleons in different orbitals can lead to co-existence of different shapes.

A high-statistics experiment aiming at the identification of hyperdeformed states [1] in A$\simeq$120 nuclei has also provided valuable data for studying the normal deformed states at the highest spins in this mass region. The aim of this work is to search for terminating bands in ^{121}Xe and ^{122}Xe as well as to test the cranked shell model at high spins.

The fusion-evaporation nuclear reactions ^{64}Ni(^{64}Ni,α3n) and ^{64}Ni(^{64}Ni,α2n) were used to populate high-spin states in ^{121}Xe and ^{122}Xe, respectively. The beam with energies of 255 and 261 MeV was provided by the VIVITRON tandem accelerator at IReS, Strasbourg. The emitted γ-rays were detected by the EUROBALL IV spectrometer [2]. The detection of light charged particles was performed by means of the highly efficient DIAMANT array [3,4], which was mounted inside the target chamber.

A total of about 3.7 $\times 10^9$ Compton suppressed events was recorded when one charged particle has been detected in DIAMANT array. For the analysis of the one-α gated triple-coincidence cube a standard gating procedure was carried out with the help of the RADWARE software package [5].

As an illustration Fig. 1 shows γ-lines of the dominant (α,2n) and (α,3n) channels.

The data are presently being analyzed.

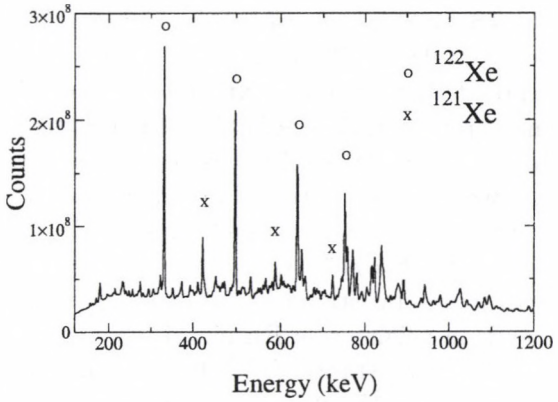

Figure 1. Part of the γ-spectrum demonstrating the selectivity on the 1α channel for the ^{64}Ni(^{64}Ni,α) reaction at 261 MeV. The strongest γ-lines from (α,2n) and (α,3n) channels are indicated by o and x symbols.

a) see P. Mason *et al.*, ATOMKI Ann. Rep. (2005)

[1] B.M. Nyakó *et al.*, ATOMKI Ann. Rep. (2005)

[2] J. Simpson, Z. Phys. A 358 (1997) 139.

[3] J.N. Scheurer *et al.*, NIM A 385 (1997) 501.

[4] J. Gál *et al.*, NIM A 515 (2004) 502.

[5] D.C. Radford, NIM A 361 (1995) 297.

2.15 The role of the core in degeneracy of chiral candidate band doubling

J. Timár, C. Vaman[a,b], K. Starosta[a], D.B. Fossan[b], T. Koike[b,c], D. Sohler, I.Y. Lee[d], A.O. Macchiavelli[d]

Nearly degenerate ΔI=1 rotational bands have been observed recently in several odd-odd nuclei in the $A\approx130$ and $A\approx100$ mass regions. The properties of these doublet bands have been found to agree with the scenario of spontaneous formation of chirality and disagree with other possible scenarios. However, the most recent results obtained from lifetime experiments for some chiral candidate nuclei in the $A\approx130$ mass region seem to contradict the chiral interpretation of the doublet bands in these nuclei based on the observed differences in the absolute electromagnetic transition rates; the transition rates expected for chiral doublets are predicted to be very similar. Therefore it is interesting to search for new types of experimental data that may provide further possibilities to distinguish between alternative interpretations, and may uncover new properties of the mechanism that is responsible for the band doubling in these nuclei. Such a new type of experimental data was found by studying the chiral candidate bands in neighboring Rh nuclei [1].

High-spin states of ^{103}Rh were studied using the ^{96}Zr(^{11}B,4n) reaction at 40 MeV beam energy and chiral partner candidate bands have been found in it. As a result of this observation a special quartet of neighboring chiral candidate nuclei can be investigated for the first time. With this quartet identified a comparison between the behavior of the nearly degenerate doublet bands belonging to the same core but to different valence quasiparticle configurations, as well as belonging to different cores but to the same valence quasiparticle configuration, becomes possible. The comparison shows that the energy separation of these doublet band structures depends mainly on the core properties and only at less extent on the valence quasiparticle coupling. This observation sets up new criteria for the explanations of the band doublings, restricting the possible scenarios and providing new information on the characteristics of the underlying mechanism; it is in a qualitative agreement with the chiral scenario.

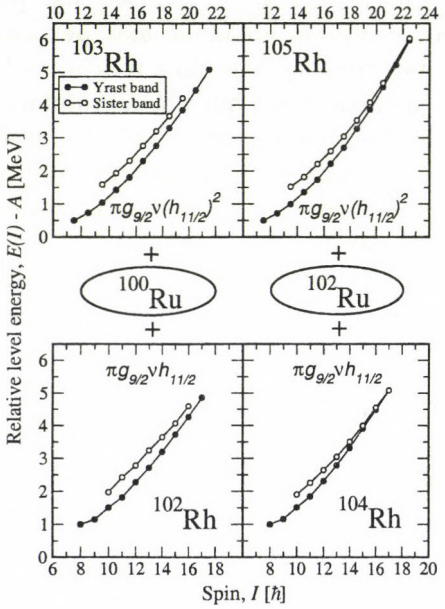

Figure 1. Comparison of the relative energy vs. spin plots of the chiral candidate bands in the neighboring ^{102,103,104,105}Rh nuclei. The energy of the yrast band head is shifted to 1 MeV in the odd-odd cases and to 0.5 MeV in the odd-A cases.

Acknowledgements

This work was supported in part by the Hungarian Scientific Research Fund, OTKA (contract numbers T046901 and T038404).

a) NSCL, Cyclotron Laboratory, Michigan State University, East Lansing, MI 48824-1321, USA

b) Department of Physics and Astronomy, SUNY, Stony Brook, New York, 11794-3800, USA

c) Graduate School of Science, Tohoku University, Sendai, 980-8578, Japan

d) Nuclear Science Division, Lawrence Berkeley National Laboratory, Berkeley, California 94720, USA

[1] J. Timár *et al.*, Phys. Rev. C 73 (2006) 011301(R)

2.16 Search for hyperdeformation at high spins in A≈120 nuclei using charged particle-xn data

B.M. Nyakó, B. Herskind[a], K. Juhász[b] and the HLHD collaboration[1]

The formation of hyperdeformed (HD) shapes in nuclei at high spins is a consequence of fast rotational motion. With increasing angular momentum, as recent LSD theory [1] predicts, nuclei undergo a Jacobi shape transition from normaldeformed to extremely elongated axially symmetric shape. Stable HD shapes can be formed, if the Jacobi instability spans over a wide-enough spin range before the nucleus becomes unstable against fission. This is expected to happen in some nuclei near the highest spins nuclei can sustain. Their deexcitation happens primarily by fast γ-ray cascades, but the emission of light charged particles from the tips of HD nuclei may also be possible, with enhanced probability. It is, therefore, important to find the best experimental conditions to optimize the population, and to choose the proper data evaluation techniques to select the signatures of HD structures.

The main aim of the HLHD collaboration, named after a one-month-long Hyper-Long HD experiment, was to find discrete-line HD bands in ^{126}Ba. The symmetric ^{64}Ni+^{64}Ni fusion-evaporation reaction was utilised at E_{beam} = 255 and 261 MeV. γ-rays were detected by the highly efficient EUROBALL-IV array at IReS (Strasbourg), equipped with two 4π ancillary detector systems: the BGO InnerBall γ-calorimeter and the 84-element light charged particle detector DIAMANT, which served to eliminate (to select) charged particle-related γ-rays from the xn- (particle-xn)-type coincidence data. The *elimination* of such data enabled a study of the population of HD structures in ^{126}Ba, but no discrete band(s) were identified in the experiment [2].

The *selection* of particle-xn-type data enabled the search for extremely deformed structures in the corresponding residual nuclei, which were also predicted to possess Jacobi instability. To enhance data quality γ-ray energies in the particle-xn channels were Doppler-corrected for the change in the velocity and direction of the recoiling residual nuclei when one or two alpha particle(s) were emitted. The γ-energy correlation methods were used for the identification of collective structures. Preliminary results showed the presence of many normal or highly deformed bands with almost constant moment of inertia both in the α and proton channels [3]. To investigate if extreme deformations in these nuclei exist or not a further analysis of diagonal cut spectra created from 2D and 3D rotational plane mapped energy correlation data have been carried out.

A breakthrough was recently obtained in this type of analysis [4]: rotational patterns in the form of ridge-structures in the 3D rotational mapped spectra have been observed with dynamic moments of inertia $J^{(2)}$ ranging from 71 to 111 $\hbar^2$/MeV in 11 different nuclei specifically selected by combination of charged particle and/or γ-gating. The 4 nuclei, ^{118}Te, ^{124}Cs, ^{125}Cs, ^{124}Xe found with moment of inertia $J^{(2)}\approx100$ $\hbar^2$/MeV, are most likely hyperdeformed, the remaining nuclei with smaller values of $J^{(2)}$ are considered to be superdeformed, in qualitative agreement with recent theoretical calculations [4]. A comparison of such data obtained with and without Doppler correction resulted no conclusive evidence for the presence of the otherwise possible particle decay-out from the expected HD bands.

a) Niels Bohr Institute, Copenhagen Ø, Denmark

b) Dept. of Inf. Techn., Univ. of Debrecen, Hungary

[1] K. Pomorski and J. Dudek, Phys. Rev. C67 (2003) 044316.

[2] B. Herskind *et al.*, AIP Conf. Proc. 701 (2004) 303-315.

[3] B.M. Nyakó *et al.*, Acta Physica Polonica, B36 (2005) 1033.

[4] B. Herskind *et al.*, Int. Conf. on Finite Fermionic Systems - Nilsson Model 50 years, to appear in Phys. Scripta (2006).

[1] For the list of participants see Ref. [3]

2.17 Evidence for octupole correlations in ^{124,125}Ba

P. Mason[a], G. Benzoni[a], A. Bracco[a], F. Camera[a], B. Million[a], O. Wieland[a], S. Leoni[a], A.K. Singh[b], A. Al-Khatib[b], H. Hübel[b], P. Bringel[b], A. Bürger[b], A. Neusser[b], G. Schönwasser[b], B.M. Nyakó, J. Timár, A. Algora, Zs. Dombrádi, J. Gál, G. Kalinka, J. Molnár, D. Sohler, L. Zolnai, K. Juhász[c], G.B. Hagemann[d], C.R. Hansen[d], B. Herskind[d], G. Sletten[d], M. Kmiecik[e], A. Maj[e], J. Styczen[e], K. Zuber[e], F. Azaiez[f], K. Hauschild[f], A. Korichi[f], A. Lopez-Martens[f], J. Roccaz[f], S. Siem[f], F. Hannachi[g], J.N. Scheurer[g], P. Bednarczyk[h], Th. Byrski[h], D. Curien[h], O. Dorvaux[h], G. Duchene[h], B. Gall[h], F. Khalfallah[h], I. Piqueras[h], J. Robin[h], S.B. Patel[i], O.A. Evans[j], G. Rainovski[j], C.M. Petrache[k], D. Petrache[k], G. La Rana[l], R. Moro[l], G. De Angelis[m], P. Fallon[n], I.-Y. Lee[n], J.C. Lisle[o], B. Cederwall[p], K. Lagergen[p], R.M. Lieder[q], E. Podsvirova[q], W. Gast[q], H. Jäger[q], N. Redon[r], A. Görgen[s]

Octupole correlations in atomic nuclei are due to the interaction between orbitals of opposite parity, whose angular momenta differ by $3\hbar$, lying in the proximity of the Fermi surface. In general, this situation occurs when the Fermi level is found between an intruder orbital and the normal-parity subshell. Experimental fingerprints of octupole correlations, such as alternate-parity bands linked by enhanced E1 transitions, very collective E3 transitions, and parity doublets in odd nuclei, are in fact long established in the proximity of both the double octupole shell closures Z = 56,N = 88 (corresponding to the nucleus ^{144}Ba) and Z = 56,N = 56 (corresponding to the so far unidentified-and perhaps unbound-nucleus ^{112}Ba). Octupole features of Ba nuclei situated between these two regions were studied [1].

The γ decay of the nuclei ^{124,125}Ba has been investigated by means of the EUROBALL spectrometer, coupled to the DIAMANT array of charged-particle detectors, using the reaction ^{64}Ni+^{64}Ni at E_{beam}=255 and 261 MeV. In the nucleus ^{125}Ba six new E1 transitions have been found to link opposite-parity bands currently interpreted as $\nu d_{5/2}(+g_{7/2})$, $\nu h_{11/2}$ structures. The previously unknown $J^\pi = 3^-$ level in the nucleus ^{124}Ba has also been identified; its excitation energy is accurately reproduced by a microscopic calculation including octupole correlations. Both issues are bolstered by sizable B(E1)/B(E2) ratios.

a) INFN and Dipartimento di Fisica, Universita degli Studi di Milano, via Celoria 16, I-20133 Milano, Italy

b) Helmholtz-Institut für Strahlen-und Kernphysik, Universität Bonn, Nussallee 14-16, D-53115 Bonn, Germany

c) Faculty of Informatics, University of Debrecen, Hungary

d) Niels Bohr Institute, Blegdamsvej 17, DK-2100 Copenhagen Ø, Denmark

e) Niewodniczański Institute of Nuclear Physics, PAN, 31-342 Kraków, ul. Radzikowskiego 152, Poland

f) CSNSM Orsay, IN2P3/CNRS, F-91405 Orsay, France

g) Centre d Etudes Nuclèaires deBordeaux-Gradignan, F-33175 Gradignan, France

h) Institut de Recherches Subatomiques, CNRS-IN2P3, F-67037 Strasbourg, France

i) Department of Physics, University of Bombay, Mumbai, India

j) Oliver Lodge Laboratory, University of Liverpool, Liverpool L69 7ZE, United Kingdom

k) INFN and Dipartimento di Fisica, Università di Camerino, via Madonna delle Carceri, I-62032 Camerino, Italy

l) INFN and Physical Science Department, Complesso Universitario di Monte S.Angelo, via Cinthia, I-80126 Napoli, Italy

m) INFN, Laboratori Nazionali di Legnaro, via Romea 4, I-35020 Legnaro, Italy

n) Lawrence Berkeley Laboratory, Berkeley California 94720, USA

o) Schuster Laboratory, University of Manchester, Brunswick Street, Manchester M13 9PL, United Kingdom

p) Department of Physics, Royal Institute of Technology, SE-10691 Stockholm, Sweden

q) Institut für Kernphysik, Forschungszentrum Jülich, D-52425 Jülich, Germany

r) IPN Lyon, IN2P3/CNRS, Universitè Lyon-1, F-69622 Villeurbanne, France

s) DAPNIA/SPhN, CEA-Saclay, F-91191 Gif-sur-Yvette, France

[1] P. Mason *et al.*, Phys. Rev. C 72 (2005) 064315.

2.18 Systematic investigations on the decay properties of the Isoscalar Giant Dipole Resonance

M. Hunyadi, A.M. van den Berg[a], M. Csatlós, U. Garg[b], J. Gulyás, M. Fujiwara[c], M.N. Harakeh[a], A. Krasznahorkay, T. Li[b], A. Matić[a], D. Sohler, A. Vitéz, H.J. Wörtche[a]

An experiment to study the direct proton-decay properties of the Isoscalar Giant Dipole Resonance (ISGDR) was carried out at the superconducting cyclotron facility of KVI using of the $(\alpha, \alpha'\mathrm{p})$ reaction on ^{90}Zr and ^{208}Pb targets at E_α=200 MeV. A proton-decay experiment was first performed by our group for the ISGDR in ^{208}Pb [1], and later in Osaka in ^{58}Ni [2], which yielded partial branching ratios of the ISGDR for the first time. The primary motivation was to extend these studies and to pursue a systematic investigation of the direct-decay branching ratios to the single hole-states. These can be compared to the results of recent continuum-RPA calculations [3] in order to learn about the microscopic structure and the subsequent damping mechanism of the ISGDR. Previously, systematics were established only for the direct-neutron decay of the ISGDR in ^{90}Zr,^{116}Sn and ^{208}Pb [4], but the moderate resolution ($\approx$1500 keV) of the neutron energies in the TOF measurements did not allow to resolve the individual final states in the daughter nuclei, and therefore the determination of partial branching ratios was not possible.

The experiment was performed with the Big-Bite Spectrometer (BBS) in conjunction with the EuroSupernova focal-plane detector-system. The BBS was set at Θ_{lab}=4° and 5° for ^{208}Pb and ^{90}Zr targets, respectively, covering a solid angle of 6 msr in both cases. The decay-protons were detected by a Si-ball consisting of 16 Si(Li)-detectors with a thickness of 5 mm each. These were placed in the backward hemisphere of the scattering chamber at a distance of 10 cm from the target, as in our previous experiment [1].

In Fig. 1 the final-state spectrum populated by proton decay from a part of the ISGDR region (20-24 MeV) in ^{90}Zr is shown, which well represents the effective selection of single hole-states (2p1/2, 2p3/2, 1f5/2) in ^{89}Y. Projecting events populating these hole-states resulted in a better definition of the giant resonance strengths compared to multipole decomposition analyses of singles data. This is due to suppression of the underlying nuclear continuum, which decays by statistical evaporation of particles to complex configurations. The multipolarity to be studied (L=1 in our case) was selected in the coincidence spectra by the application of the difference-of-spectra technique, which exploits differences in the shapes of the angular distributions for various multipolarities. Preliminary values of the partial branching ratios were determined for the ISGDR strength, and were compared to theoretical predictions. The analysis and the interpretation of the results is still in progress.

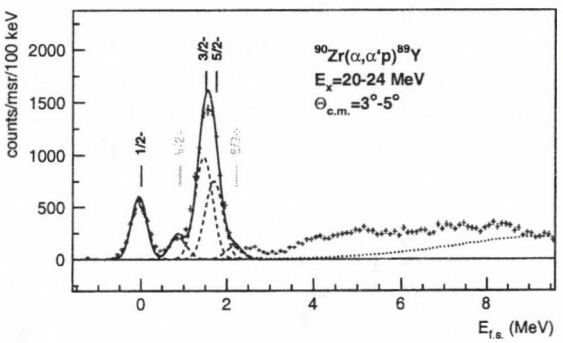

Figure 1. Final-state energy spectrum following proton decay from a part of the ISGDR region (20-24 MeV) in ^{90}Zr. Single proton-hole states are marked with black labels. The dotted curve represents the statistical decay contribution.

a) KVI, Groningen, The Netherlands

b) University of Notre Dame, USA

c) RCNP, University of Osaka, Japan

[1] M. Hunyadi *et al.*, Phys. Lett. B**576**, 253 (2003).

[2] U. Garg, private communication.

[3] M.L. Gorelik *et al.*, Phys. Rev. C **69**, 054322 (2004).

[4] M. Hunyadi *et al.*, prep. for submission.

2.19 First observation of low-lying excited states in ^{232}Pa

M. Csatlós, L. Csige, T. Faestermann[b], Z. Gácsi, J. Gulyás, D. Habs[a], R. Hertenberger[a], M. Hunyadi, A. Krasznahorkay, H.J. Maier[a], P.G. Thirolf[a] and H.F. Wirth[a]

The actinide region is very rich in interesting nuclear phenomena (fission, super- and hyperdeformed shapes, cluster decay, superheavy elements etc.) and contains important isotopes (Th, Pa, U) also for energy production (fission). However, the spectroscopic information for the low-lying excited states are scarce. The well known spectroscopic tools like one particle transfer reactions could not be used because of the lack of suitable targets. With respect to the hyperdeformation, the double-odd ^{232}Pa nucleus is of great interest. The level scheme of this isotope is completely unknown except for the ground-state level ($I^{\pi}_{gs} = 2^-$) [1], although it could be important in fixing the proton-neutron residual interaction part of the shell model description in this mass region. The aim of this work was to study the low-lying excited states in ^{232}Pa using (d,p) reaction on the radioactive ^{231}Pa target.

The experiment was performed at the Munich Tandem accelerator. The deuteron beam energy was $E_d = 12$ MeV. A 80 μg/cm^2 thick ^{231}Pa target on a 20 μg/cm^2 thin carbon backing was used. The kinetic energy of the proton ejectiles was analysed with a Q3D magnetic spectrometer placed at $\Theta_L = 140°$ relative to the incident beam, covering a solid angle of 10 msr. The position of the analyzed particles in the focal plane was measured with a position-sensitive light ion focal plane detector with individual cathode strip readout of 890 mm active length.

The spectrum was analyzed with a fitting program GASPAN [2]. The energy and the relative differential cross section were determined for 35 new excited states below 900 keV.

A typical part of the fit is shown in Fig. 1. The spin and parity assignment is still the subject of further measurements of the angular distribution.

a) LMU, München, Germany.

b) TU, München, Germany.

[1] http://www.nndc.bnl.gov/nudat2/

[2] F. Riess, Ann. Rep., Munich Tandem Accelerator Laboratory, 1991, p.168.

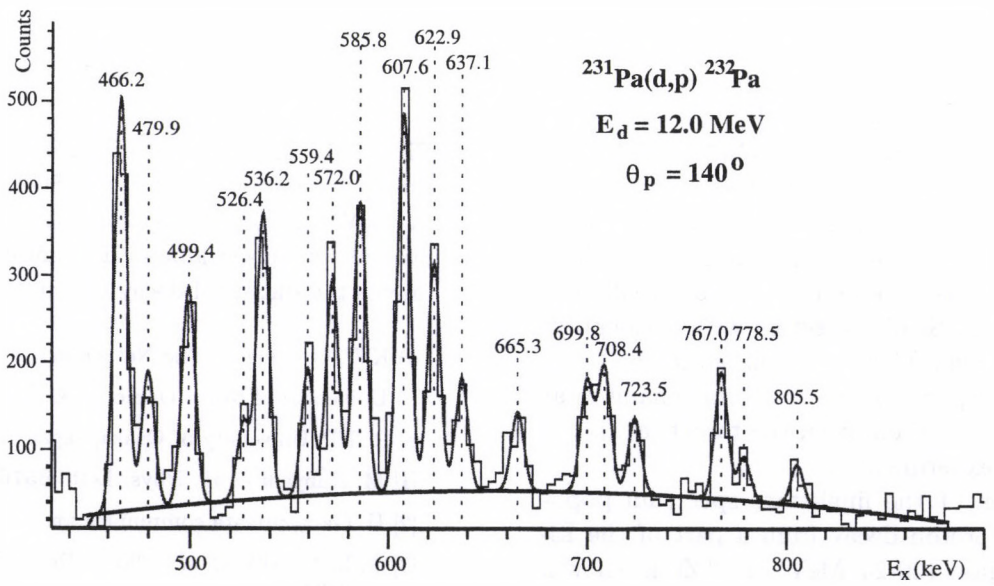

Figure 1. Part of the result of the fit. The dotted lines show the position of the peak in energy.

2.20 Angular distribution of fission fragments from ^{236}U(d,pf)

L. Csige, M. Csatlós, T. Faestermann[b], Z. Gácsi, J. Gulyás, D. Habs[a], R. Hertenberger[a], M. Hunyadi, A. Krasznahorkay, H.J. Maier[a], Z. Máté, O. Schaile[a], P. Thirolf[a], H. Wirth[a]

^{236}U is the only isotope in the actinide region in which transmission fission resonances observed [1] and at the same time a superdeformed fission isomer is well-established [2]. We have been investigating these transmission resonances for several years.

The aim of our latest experiment was to measure the angular distribution of the fission fragments in order to determine the spin and K-values of the resonances and to improve the statistics compared to the previous experiment [3].

An experiment was performed to study the fission resonances of ^{236}U at the Munich Tandem Laboratory using ^{235}U(d,p) reaction at 13 MeV. A $^{235}U_2O_3$ target was used with a thickness of 90 μg/cm^2. The outgoing proton energy was determined by a Q3D magnetic spectrometer at an angle 139.4°. An energy resolution of ΔE=5keV was achieved. Fission fragments were detected by two position sensitive avalanche detectors (PSAD) consisting of two wire planes corresponding to horizontal and vertical directions. Thus, the spatial positions of the fragments and their angular correlation with respect to the recoil axis could be determined.

High resolution measurement of the angular distribution allowed us to determine the spin and K-values of the observed resonances individually. The angular correlation was parametrized with coefficients a_2 and a_4 of even Legendre polynomials. Fig. 1b) shows the a_2 coefficient belonging to the different resonances. The a_2 values are agree with the values of Ref. [4], which were used to determine the K-values in the data analysis of the previous experiment [3]. The most interesting energy region is around 5.1 MeV, where hyperdeformed resonances were identified recently [3] in contrast to the superdeformed interpretation published so far [5].

The high-resolution excitation energy spectrum, which was deduced from the proton kinetic energy is shown in Fig. 1a). A combined analysis of the energy spectrum and the angular distribution confirms that the resonances around 5.1 MeV correspond to resonances in the hyperdeformed third minimum rather than in the superdeformed second well of the potential energy surface as found in [3].

The rotational parameter was determined as $\hbar^2/\Theta = 2.35^{+0.2}_{-0.65}$ keV, which is in good agreement with the previous result of $\hbar^2/\Theta = 2.4^{+0.6}_{-0.3}$ keV.

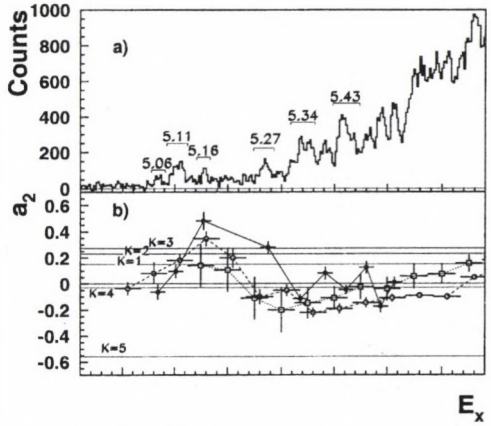

Figure 1. (a) Excitation energy spectrum of ^{236}U. Known hyperdeformed resonance regions are marked. (b) Full dots represent the a_2 values determined in this experiment, while the open circles and squares show the coefficients from Ref. [4] and [6], respectively. The horizontal lines indicate theoretical values for different K-values.

a) LMU, Munich, Germany

b) TUM, Munich, Germany

[1] A. Krasznahorkay *et al.*, Phys. Rev. Lett. 80(1998) 2073.

[2] S. B. Bjornholm, J.E. Lynn, Rev. Mod. Phys. 52(1980) 725.

[3] M. Csatlós *et al.*, Phys. Lett. B615(2005) 175.

[4] M. Just *et al.*, Proc. of the Int. Symp. on the Phys. and Chem. of Fission, Jülich, 1979, IAEA,71.

[5] P. D. Goldstone *et al.*, Phys. Rev. C18(1978) 1706.

[6] H. C. Britt *et al.*, Phys. Rev. 175(1968) 1525.

2.21 Extending the nuclear cluster supersymmetry scheme to $A = 18$ nuclei

G. Lévai

The U(4|12) nuclear cluster supersymmetry has been proposed as a framework that allows unified description of core+α-particle type cluster configurations in the $A \leq 20$ domain [1]. In particular, the bosonic sector of this scheme describes the relative motion of the clusters in terms of monopole (σ) and dipole (π) bosons, while the fermionic sector accounts for hole configurations in the p shell within the Elliott model. The group structures associated with the two sectors, $U_B(4) \supset SU_B(3)$ and $U_F(12) \supset SU_F(3) \times U_F^{ST}(4)$ both contain the SU(3) group accounting for three-dimensional oscillators, and this fact can be used to couple the spatial structure of the two sectors to describe that of the unified nucleus. In fact, this construction corresponds to embedding the algebraic structure of the semimicroscopic algebraic cluster model (SACM) into a superalgebra. The assumed supersymmetry (SUSY) imposes correlations between the spectroscopic properties of the members of the supermultiplet, and these can be checked against the available experimental data. The actual physical systems corresponding to N_F=0, 1 and 2 fermions are the α-cluster states of the A=20, 19 and 18 nuclei ^{20}Ne, ^{19}F, ^{19}Ne, ^{18}O, ^{18}F and ^{18}Ne.

Similarities between various α-cluster bands of these nuclei have been pointed out previously, so attempting their interpretation in terms of the supersymmetry scheme is a natural choice. As a first attempt the spectroscopic properties (energy spectrum, E2 transitions and one-nucleon transfer amplitudes) of α-cluster states of ^{20}Ne and ^{19}F have been analysed in terms of the U(4|12) SUSY scheme, and it was shown that the performance of this model is at least as good [1] as that of other nuclear supersymmetry schemes.

As the next natural step we extended this scheme to all six nuclei corresponding to fermion number N_F=0, 1 and 2. Perhaps the most decisive observables are the spectroscopic factors of one-nucleon transfer reactions between pairs of these nuclei, because these are described by SUSY generators. These spectroscopic factors can be calculated in terms of SU(3) and SO(3) $9j$-coefficients and other factors, however, the validity of the selection rules dictated by the SUSY scheme can be analysed directly without any calculations, simply by comparing the SU(3) (and SO(3)) quantum numbers associated with the experimental levels. The results of this analysis are displayed in Table 1 for six reactions for which data were available [2]. The results indicate that the selection rules are realized rather well. (There are some transitions to levels which cannot be resolved or do not have α-cluster character, but the corresponding C^2S values are smaller than in the case of allowed transitions.)

Work is in progress to account for quantitative data on one-nucleon transfer spectroscopic factors and B(E2) values [3]. Our aim is giving a unified description on these quantities for all six nuclei mentioned above, using the *same* operators. The most complex system is ^{14}N+α, in which case both $T = 1$ and $T = 0$ states appear in the core nucleus, and these are combined with spin values $S = 0$ and $S = 1$.

Table 1. The number and average C^2S_{Exp} spectroscopic factor of one-nucleon transfer reactions allowed (All.) and forbidden (Forb.) by the supersymmetry-dictated selection rules.

Reaction	No.($\langle C^2S_{\mathrm{Exp}} \rangle$)	
	All.	Forb.
^{20}Ne(t,α)^{19}F	6(0.83)	0(0)
^{19}F(p,d)^{18}F	11(0.55)	8(0.03)
^{19}F(d,^{3}He)^{18}O	3(1.23)	0(0)
^{20}Ne(^{3}He,α)^{19}Ne	6(0.89)	0(0)
^{18}O(d,n)^{19}F	3(0.29)	5(0.043)
^{19}F(^{3}He,d)^{20}Ne	2(0.36)	3(0.02)

[1] G. Lévai, J. Cseh, P. Van Isacker, Eur. Phys. J. A **12** (2001) 305.

[2] G. Lévai, AIP Conf. Proc. **802** (2005) 65.

[3] G. Lévai, J. Cseh, P. Van Isacker, in preparation.

2.22 Dynamical versus kinematical symmetry breaking is revisited

J. Cseh and G. Tímár

Quantum algebras are deformed versions of the classical Lie-algebras, therefore, the symmetries based on them are more general, than those appearing in Lie-algebraic models. One of the interesting questions one can address is: if the quantum deformation of the algebraic structure (in other words: the kinematical breaking of the symmetry) can bridge the gap between the dynamical symmetries of the algebraic models. These symmetries, described by a nested chain of Lie-subalgebras, show up as analytically solvable limits of the models, and correspond to well-defined physical situations, e.g. the rotational or vibrational behaviour of a many-body system. The regions in between the dynamical symmetries, however, need numerical treatment in the usual approach. On the other hand quantum algebraic descriptions provide us with analytical solutions even if we move away from the classical Lie-algebraic symmetry. The question is: how far one can go in this way along the path to the other classical limit.

Recently we have reinvestigated [1] the question of the kinematical versus dynamical symmetry-breaking within the framework of the two-dimensional interacting boson model of $SU(3)$ group-structure [2]. This model seems to be very well-suited for this kind of study, since it is simple enough, yet it is not trivial: it contains two dynamical symmetries, corresponding to the rotational (SO(3)) and vibrational (SU(2)) limits.

The novel features of the present work in comparison with the previous ones are as follows. i) Here we measure quantitatively the similarity of the quantum-deformed spectrum to those of the corresponding classical Lie-algebraic dynamical symmetries. The conclusions so far were based on qualitative comparisons between the spectra. ii) We perform a systematic search in fitting the kinematically broken spectrum to the ones with exact dynamical symmetries. iii) We investigate the problem from both sides, i.e. trying to reach the classical rotational spectrum with the quantum-deformed vibrational one, and vice versa, based on more recent works [3]. (At the time of the earlier works, only the deformation of the vibrational $SU(2)$ was known.) As for the deformation parameter, we take real numbers, or pure phase values, for which the generalised algebraic model has real physical quantities.

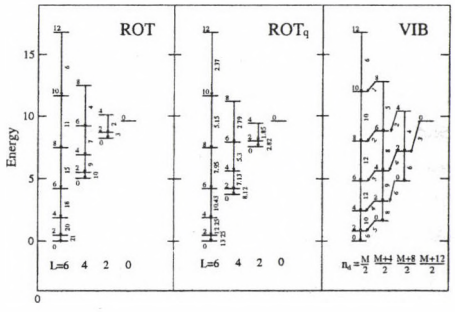

Figure 1. Classical rotational (left side) and vibrational (right side) spectrum of the two-dimensional IBA model. The central part shows the best approximation (phase-deformed rotational spectrum) which can be reached by performing algebraic deformation of one classical limit towards the other one.

It turned out that quantum-deformed dynamical symmetries can not take the system from one classical limit to the other, on the contrary, they can cover only a tiny part of the gap between them. Only the phase-deformed rotational limit could govern the system towards the other classical limit, but its similarity is only slightly better (14.7 %), than that of the two classical limits.

This work was supported by the OTKA (Grant No. T37502).

[1] J. Cseh, G. Tímár, in preparation.

[2] D. Bhaumik, S. Sen, and B. Dutta–Roy, Am. J. Phys. **59** (1991) 719.

[3] D. Bonatsos, C. Daskaloyannis, Progr. Part. Nucl. Phys. **43** (1999) 537; and references therein.

2.23 From Finite Nuclei to the Nuclear Liquid Drop: Leptodermous Expansion Based on the Self-consistent Theory

P.-G. Reinhard[a,b], *M. Bender*[c,d] *W. Nazarewicz*[e,f,g] *T. Vertse*

In the work to be published soon [1], we extract the macroscopic liquid drop model (LDM) parameters by using a large sample of finite, spherical nuclei, including huge systems having 10^5-10^6 nucleons. Based on the self-consistent SHF and RMF results, we extract the macroscopic information from the large scale trends by subtracting fluctuating shell corrections. The parameters of the nuclear LDM, such as the volume, surface, symmetry, and curvature constants, as well as bulk radii, are extracted from the non-relativistic and relativistic energy density functionals used in microscopic calculations for finite nuclei. The microscopic liquid drop energy, obtained self-consistently for a large sample of finite, spherical nuclei, has been expanded in terms of powers of $A^{-1/3}$ (or inverse nuclear radius) and the isospin excess (or neutron-to-proton asymmetry). In order to perform a reliable extrapolation in the inverse radius, the calculations have been carried out for nuclei with huge numbers of nucleons, of the order of 10^6. The Coulomb interaction has been ignored to be able to approach nuclei of arbitrary sizes and to avoid radial instabilities characteristic of systems with very large atomic numbers. The main contribution to the fluctuating part of the binding energy has been removed using the Strutyinsky's shell correction with generalized plateau condition [2] and applying the Green's function method specified in ref.[3,4]. The leptodermous expansion however, has certain limitations for finite nuclei. While the leading terms in the macroscopic energy expansion can be extracted very precisely, the higher-order, isospin-dependent terms are prone to large uncertainties due to finite-size effects.

Acknowledgements This work was supported in part by the Hungarian OTKA T037991, T046791, by the U. S. National Nuclear Security Administration under the Stewardship Science Academic Alliances program through the U.S. Department of Energy Research Grant DE-FG03-03NA00083; by the U.S. Department of Energy under Contracts Nos. DE-FG02-96ER40963 (UT), DE-AC05-00OR22725 with UT-Battelle, LLC (ORNL), DE-FG05-87ER40361 (JIHIR), DE-FG02-00ER41132 (Institute for Nuclear Theory), W-31-109-ENG-38 (ANL), by the NSF Grant No PHY-0456903, by the Bundesministerium für Bildung und Forschung (BMBF), Project Nos. 06 ER 808 and 06 ER 124.

a) Institut für Theoretische Physik II, Universität Erlangen–Nürnberg, Staudtstrasse 7, D–91058 Erlangen, Germany

b) Joint Institute for Heavy Ion Research, Oak Ridge National Laboratory, P. O. Box 2008, Oak Ridge, Tennessee 37831, U.S.A.

c) Institute for Nuclear Theory, University of Washington, Box 351550, Seattle, WA 98195-1550, U.S.A.

d) Physics Division, Argonne National Laboratory, 9700 S. Cass Avenue, Argonne, IL 60439, U.S.A.

d) Department of Physics and Astronomy, The University of Tennessee, Knoxville, Tennessee 37996, U.S.A.

e) Physics Division, Oak Ridge National Laboratory, P. O. Box 2008, Oak Ridge, Tennessee 37831, U.S.A.

f) Institute of Theoretical Physics, Warsaw University, ul. Hoża 69, PL-00681, Warsaw, Poland

[1] P.-G. Reinhard, M. Bender, W. Nazarewicz, T. Vertse, Phys. Rev C in press

[2] T. Vertse, A.T. Kruppa, R.J. Liotta, W. Nazarewicz, N. Sandulescu, T.R. Werner, Phys. Rev. C 57 (1998) 3089.

[3] T. Vertse, A.T. Kruppa, W. Nazarewicz , Phys. Rev. C 61 (2000) 064317.

[4] A.T. Kruppa, M. Bender, W. Nazarewicz, P.-G. Reinhard, T. Vertse, S. Cwiok, Phys. Rev. C 61 (2000) 034313.

3.1 Plasmon excitation in amorphous silicon by electron impact: dependence of the surface and bulk plasmon yield on the angle of incidence

T. Ricsóka, S. Ricz, Á. Kövér, J. Gervasoni[a] *and D. Varga*

A new double pass and second order focusing electron spectrometer (called ESA-22D) was designed and built in the Institute of Nuclear Research of the Hungarian Academy of Sciences to study the energy and angular distribution of electrons ejected in different processes from solids.

This electron analyzer is similar to our earlier electron spectrometer (ESA-22L), which is used in Lund, Sweden in cooperation with Electron-spectroscopy Group of Department of Physical Sciences (Oulu, Finland) [1]. The spectrometer consists of a combination of a spherical and a cylindrical mirror analyzer. The spherical mirror focuses the electrons from the scattering plane to the entrance slit of the cylindrical analyzer performing the energy analysis of the electrons. A spherical deceleration lens is placed around the source region to improve the energy resolution of the system. The residual magnetic field is reduced less than 5 mG in the scattering plane and in the analyzer. Furthermore, the outer sphere and cylinder are cut in two parts resulting two spectrometers. This concept enables us to analyze two independent angularly resolved electron spectra in different energy regions, simultaneously.

Silicon is a standard sample in plasmon investigations [2]. In the present work, the incident angle dependence of the surface and bulk plasmon excitations was measured in amorphous silicon by electron impact at 2000 eV electron energy and at 45° and 89° (glancing angle) incident angles relative to the surface normal. The scattered electrons were detected with a position sensitive detector (PSD) between -90° and 90° relative to the surface normal.

Figure 1 shows the scattered electron spectra in silicon at 45° and 89° (glancing angle) incident angles. The measured intensity was integrated between -90° and 90° relative to the surface normal. At 45° incident angle the peak of the surface plasmon can be seen as a shoulder on the bulk peak while at glancing angle the bulk and surface plasmon peak can be separated well.

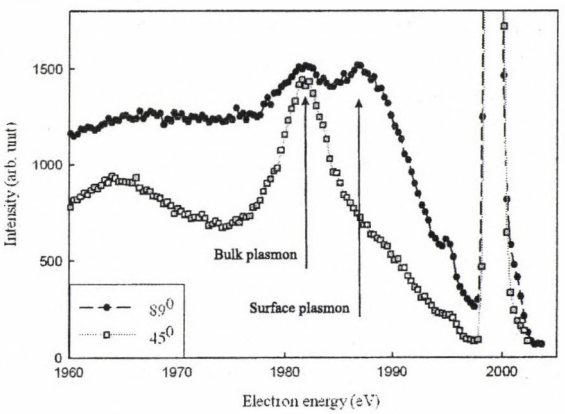

Figure 1. Elastic and inelastic scattered spectra of Si surface.

Acknowledgements

This work was supported by the Hungarian Scientific Research Foundation (OTKA Grant No. T037203) and by the Hungarian-Argentinean Intergovernmental S and T Cooperation Programme of the Research and Technology Innovation Fund (KTIA) and SECyT (Grant No. ARG-13/04).

a) Instituto Balseiro, Centro Atómico Bariloche, 8000 S. C. Bariloche, Argentina

[1] S. Ricz, Á. Kövér, M. Jurvansuu, D. Varga, J. Molnár, and S. Aksela, Phys. Rev. A **65** (2002) 042707 .

[2] L. Kövér, S. Egri, I. Csernyi, Z. Berényi, J. Tóth, J. Végh, D. Varga and W. Drube, Journal of Surface Analysis (Japan) Vol. **12** No. 2 (2005) in press.

3.2 Fragmentation of H_2O and CH_4 molecules following 800 keV He^+ impact

B. Sulik, T. Ricsóka, Z. Juhász, F. Gáll and N. Stolterfoht[a)]

Fragmentation mechanisms of H_2O and CH_4 molecules are important for understanding direct and indirect radiation damages in biological tissues [1].

The energy distributions of fragments produced in 800 keV $He^+ + H_2O$, and $He^+ + CH_4$ collisions have been measured at the beamline of a Van de Graaff electrostatic accelerator in ATOMKI, Debrecen. An electrostatic analyzer, ESA-21 has been utilized for taking the ion spectra simultaneously at 13 different observation angles. The data compare well to those measured earlier for He^{2+} and $Ne^{q+} + H_2O$ collisions at much lower projectile energies in HMI, Berlin [1,2].

In the present work, we study only the low recoil-ion energy group, which extends up to 50 eV, and corresponds to Coulomb explosion (CE) of the ionized target. The ionization mechanisms are direct ionization and excitation for the present ATOMKI data, while it was mainly electron capture for the earlier HMI data [1,2].

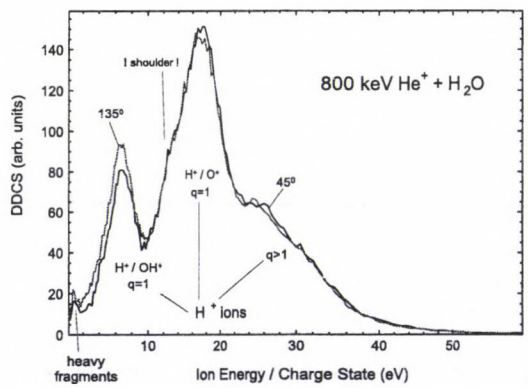

Figure 1. Energy spectra of the ion-fragments O^{q+}, OH^{q+} and H^+ in 800 keV $He^+ + H_2O$ collisions at 45° and 135° observation angles. The supposed charge state of the heaviest fragment is denoted by q.

Coulomb explosion is a common mechanism for fragmentation in both fast and slow ion impact. Accordingly, in the case of water target, the structure of the spectra of fragments are similar, the characteristic energies for the fragments are the same for the HMI [1,2] and the ATOMKI data.

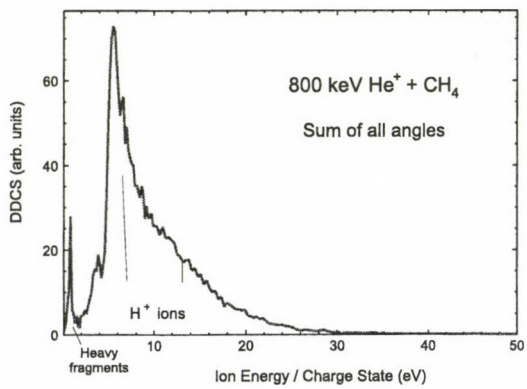

Figure 2. Energy spectra of the heavy and H^+ ion-fragments in 800 keV $He^+ + CH_4$ collisions, after summation of the spectra over all the observation angles.

The spectrum of ion fragments from CH_4 is different from that of water, especially for the relative yields belonging to low energy dissociation channels. Further measurement and interpretation are in progress.

Acknowledgements

This work was supported by Hungarian OTKA Grant (T046905) and the COST P9 Action (Radiation Damages In Biomolecular Systems).

a) Hahn-Meitner Institute Berlin, Glienickerstr. 100, D-14109 Berlin, Germany

[1] Z.D. Pešić, J.-Y. Chesnel, R. Hellhammer, B. Sulik and N. Stolterfoht, J. Phys. **37** (2004) 1405.

[2] P. Sobocinski, Z.D. Pešić, R. Hellhammer, N. Stolterfoht, J.-Y. Chesnel, S. Legendre and B. Sulik, Nucl. Instr. Meth. B **233** (2005) 207.

3.3 Cusp formation in classical trajectory Monte Carlo calculations of single atomic ionization by the impact of neutral projectiles

L. Sarkadi, P. Macri [a] *and R.O. Barrachina* [b]

The velocity distribution of electrons emitted in atomic collisions often exhibits a peak centered at the velocity $\mathbf{v}_P$ of the incident projectile [1]. Classical trajectory Monte Carlo (CTMC) simulations provide an excellent description of this structure whenever the interaction between the electron and the outgoing projectile is of a Coulomb [2] or even of a dipolar type [3,4]. However, serious doubts were recently cast over the general validity of any classical approach for the description of more general atom-atom ionization collisions [5]. These questionings are due to the visualization of the cusp as the result of a smooth continuation across the ionization limit of *capture* into highly excited electron-projectile bound states [6,7]. By mimicking a bound spectrum accumulating at zero energy by a continuum, any classical description would succeed in describing the "electron capture to the continuum" divergence observed whenever the electron-projectile interaction is of Coulomb or dipolar nature. But, whenever the electron-projectile interaction decreases faster than a dipole potential at large distances, the energy spectrum does not accumulate at zero energy, and any classical description should be doomed to failure. Our purpose in this communication is to elucidate, through CTMC calculations [8], this limitation of the classical description of cusp formation. To this end we consider the ECC peak formed in He-Ar ionization collisions for the case of neutral He outgoing projectiles in the 2^1S metastable state, as first measured by the Debrecen group in 1989 [9]. Both the experimental data and the quantum-mechanical calculations show a cusp that is much sharper than the one produced by He^{2+} projectiles [10]. This phenomenon was attributed to a low-lying virtual state on the electron-projectile system [11], an effect that no classical description can reproduce. Actually, as it is shown in the figure, the CTMC calculation produces a peak that is much broader and smaller than for a Coulomb interaction, a result that testifies against any supposedly classical origin of the ECC phenomenon.

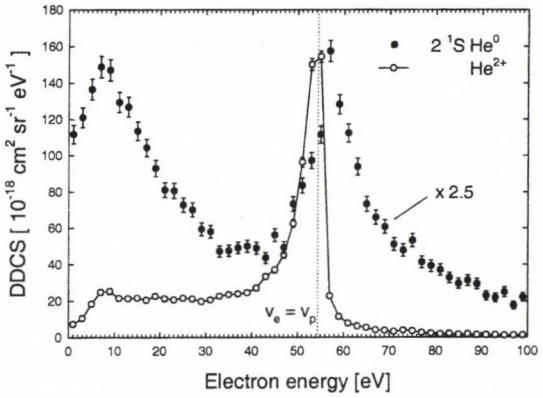

Figure 1. CTMC calculation of the double differential cross section (DDCS) in the forward direction for 2^1S He^0 outgoing projectiles, in a 400 keV He+Ar collision. The result for a He^{2+} projectile is also shown for comparison. The acceptance angle is 1°. These results were obtained by integrating 0.36×10^9 trajectories.

a) Instituto de Astronomía y Física del Espacio, CC. 67, Suc. 28, 1428 Buenos Aires, Argentina

b) Centro Atómico Bariloche and Instituto Balseiro, 8400 Bariloche, Argentina

[1] C. B. Croooks and M. E. Rudd, Phys. Rev. Lett. 25 (1970) 1599.

[2] C. O. Reinhold and R. E. Olson, Phys. Rev. A 39 (1989) 3861.

[3] K. Tőkési et al., J. Phys. B 30 (1997) L123.

[4] L. Sarkadi et al., J. Phys. B 33 (2000) 847.

[5] R. O. Barrachina and C. Courbin, J. Phys. 35 (2002) 3157.

[6] J. Macek, Phys. Rev. A 1 (1970) 235.

[7] M. E. Rudd and J. Macek, Case Studies in Atomic Physics 3 (1972) 48.

[8] L. Sarkadi and R. O. Barrachina, Phys. Rev. A 71 (2005) 062712.

[9] L. Sarkadi et al., Phys. Rev. Lett. 62 (1989) 527.

[10] A. Báder et al., Phys. Rev. A 55 (1997) R14.

[11] R. O. Barrachina, J. Phys. B 23 (1990) 2321.

3.4 A time-of-flight electron spectrometer for the study of the electron correlation in atomic collisions

L. Sarkadi and A. Orbán

Recently we have tested and improved our new time-of-flight (TOF) electron spectrometer [1,2]. The spectrometer was designed to study the electron correlation in low energy double continuum states of atoms. These experiments regarding the measurements of very low energy electron (typically lower than 100 meV) are based on projectile electron spectroscopy at 0° relative to the incoming projectile direction. We are going to carry out experiments obeyed to triple coincidence conditions: Detecting the two ejected electrons in coincidence with the charge state analyzed scattered projectile.

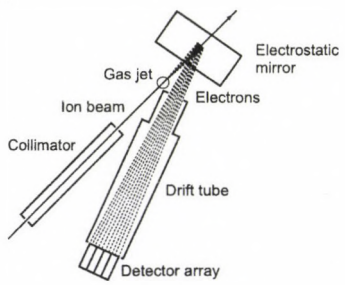

Figure 1. Scheme of the TOF spectrometer.

For a good detection efficiency of the event in triple-coincidence measurements we increased the transmission of the spectrometer. In time-of-flight measurements usually the particles (in our case the electrons) traverse a field free region, the so-called drift region before they reach the detector. At the beginning of the test measurements with double coincidence condition the number of the background events were too high. In order to reduce the background, created mostly by the secondary electrons from the collimator, we closed the entrance part of our detectors, using a tube in the drift region between the electrostatic mirror and detectors (see Fig. 1). This so-called drift tube reduced the background with order of magnitudes. Besides this effect the tube also reduces the effect of stray fields on the electrons reflected by the mirror. Since we measure low energy electrons (several eV in the laboratory frame), those ones whose transversal velocity component is higher than a given value, will never reach the detector located at relative large distance. In order to collect a part of those electrons we may apply week electrostatic and magnetic fields within the drift tube to 'direct' them to the detector. The test measurements have been done at the 1.5 MeV Van de Graaff generator of ATOMKI. The studied phenomena in these measurements was the already well understood cusp problem (e.g. [3]). Performing double coincidence measurements in C^{q+} $(q = 0, 1, 2)$ on Ar collisions we made the energy calibration of the spectrometer, based on SIMION calculations and the measured positions of the cusp peak and Auger-lines in the time spectra. In Fig. 2 the cusp peaks are seen resulted from different mechanisms: Electron loss to the continuum (ELC), electron capture to the continuum (ECC) and transfer ionisation (TI). These results are in good accordance with previous knowledge. The relative energy resolution for the studied 5-20 eV energy region is between 6% and 10.5%.

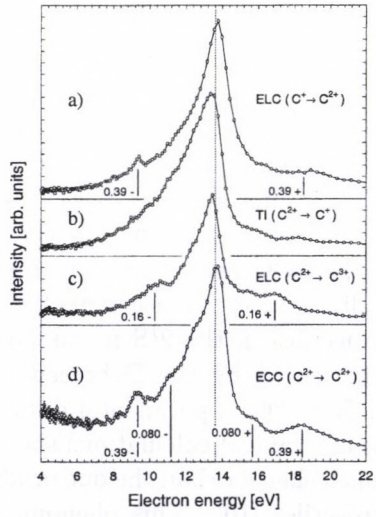

Figure 2. Measured electron energy spectra at 0°.

[1] L. Sarkadi, A. Orbán, Atomki Ann. Rep. (2005) 85.

[2] L. Sarkadi, A. Orbán, Meas. Sci. Tech. 17 (2006) 84.

[3] L. Víkor *et al.*, Nucl. Instr. Meth. B107 (1996) 79.

3.5 Energy-Sharing Asymmetries in Ionization by Positron Impact

C. Arcidiacono[a], Á. Kövér and G. Laricchia[a]

The problem of few-body dynamics in ionization by charged projectiles is particularly challenging in scattering theory. The main difficulty is represented by the high correlation and interference among particles. Such effects can be probed with great sensitivity through differential studies. A special kind of ionization is electron-capture, where the ejected electron is captured by the projectile to a bound or low-lying continuum state. This latter process is often referred to as electron capture to the continuum (ECC) and was first observed for positron impact by Kövér and Laricchia [1]. The signature of this process is a cusp-like peak feature in the electron spectrum at an energy corresponding to half of the residual kinetic energy ($E_r/2$ where $E_r = E_i - I$, I is the ionization energy of the target and E_i is the positron kinetic energy). The peak arises from the post-collision Coulomb attraction between the scattering positrons and the ionized electrons in the final state. In fact, due to the identical mass of the particles, the projectile transfers nearly one half of its kinetic energy to accelerate the outgoing electron to the same velocity.

In our previous work [2], the triply-differential cross-section (TDCS) has been determined for positrons at an incident energy of 50 eV for collision with a H_2 target. On contrasting the experimental and theoretical results [3], an energy shift of 1.6eV between the two distributions was observed but not understood. Among the possible causes of this energy shift the authors cited a systematic experimental error (e.g. energy miscalibration of the PPA, contact potential effects, etc.) or a physical effect (e.g. vibrational excitation or molecular disintegration of the target). If ECC resulted in dissociation of the remnant ion, the energy of the cusp peak would be decreased by around $E_d/2$ where $E_d = 2.65eV$ is the dissociation energy of H_2^+.

In our recent study [4], (i) we resolve the main uncertainties of the work mentioned above, by calibrating the absolute energy through the identification of the threshold for positronium formation and by checking the remnant Hydrogen ion for possible dissociation; (ii) we determine, for the first time, the energy spectrum of the positrons scattered from molecular Hydrogen and (iii) we measure, also for the first time, the energies of electrons ejected by positron impact ionisation of Helium at the same excess energy as in the molecular Hydrogen study.

An unexpected asymmetry in the energy sharing between the two light particles in the final state has been observed around half-of-the residual energy, with the electron (positron) spectrum being shifted to lower (higher) energies than predicted by perturbative calculations. At present, the data have no consistent description by quantum-mechanical theoretical treatments and, in this respect, might be a suitable testing ground for recently developed ab-initio approaches.

Acknowledgements

This work is kindly supported by the Engineering and Physical Science Research Council UK (grant No GR/S16041/01), the Royal Society East European project, the Hungarian Scientific Research Found (OTKA No. T037203) and the European Union (HPRN-CT-2002-00179 EPIC).

(a) Department of Physics and Astronomy, University College London, Gower Street, London, WC1E 6BT, UK

[1] Á. Kövér and G. Laricchia, Phys. Rev. Lett. **80** (1998) 5309.

[2] Á. Kövér, K. Paludan and G. Laricchia, J. Phys. B **34** (2001) L219.

[3] J. Fiol, V. D. Rodríguez and R. O. Barrachina, J. Phys. B **34** (2001) 933.

[4] C. Arcidiacono, Á. Kövér and G. Laricchia, Phys. Rev. Lett. **95** (2005) 223202.

3.6 Quality Assurance Challenges in X-ray Emission Based Analyses

T. Papp

There is a large scatter in the results of X-ray analysis with solid-state detectors suggesting methodological origin. Although the PIXE (proton induced X-ray emission) analytical technique can work without relation to any physics, as was commented at the recent PIXE conference, one could argue that if the same technique is used for measuring physical quantities reveals problems, then perhaps potential methodological issues can not apriory be excluded. We present a simple example which could be interpreted as indications for methodological considerations.

Recently an inter-comparison was made of analysis of the spectra measured at the laboratory of the International Atomic Energy Agency (IAEA). Four participating analytical software packages were used to evaluate the X-ray spectra [1]. There are several thin metal samples spectra, for which common energy scale could not be established. The quality of the spectrum can be judged from the line shape. The line shape is parametrized by the full widths at half maximum (FWHM) of a peak and the so-called low energy tailing.

Fitting the spectra individually we obtained FWHM squared values at different energies and determined the linear regression parameters. The parameters suggest a rather poor detector performance. It is generally assumed that the $(\mathrm{FWHM})^2$ values have a first order polynomial form as a function of X-ray energy. Having done a linear regression analysis, we can plot the standard residual, presented in Fig. 1, which clearly shows a three-sigma deviation. The probability to having a three-sigma deviation is 1%. In other words, the probability that these spectra are in accordance with the expected FWHM functional form is less than 1%.

The main problem is that, although the composite spectra were analyzed using four different programs, the difficulty in interpreting the spectra was not commented upon by any of the participants in the inter-comparison.

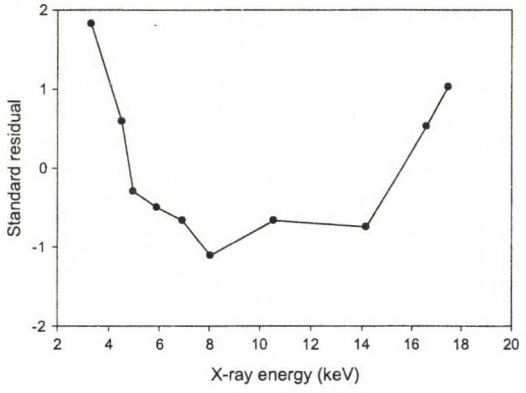

Figure 1. The FWHM^2 is expected to be a linear function of the energy in the field of analytical applications, but the standard residual clearly indicates that it was not fulfilled. Would this affect the relative line intensities across the spectral energy range? The inter-comparison data from IAEA was used to demonstrate that there are quality control challenges.

[1] Intercomparison of PIXE spectrometry software packages, IAEA-TECDOC-1342, February, 2003; M. Blaauw, J.L. Campbell, S. Fazinic, M. Jaksic, I. Orlic and P. Van Espen, Nucl. Inst. Meth. B, 2002, 189, 113.

3.7 On the accuracy of L subshell ionization cross sections: II. Coster-Kronig transition probabilities

T. Papp

Recently the experimental data on the fluorescence yields and Coster-Kronig probabilities were reviewed and recommended values were adopted [1]. Since they are widely used in nuclear and atomic physics, beside their vital importance in x-ray based analytical methods, it is perhaps justifiable to check the internal consistency of the data.

The L1 subshell fluorescence yield ($\omega 1$) is the ratio of X-ray rate (X) to the total decay rate. The total decay rate is the sum of radiate (X) and non radiate yields. The non radiate yields can be separated to Coster-Kronig rates (f12+f13) and the non Coster-Kronig Auger rates (A). The f12 and f13 rates are the L1 to L2 and L1 to L3 Coster-Kronig transition rates. Therefore $\omega 1$ can be expressed as $\omega 1$=X/(X+A+f12+f13). For the Z>70 atomic number range probably the sum of f12 and f13 is above 50%, and can reach 80% therefore, it can be considered as the dominant process. At certain Z numbers around Z=75 the L1-L3M5 Coster-Kronig transitions become energetically allowed, and the probability will have a jump to a higher value from about 50% to 70%. A second jump when the L1-L3M4 Coster-Kronig transitions become energetically allowed is expected around Z=78. Since X and A do not have jumps, and are rather smooth functions of Z, therefore when f13 jumps upwards, we would expect a drop in the $\omega 1$ value.

The data from [1] is plotted in fig. 1. The theoretical Dirac Hartree Slater values represented by symbols filled with black, while the experimental values from [1] are presented with symbols filled with white. The f12+f13 values are denoted by circle, while the omega1 values with squares. The theoretical values pass the simple expectations. When the DHS (f12+f13) jumps at Z=75 omega1 drops. If we increase the denominator, the ratio should decrease. Similarly at Z=78, the upward jump in the denominator, coincides with the drop in the ratio. The experimental data do not follow such a trend, and remained to be explained.

It should be noted, that the experimental data is from a very extensive review, therefore could be considered as the experimental data either need to be explained or had to be accepted that there is a methodological problem.

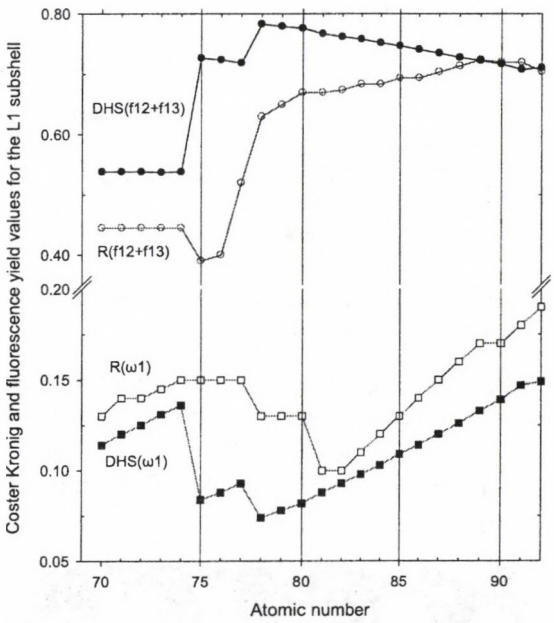

Figure 1. Comparison of the experimental and theoretical L1 subshell fluorescence yield and Coster-Kronig transition probabilities. The experimental data is inconsistent in an extent of more than 100%.

[1] J.L. Campbell, Fluorescence yields and Coster-Kronig probabilities for the atomic L subshell Atomic Data and Nuclear Data Tables 85 (2003) 291-315

3.8 Transmission of highly charged ions through Al_2O_3 capillaries

Z. Juhász, Gy. Víkor, S. Biri, É. Fekete, I. Iván, F. Gáll, K. Tőkési, S. Mátéfi-Tempfli[a)], M. Mátéfi-Tempfli[a)], N. Stolterfoht[b)], E. Takács[c)], J. Pálinkás[c)], B. Sulik

Nanocapillaries are frequently used tools to investigate ion - surface interactions. Insulating nanocapillaries have been studied recently and an interesting phenomenon has been discovered: slow ions are guided within the capillaries without close contacts with the capillary walls [1].

In 2005, first experiments with nanocapillaries have been performed at ATOMKI, Debrecen. We set up our experimental apparatus at the ECR ion source, which provided the slow, highly charged ions.

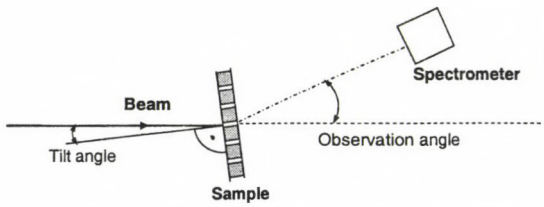

Figure 1. Experimental setup with the definition of the tilt and observation angles.

Parallel plate electrostatic analyzers have been used for selecting the transmitted ions according to their charge state. The Al_2O_3 capillaries were produced at Université Catholique de Louvain, Belgium [2].

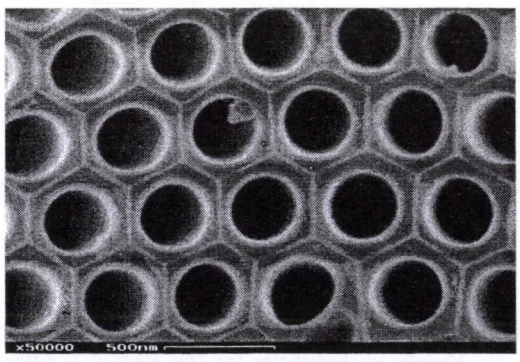

Figure 2. SEM view of an array of Al_2O_3 capillaries.

The capillaries are hexagonally ordered in a thin membrane of 15 μm thickness. The top and bottom sides are covered by conductive niobium layers in order to ensure ground potential on the surfaces of the membrane.

We have measured the angular distribution of the ions passing through the capillaries with different target tilt angles. So far we have used Al_2O_3 capillaries with diameters of 150 and 290 nm as target and Ne^{6+} ions with energies of 3 and 6 keV as projectile. The measurements were started after a few tens of minutes charge up time, when an equilibrium state developed and constant fraction of the incident ions were transmitted.

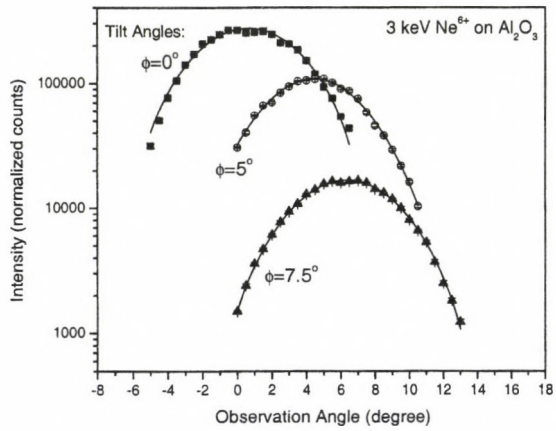

Figure 3. Angular distribution of the observed Ne^{6+} ions after passing through the capillary sample with pore diameters of 290 nm at tilt angles of 0°, 5° and 7.5°. The solid lines represent Gaussian fits to the data, with an almost common FWHM of ~5.5°.

The observed angular distributions are relatively broad (4-6° FWHM) and nearly independent of the tilt angle of the target, similarly to the previous observations for the case of polymer foils [1]. There is a measurable intensity even for as large tilt angle as 7.5°, and the intensities maximize around the capillary axis for all cases. More than 95% of the transmitted ions remain in their original charge state. These facts clearly demonstrate the guiding ability of the Al_2O_3 capillaries. In the future we intend to perform experiments

with different kinds of ions and target materials. We are going to use a position sensitive detector to observe the time dependency of the two-dimensional angular distributions for getting a better view of the guiding process.

Acknowledgements

This work was supported by the Hungarian National Science Foundation OTKA (Grant No's: T046905, T046454, T042729 and PD050000), and in part by the Belgian Science Policy through the Interuniversity Attraction Pole Program IAP (P5/1/1).

a) Unité de Physico-Chimie et de Physique des Matériaux, Université Catholique de Louvain, Place Croix du Sud, 1, 1348-Louvain-la-Neuve, Belgium

b) Hahn-Meitner Institute Berlin, Glienickerstr. 100, D-14109 Berlin, Germany

c) Department of Experimental Physics, University of Debrecen, Egyetem tér 1, H-4032 Debrecen, Hungary

[1] N. Stolterfoht, J.-H. Bremer, V. Hoffmann, R. Hellhammer, D. Fink, A. Petrov and B. Sulik, Phys. Rev. Lett. **88** (2002) 133201-1.

[2] S. Mátéfi-Tempfli et. al. to be published (2006)

3.9 Simulation of ion guiding through nanocapillaries

Z. Juhász, K. Tőkési, B. Sulik

The ion guiding capability of nanocapillaries etched in polymer foils has recently been discovered [1]. According to our recent knowledge, the guiding effect may be a result of charge deposition on the capillary walls. The accumulated charges on the inner surfaces of the capillary repel the latter arriving ions, thereby close collisions with the walls can be avoided. Theoretical description of these processes is difficult and the existing models fail to reproduce all experimental observations [2]. To understand the phenomenon better, a microscopic model was developed.

In our model the individual local events of charge deposition and migration are traced. The electric potential of the deposited charges is numerically calculated. The calculation is performed for a single capillary, but the effects of the other capillaries in the foil are included by setting up periodic boundary conditions in the x, y directions. In this way the simulation describes the case, where all the capillaries charge up in the same manner. The ion trajectories in the electric filed are calculated numerically. When an ion trajectory crosses the capillary surface the trajectory calculation is stopped. Than the charge of the ion is deposited at the surface. The potential of the corresponding charge is calculated and added to the previous potential. Until the next ion is coming (roughly a few tenth of second) the charges are migrating, which is driven by the electric field. If a charge reaches the conductive layers, it is neutralized instantly. As an example, Fig. 1 shows typical trajectories for 3 keV Ne^{7+} ions passing through a polyethylene terephthalate nanocapillary with a diameter of 100 nm and length of 6.5 μm. Both sides of the capillary are covered by conductive layers.

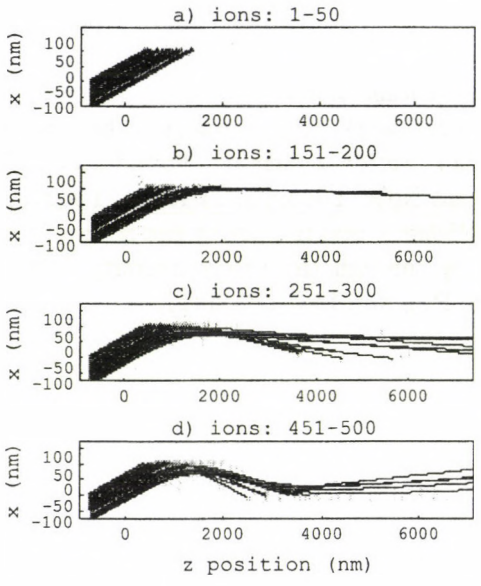

Figure 1. Simulated trajectories of 3 keV Ne^{7+} ions in a polyethylene terephthalate capillary. The numbers of entering ions into the capillary are indicated on the top of each figure. The incidence angle is 5°. a) The first ions reach the capillary surface with almost straight-line trajectories. b) The deposited charges start to deflect the incoming ions. Some of them can escape from the capillary. c) Guiding is developed, meanwhile a second patch of charges is deposited on the opposite side due to the ions that suffered very large angular deflection. d) The second patch is also contributing to the guiding.

Acknowledgements

This work was supported by the Hungarian National Science Foundation, OTKA (Grants: PD050000 and T046905).

[1] N. Stolterfoht, J.-H. Bremer, V. Hoffmann, R. Hellhammer, D. Fink, A. Petrov and B. Sulik, Phys. Rev. Lett. **88** (2002) 133201-1.

[2] K. Schiessl, W. Palfinger, C. Lemmel, J. Burgdörfer, Nucl. Instr. Meth. B **232** (2005) 228.

3.10 Simulation of guiding of multiply charged projectiles through insulating capillaries

K. Schiessl[a)], W. Palfinger[a)], K. Tőkési, H. Nowotny[a)], C. Lemell[a)], J. Burgdörfer[a)]

Recent experiments have demonstrated that highly charged ions can be guided through insulating nanocapillaries along the direction of the capillary axis for a surprisingly wide range of injection angles [1]. Even more surprisingly, the transmitted particles remain predominantly in their initial charge state, thus opening the pathway to the construction of ion-optical elements without electric feedthroughs.

We develop a classical trajectory transport theory that relates the microscopic charge-up with macroscopic material properties. We present a simulation for ion guiding through insulating nanocapillaries within the framework of a mean field classical transport theory [2]. We combine a microscopic trajectory simulation with macroscopic material properties for bulk and surface conductivities of highly insulating materials (PET, Mylar). Projectiles hitting the inner wall of the insulating material in the early stage of the irradiation deposit their charge on the capillary surface. These charges diffuse along the surface and, eventually, into the bulk due to the small but finite surface and bulk conductivities of the insulator. Projectiles entering the capillary at a later stage are deflected by the Coulomb field of a self-organized charge patch close to the entrance of the capillary. Invoking this scenario we are able to reproduce a range of experimental findings, e.g., ion guiding even for large incidence angles, the temporal decrease of transmission during beam-off times, and, in part, a relatively large angular spread of the transmitted beam. We have shown that these results can be interpreted on the basis of a linear model including transport of deposited charges along the surface without resorting to freely adjustable parameters. The present simulation treats only the case of ideal cylindrically shaped and well aligned capillaries with fixed diameter. Variations of surface structure, surface roughness, clustering of capillaries, capillary alignment, and capillary diameter within the target foil resulting from target preparation are not yet included in our simulation. Future investigations should therefore address the dependence on material properties. In particular, measurements for other insulating materials (SiO_2, Al_2O_3) should provide for benchmark data and critical tests for the theoretical framework presented here as for these materials the target properties such as capillary diameter, ordering and alignment of capillaries, and possibly also surface roughness can be controlled much more accurately.

Acknowledgements

The work was supported by the Austrian Fonds zur Förderung der wissenschaftlichen Forschung under proj. nos. FWF-SFB016 "ADLIS" and P17449-N02, the Hungarian Scientific Research Found: OTKA Nos. T046095, T046454, the grant "Bólyai" from the Hungarian Academy of Sciences, the TéT Grant No. A-15/04, by the EU under contract No. HPRI-CT-2001-50036 and by the Donostia International Physics Center (DIPC).

a) Inst. f. Theoretical Physics, Vienna University of Technology, Wiedner Hauptstr. 8-10, A–1040 Vienna, Austria

[1] N. Stolterfoht, J.-H. Bremer, V. Hoffmann, R. Hellhammer, D. Fink, A. Petrov, and B. Sulik, Phys. Rev. Lett. 88, (2002) 133201-1-4.

[2] K. Schiessl, W. Palfinger, K. Tőkési, H. Nowotny, C. Lemell, and J. Burgdörfer, PRA 72 (2005) 062902

3.11 Resonances in atomic few-body systems

J.Zs. Mezei and A.T. Kruppa

The variational method using a correlated Gaussian basis (SVM, see [1]) has proved to be an excellent method in calculating the characteristics of bound-states. Its trial and error procedures are very powerful to select an optimal basis, while the simple form of the trial function simplifies the calculations, because most of the matrix elements have analytic form.

Combining the SVM with the complex rotational technique we are able to determine auto-ionizing states of Coulombic systems with three or more charged particles. Performing the complex rotation of the coordinates ($r \rightarrow re^{i\theta}$) the complex scaled Hamiltonian of a Coulombic system – only Coulomb interactions act between the particles – is a simple function of the rotational angle $H(\theta) = Te^{-2i\theta} + Ve^{-i\theta}$, where T, V are the kinetic and the potential energies of the system. In order to find the complex eigen energies of the rotated Hamiltonian, we have to solve the equation $\det|e^{-i2\theta}T_{i,j} + e^{-i\theta}V_{ij} - E\Delta_{ij}| = 0$, where T_{ij} and $V_{i,j}$ are the matrix elements of the original kinetic energy operator and the potential energy operator, while Δ_{ij} are the overlap integrals of the basis elements.

The SVM optimizes the non-linear parameters of the basis in a very specific way in order to get the best ground state energy. In the calculation of the excited auto-ionizing states we used the same set of parameters as for the ground state, because there are no simple recipes to optimize the parameters of a basis in a resonance state calculation. We have found that with the same set of non-linear parameters as for the ground state, we are able to describe all resonances of the $Ps^- = (e^+ + e^- + e^-)$ system calculated by Ho [2].

Table 1. The results of present method are compared with the results of Ho [2] for a few resonances of Ps^- system.

$E_r^{SVM} - i\Gamma/2$ (a.u.)	$E_r^{Ho} - i\Gamma/2$ (a.u.)
$-0.0760304 - i2.153410^{-5}$	$-0.0760305 - i2.1510^{-5}$
$-0.0636496 - i4.810^{-6}$	$-0.0636 - i4.010^{-5}$
$-0.0353416 - i3.7710^{-5}$	$-0.035341881 - i3.72110^{-5}$
$-0.0202133 - i6.4510^{-5}$	$-0.020213985 - i6.50610^{-5}$

We get almost the same accuracy as Ho, although Ho uses different bases for each resonant state. For the second resonance state in Table 1, our width is an order-of-magnitude smaller than Ho's, but our result is in a good agreement with recent calculations of Shakeshaft et al. [3] and Papp et al. [4]. We think that the good performance of the SVM method for the description of the auto ionizing state is due to the fact that the non-linear parameters are determined by a stochastic method. An advantage the complex scaled SVM method is that it can be easily extended to four- or five-particle problems.

[1] Y. Suzuki and K. Varga, Stochastic Variational Approach to Quantum-Mechanical Few-Body Problems

[2] Y.K Ho, Phys. Lett., A **102**, 348 (1984)

[3] T. Li, R. Shakeshaft, Phys. Rev. A, **71**, 052505 (2005)

[4] Z. Papp, J. Darai, A. Nishimura, Z.T. Hlousek, C.-Y. Hu, and S.L. Yakovlev, Phys. Lett. A **304**, 36 (2002)

3.12 Efimov resonances in atomic three-body systems

J.Zs. Mezei and Z. Papp [a)]

Using our newly developed code which locates resonant states in three-body Coulombic systems by solving homogeneous Faddeev-Merkuriev integral equations, we studied the negative positronium ion $(e^- - e^+ - e^-)$. We located all the known resonances found before by using complex rotation techniques.

Besides these, however, we found numerous resonances, all attached to threshold. We even found them attached to the first, $n = 1$, threshold (see the figures). They are all aligned along a line in the complex energy plane pointing towards the two-body threshold. Based on the pattern of accumulation it is very suggestive that there are infinitely many resonances accumulating at the two-body threshold of the three-body Coulomb system [1,2].

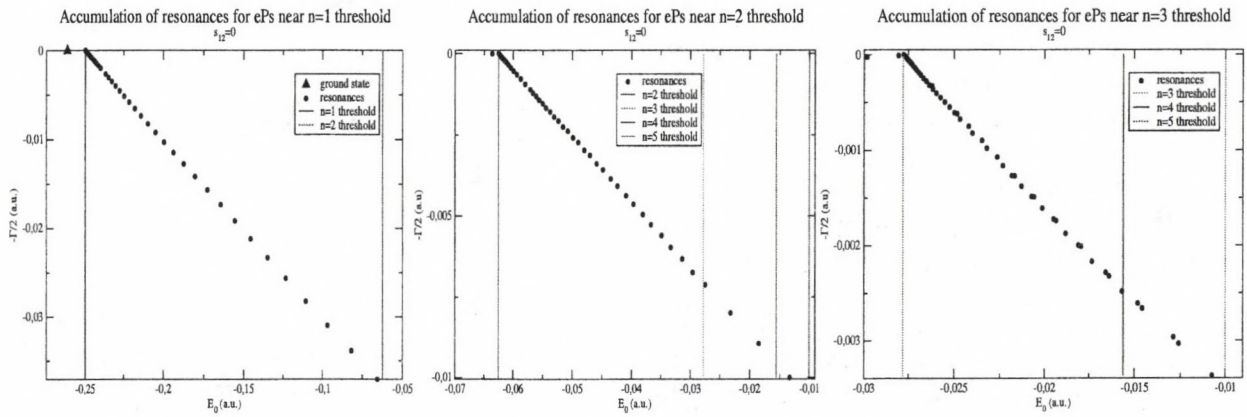

Figure 1. Accumulation of resonances above the two-body thresholds when the electrons spin are coupled to $s_{12} = 0$. The dots stand for the resonances, while the solid lines represents the two-body $(Ps = (e^+ - e^-))$ thresholds.

The only possible explanation we found is that these resonances are due to the Efimov effect. Efimov pointed out that if the two-body subsystem has a bound state at zero energy the three-body system has infinitely many bound states [2]. They become resonant states if they are embedded into the continuum associated with other deeper two-body bound states. In atomic three-body systems the two-body attractive Coulomb potential has bound states accumulating at zero energy. So, all the requirement of Efimov resonances are met in atomic three-body systems.

This research has been supported by the Cottrell Research Corporation and by the OTKA # T46791.

a) Department of Physics and Astronomy, California State University, Long Beach, California 90840

[1] Z. Papp, J. Darai, J.Zs. Mezei, Z.T. Hlousek, and C-.Y. Hu, Phys. Rev. Lett., **94**, 143201 (2005); J.Zs. Mezei and Z. Papp, Phys. Rev. Lett., submitted

[2] V. Efimov, Phys. Lett. **33 B**, 563 (1970).

4.1 Resonant Ni and Fe KLL Auger spectra photoexcited from NiFe alloys

L. Kövér, W. Drube[a)], I. Cserny, Z. Berényi, S. Egri and M. Novák

KLL Auger spectra of *3d* transition metal atoms in solid environment, measured using high energy resolution, give an insight into the details of the local electronic structure surrounding the particular atoms emitting the signal Auger electrons [1]. Fine tuning the energy of the exciting monochromatic photons across the K-absorption edge, features characteristic to resonant phenomena can be identified in the spectra. The shapes of the resonantly photoexcited KLL Auger spectra induced from *3d* transition metals and alloys are well interpreted by the single step model of the Auger process, based on the resonant scattering theory. The peak shapes are strongly influenced by the *4p* partial density of unoccupied electronic states around the excited atom.

High energy resolution studies of KLL Auger spectra of *3d* transition metals using laboratory X-ray sources [1], however, request very demanding experiments and yield spectra of limited statistical quality making the evaluation of the fine details in the spectra difficult. The Tunable High Energy XPS (THE-XPS) instrument at BW2 offers optimum photon flux and energy resolution for spectroscopy of deep core Auger transitions. For the present measurements high purity polycrystalline Ni and Fe sheets as well as NiFe alloy samples of different compositions ($Ni_{80}Fe_{20}$, $Ni_{50}Fe_{50}$, $Ni_{20}Fe_{80}$) were used. The surfaces of the samples were cleaned by *in-situ* argon ion sputtering.

The measurements of the Ni and Fe $KL_{23}L_{23}$ Auger spectra of the metal and alloy samples were performed with the THE-XPS instrument using high electron energy resolution (0.2 eV).

In Fig.1, the measured Fe $KL_{23}L_{23}$ spectrum, photoexcited at the Fe K absorption edge from Fe metal, is compared with the respective spectrum excited from a $Ni_{50}Fe_{50}$ alloy. A significant broadening of the $^1D_2$ peak and an enhancement of the spectral intensity at the low energy loss part of this peak is observed in the alloy sample, while the corresponding Ni KLL spectra are similar both in the alloy and Ni metal. These differences suggest an increased role of the *4p* unoccupied electronic states in the proximity of the Fe component atoms in the alloy compared to the case of Fe metal, when resonant excitation is taking place.

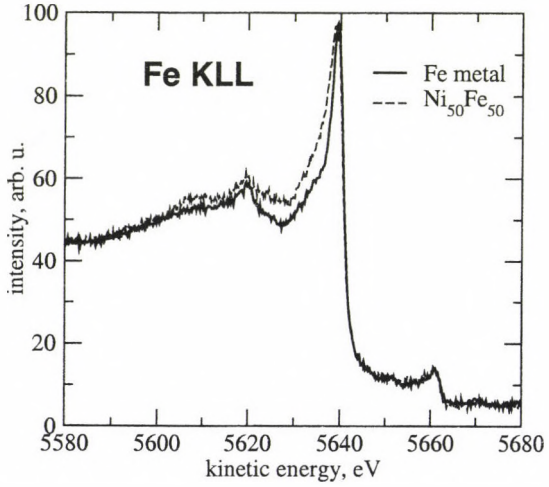

Figure 1. Resonant Fe $KL_{23}L_{23}$ Auger spectra excited at the Fe K-shell ionization threshold from a Fe metal (solid line) and a $Ni_{50}Fe_{50}$ (dotted line) sample.

Acknowledgements

The authors are indebted to Prof. S. Thurgate for providing the NiFe alloy samples. This work was supported by the European Community - Research Infrastructure Action under the FP6 "Structuring the European Research Area" Programme (through the Integrated Infrastructure Initiative "Integrating Activity on Synchrotron and Free Laser Science") and by the Hungarian Project OTKA T038016.

a) HASYLAB/DESY, Notkestraße 85, 22603 Hamburg, Germany

[1] L. Kövér, Zs. Kovács, J. Tóth, I. Cserny, D. Varga, P. Weightman and S. Thurgate, Surf. Sci. 433-435, 833 (1999)

4.2 Surface modifications with highly charged Xe ions

I. Iván, S. Kökényesi[a)], É. Fekete, S. Biri, J. Pálinkás[a)]

Interactions of ions with solid surfaces result in a great variety of effects that depend on the material and the type and energy of the impinging ion. Ion implantation and surface etching are the most investigated processes that find a wide range of industrial applications. In such processes the kinetic energy of the given single or multiple-charged ion is of the primary importance. For the case of highly-charged ions (HCI) the potential energy of ions also can become important and give rise to new effects, such as Coulomb explosion and nanohillock formation. These phenomena are connected to the potential energy induced electron emission and subsequent collective displacement due to local charge imbalance. The underlying mechanism, especially in the case of nanohillock formation is controversial, further experimental work is needed to improve the understanding of the phenomena.

For the first investigations we have selected two types of samples which surface was found to be smooth enough for such investigations: amorphous selenium layers with total thickness of about 500 nm deposited onto Corning glass or mica crystalline substrata by vacuum thermal evaporation and SbSI needle crystals with smooth $\sim 1.5 \times 10$ mm^2 natural facets grown by the gaseous transport reactions. The samples were mounted on a special metallic sample holder and transported in a closed dust-protected box at atmospheric pressure to the ECR-connected collision chamber.

The samples were irradiated with Xe^{20+} and Xe^{24+} ions delivered by the ATOMKI ECR ion source [1] with total beam current in the 50-500 pA range for 0.5-30 min exposure times. This assumed to produce 1-300 impacts on a 100×100 nm^2 area of the target surface.

Atomic force microscope (AFM) investigations (tapping mode at atmospheric pressure) revealed nanohillock formation on the irradiated areas of both samples. A typical image on an irradiated surface is shown in Fig. 1. The hillocks were 1-2 nm high and had diameter between 20 and 60 nm; the population distribution of diameters had maxima at 30 nm for Se and 50 nm for SbSI.

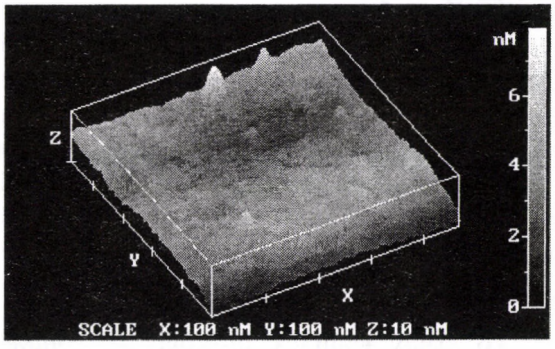

Figure 1. AFM image of a-Se surface bombarded by Xe20+ ions

The kinetic energy of the beam particles is developed by the platform potential of the ion source which was usually 10 kV. Therefore the kinetic energy of the projectiles in these experiments always exceeded the potential energy by about two orders of magnitude or more. Therefore, at this moment we do not know the hillock formation in our samples is really connected to the potential energy of the ions. To decide this question the kinetic energy of ions has to be lowered to be comparable with the potential energy. For this purpose a beam decelerator optics was constructed to decrease the beam kinetic energy down to a couple of hundreds of eV. The testing of the decelerator and the preparation of the next series of experiments are in progress.

a) Dept. of Exp. Phys, Univ. of Debrecen.

[1] S. Kökényesi *et al.*, NIM B 233, 222 (2005).

4.3 Study of magnetic phases in $La_{0.8}Sr_{0.2}Fe_xCo_{1-x}O_3$ ($0.025 \leq x \leq 0.15$)

J. Hakl, S. Mészáros, K. Vad, P.F. de Châtel, Z. Németh[a], *Z. Homonnay*[a], *A. Vértes*[a], *Z. Klencsár*[b], *E. Kuzmann*[b], *K. Kellner*[c], *G. Gritzner*[c]

The hole doped $La_{1-y}Sr_yCoO_3$ cobaltite has recently proved to exhibit particularly clear picture of magnetic phase separation. This magnetic phase separation involves the formation of a spatially heterogeneous magnetoelectric state even in the absence of chemical inhomogeneity.

The phase diagram of the compound is dominated by the crossover from a spin glass like insulator to ferromagnetic like metal. Ferromagnetism is attributed to the percolated magnetic clusters. In the process crucial role is attributed to the gradual increase of magnetic coherence, where the crossover point lies in the vicinity of $y_{crit} \approx 0.2$.

To study complex interplay of competing phases, Fe doped $La_{0.8}Sr_{0.2}Fe_xCo_{1-x}O_3$, ($0.025 \leq x \leq 0.15$) polycrystalline samples were prepared and studied by ac susceptometry. The quality of the samples was checked by XRD, TEM and SNMS.

According to the results, the dynamics of the system can be characterized as a two-level process: by the formation and subsequent low temperature freezing of ferromagnetic clusters (see fig). In contrary to usual ferromagnetic/paramagnetic phase transition the high temperature peak is frequency dependent. Clusters disappear above 15 % Fe doping level. The low temperature transition remains and shows up characteristics of spin glass freezing. In summary by Fe doping the systems evolves from cluster glass to spin glass phase and simultaneously the long range magnetic order is corrupted.

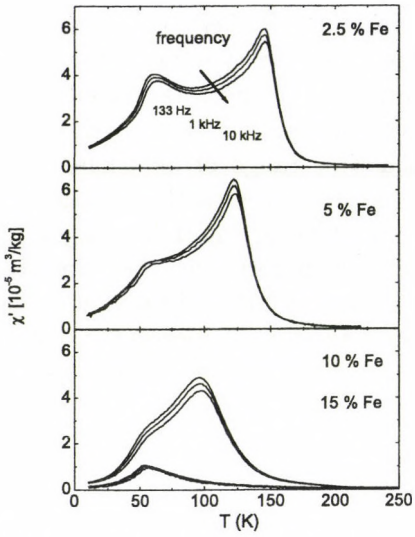

Figure 1. Temperature variation of ac susceptibilities of Fe doped cobaltite samples taken at $H_{ac} = 4.5$ Oe driving field amplitude.

Acknowledgements

This work was supported by the Hungarian Science Foundation (OTKA) under contracts KO20240, T043565, F034837, T034839 and T037976 and the Wissenschaftlich-Technische Zusammenarbeit Österreich Ungarn project A-22/01.

a) Department of Nuclear Chemistry, Eötvös Loránd University, Pázmány P. s. 1/a, Budapest 1117, Hungary

b) Research Group for Nuclear Methods in Structural Chemistry of the Hungarian Academy of Sciences and Eötvös Loránd University, Pázmány P. s. 1/a, Budapest 1117, Hungary

c) Institute for Chemical Technology of Inorganic Materials, Johannes Kepler University, Altenbergerstrasse 69, A-4040 Linz, Austria

4.4 Transport properties of $La_{0.8}Sr_{0.2}Fe_xCo_{1-x}O_3$ ($0.15 \leq x \leq 0.30$)

J. Hakl, S. Mészáros, K. Vad, P.F. de Châtel, Z. Németh[a)], Z. Homonnay[a)], A. Vértes[a)], Z. Klencsár[b)], E. Kuzmann[b)], K. Kellner[c)], G. Gritzner[c)]

Spontaneously phase separated perovskite oxides display a couple of unique physical properties, like colossal magnetoresistance effect in manganites and high-temperature superconductivity in cuprates.

The hole doped $La_{1-y}Sr_yCoO_3$ cobaltite below the percolation threshold is insulator. Surprisingly, the properties of the low temperature transport of the compound show similarities with characteristics of artificial structures fabricated by depositing nanoscale particles.

In order to study the above process, Fe doped $La_{0.8}Sr_{0.2}Fe_xCo_{1-x}O_3$ ($0.15 \leq x \leq 0.30$) polycrystalline samples were prepared and studied by transport, ac/dc magnetization and ^{57}Fe Mössbauer spectrometry. The quality of the samples was checked by XRD, TEM and SNMS.

Magnetization measurements revealed, that the compound undergoes to spin glass freezing at about 50 K, while the amplitude of the ac cusp decreases with Fe doping. Low field magnetization measurements did not show any signs of higher temperature paramagnetic/ferromagnetic phase transition.

According to our transport measurements, the resistivity increases with Fe doping. The transport mechanism can be well described by a 'granular metal in insulating matrix' model ($\rho \propto T^{-1/2}$), the goodness of fit increases with Fe doping. Magnetoresistance decreased with increasing Fe content and for samples $x \geq 0.2$ signalized the setup of magnetic order at 80/90 K. At x=0.15 traces of higher temperature ordering were found. The two transition temperatures can be associated with the setup of short range magnetic coherence and long range magnetic coherence, respectively. The setup of short range magnetic order was approved by the results of Mössbauer spectrometry, as well.

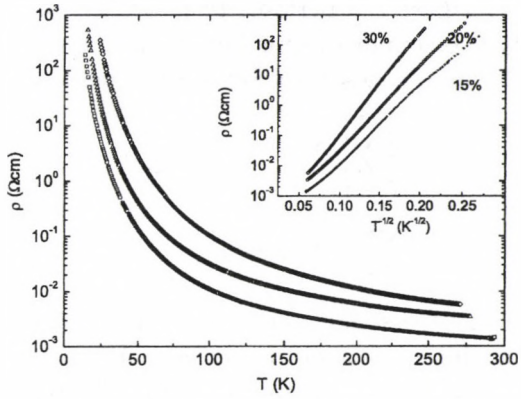

Figure 1. Temperature dependence of the resistivity of Fe doped cobaltite samples. Inset: $T^{-1/2}$ dependence of the resistivity.

Acknowledgements

This work was supported by the Hungarian Science Foundation (OTKA) under contracts KO20240, T043565, F034837, T034839 and T037976 and the Wissenschaftlich-Technische Zusammenarbeit Österreich Ungarn project A-22/01.

a) Department of Nuclear Chemistry, Eötvös Loránd University, Pázmány P. s. 1/a, Budapest 1117, Hungary

b) Research Group for Nuclear Methods in Structural Chemistry of the Hungarian Academy of Sciences and Eötvös Loránd University, Pázmány P. s. 1/a, Budapest 1117, Hungary

c) Institute for Chemical Technology of Inorganic Materials, Johannes Kepler University, Altenbergerstrasse 69, A-4040 Linz, Austria

4.5 Renormalization Group Study of the Multi-Layer Sine-Gordon Model

I. Nándori, S. Nagy[a)], K. Sailer[a)], U.D. Jentschura[b)]

We analyze the phase structure of the system of coupled sine-Gordon (SG) type field theoric models. The "pure," SG model is periodic in the internal space spanned by the field variable. The central subjects of investigation is the multi-layer sine-Gordon (LSG) model [1], where the periodicity is broken partially by the coupling terms between the layers each of which is described by a scalar field,

$$L = \frac{1}{2}\sum_{i=1}^{N}(\partial\phi_i)^2 + \frac{1}{2}J\sum_{i=1}^{N-1}(\phi_{i+1}-\phi_i)^2 + \sum_{i=1}^{N}\tilde{u}\cos(n\beta\phi_i), \quad (1)$$

where the second term on the r.h.s. describes the interaction of the layers. Here, we discuss the generalization of the results obtained for the two-layer sine-Gordon model found in the previous study [1]. Besides the obvious field theoretical interest, the LSG model has been used to describe the vortex properties of high transition temperature superconductors [2], and the extension of the previous analysis to a general N-layer model is necessary for a description of the critical behaviour of vortices in realistic multi-layer systems.

The couplings between the layers can be considered as mass terms. Since the periodicity of the LSG model has been broken only partially, the N-layer model (1) has always a single zero mass eigenvalue. The presence of this single zero mass eigenvalue is found to be decisive with respect to the phase structure of the N-layer models. By a suitable rotation of the field variables, we identify the periodic mode (which corresponds to the zero mass eigenvalue) and $N-1$ non-periodic modes (with explicit mass terms). The $N-1$ non-periodic modes have a trivial IR scaling which holds independently of β which has been proven consistently using (i) the non-perturbative renormalization group study of the rotated model [3], (ii) the Gaussian integration about the vanishing-field saddle point [4]. Due to the presence of the periodic mode the model undergoes a Kosterlitz–Thouless type phase transition which occurs at a coupling parameter $\beta_c^2 = 8N\pi$, where N is the number of layers. The critical value β_c^2 corresponds to the critical temperature which separates the two phases of the model. Its increase with increasing number of layers is in qualitative agreement with the experimentally observed thickness-dependence of the critical temperature of layered high-temperature superconductors.

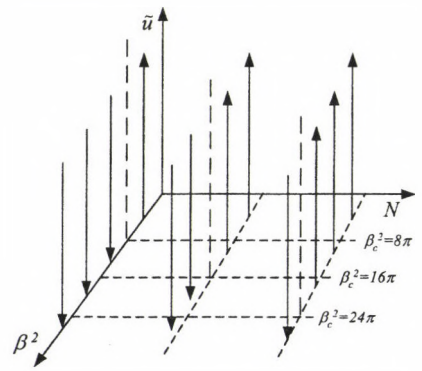

Figure 1. Schematic RG trajectories for various numbers of layers N [3,4].

Acknowledgements

This work has been supported by the Supercomputing Laboratory of the Faculty of Natural Sciences, University of Debrecen.

a) Department of Theoretical Physics, University of Debrecen, H-4032, Debrecen, Hungary

b) Max–Planck–Institut für Kernphysik, Saupfercheckweg 1, 69117 Heidelberg, Germany

[1] I. Nándori, S. Nagy, K. Sailer, U. D. Jentshura, Nucl. Phys. B**725** (2005) 467.

[2] K. Vad, *et al*, Physica C**432** (2005) 43; I. Pethes, *et al*, Phys. Rev. B**68** (2003) 184509; F. Portier, *et al*, Phys. Rev. B**66** (2002) R140511.

[3] I. Nándori, submitted to Journal of Phys. **A**

[4] U. D. Jentschura, I. Nándori, J. Zinn-Justin, Annals of Phys. (2006) at press [hep-th/0509186].

4.6 Length-scale dependence of vortex dynamics in Layered Superconductors

K. Vad and S. Mészáros

Multicontact configuration is one of the most powerful arrangements for electrical transport measurements applied to study vortex phase transition and vortex phase dimensionality in strongly anisotropic high-T_c superconducting materials. We present electrical transport measurements in $Bi_2Sr_2CaCu_2O_8$ (BSCCO) single crystals using a multiterminal configuration, which prove that secondary voltage in zero external magnetic field is induced by thermally activated vortex loop unbinding. The phase transition between the bound and unbound states of the vortex loops was found to be below the temperature where the phase coherence of the superconducting order parameter extends over the whole volume of the sample. We show experimentally that 3D/2D phase transition in vortex dimensionality is a length-scale-dependent layer decoupling process and takes place simultaneously with the 3D/2D phase transition in superconductivity at the same temperature.

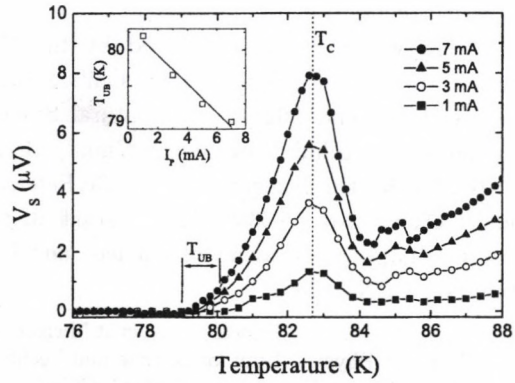

Figure 1. Temperature dependence of the secondary voltage of a BSCCO single crystal at various currents. T_c and T_{UB} are the critical and the unbinding temperatures, respectively. The inset shows the current dependence of the unbinding temperature.

Two current and potential electrodes were attached to both faces of the crystals. The current was injected into one face of the crystal through the current contacts. This is the primary current I_p. The voltage measured on the opposite face of the crystal where the current was injected is the secondary voltage V_S. In our experiments we measured the secondary voltage as a function of temperature and current density. More detailed description of the experimental arrangement is given in Ref.[1]. In Fig.1 we show the temperature dependence of the secondary voltage measured on a BSCCO single crystal in zero magnetic field with different transport currents.

We found that temperature dependence of secondary voltage has a double-peak structure and its higher maximum value is at the temperature where the phase coherence of the order parameter extends over the whole sample. Secondary voltage originates from correlated vortex-antivortex line pair unbinding, i.e., from vortex loop unbinding due to the Lorentz force of the transport current. Near the Ginzburg-Landau transition temperature, free vortex-antivortex line pairs are also generated by thermally activated vortex excitation. The two types of vortex-antivortex line pairs could be responsible for the double peak structure of the secondary voltage. Lacking of theories describing the double peak structure in BSCCO single crystals indicates a need for better description of length-scale dependence in layered superconductors. In order to improve the theoretical description, one can use e.g., field theoretical renormalization group methods [2].

Acknowledgements

This work has been supported by the project OTKA T037976.

[1] K. Vad, *et al*, Phil. Mag. (2006), in press [cond-mat/0508146]; K. Vad, *et al*, Physica C**432** (2005) 43-52;

[2] I. Nándori, *et al*, Nucl. Phys. B**725** (2005) 467; Phys. Rev. D**69** (2004) 025004; J. Phys. G**28** (2002) 607.

4.7 Monte Carlo simulation study of electron interaction with solids and surfaces

Z.J. Ding[a)], K. Salma[a)], H.M. Li[b)], Z.M. Zhang[c)], K. Tőkési, D. Varga, J. Tóth, K. Goto[d)], R. Shimizu[e)]

Monte Carlo simulation method has been playing important roles in materials analysis by electron spectroscopies, electron microscopy, and electron probe microanalysis. For a Monte Carlo modeling of electron interaction with solids, the electron inelastic scattering cross section can be calculated by the use of bulk dielectric function with optical constants in a dielectric functional approach. This has enabled to reproduce systematically the experimental energy distributions of backscattered electrons for a number of elemental materials.

An improved calculation of backscattering factor for quantitative AES analysis has been developed based on a new definition and making use of the up-to-date relevant cross sections [1]. The physical reason is given for the new feature of this backscattering factor that can be less than the unity for very low primary energies closing to the ionization energy and/or for large incident angles. For a Monte Carlo modeling of electron interaction with surfaces, the inelastic scattering of electrons moving in a surface region is treated in a self-energy formalism. The model has enabled the evaluation of surface excitation effect through the calculation of position-dependent electron inelastic scattering cross section.

As an example, a simulation of REELS spectra for Ag is compared with an experiment (see Fig. 1). A reasonable agreement found on the surface plasmon peak intensity normalized with elastic peak intensity thus verifies this modeling of electron interaction with surfaces. Finally, a Monte Carlo simulation code has been extended to deal with complex sample geometries. By using basic building blocks to construct a complex geometry and the ray-tracing technique for correction of electron flight-step-length sampling, the structured and/or inhomogeneous sample can be modeled with a quite flexibility.

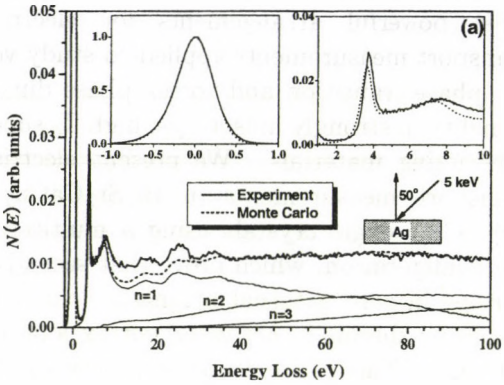

Figure 1. Comparison of the simulated REELS spectra with measurement for Ag. The primary beam is at an angle of incidence of 50 degree and a detector is at normal direction to the surface. The primary energy is 5 keV. The curves labeled by n=1, n=2, n=3 indicate the simulated components due to the respective times of inelastic event. The left inset shows the fitting to the shape of elastic peak and the right inset shows surface plasmon loss peak.

Acknowledgements

This work was partially supported by the National Natural Science Foundation of China (Grant No. 10025420 and 902060090), Natural Science Foundation of Anhui Province of China (Grant No. 05021015), the Hungarian Scientific Research Found (OTKA No. T038016), the grant Bolyai from the Hungarian Academy of Sciences, and TeT Grant No. CHN-3/2004.

a) Hefei Natl. Lab. for Physical Sciences at Microscale; Dept. of Physics, Univ. of Science and Technology of China, Hefei, Anhui 230026, China

b) High Performance Computing Lab., Univ. of Science and Technology of China, Hefei, Anhui 230026, China

c) Dept. of Astronomy and Applied Physics, Univ. of Science and Technology of China, Hefei, Anhui 230026, China

d) Dept. of Systems Engineering, Nagoya Inst. of Technology, Nagoya 466, Japan

e) Dept. of Information Science, Osaka Inst. of Technology, Osaka 573-0196, Japan

[1] Z.J. Ding *et al.* Surf. Interface Anal. 2006 in press.

5.1 Pattern formation in SiSb system

A. Csik, G. Erdélyi[a)], G.A. Langer[a)], L. Daróczi[a)], D.L. Beke[a)], J. Nyéki[a)], Z. Erdélyi[a)]

Recently much attention has been paid to study amorphous semiconductor materials because of their electronic and optical properties [1]. Besides the amorphous Si, the amorphous Si-based semiconductor alloys (for example Si-X, X=Ge, Al, Sn) have also been studied, because attractive properties can be achieved by means of alloying of the above elements. Some of them (Al, Sb, Sn) induce amorphous-crystalline transformation (metal-induced crystallization (MIC)), reducing considerably the crystallization temperature of the amorphous Si. This phenomenon offers an economical way for producing polycrystalline Si films. The effect of Sb on the crystallization of the amorphous Si was investigated by Hentzell et al.[2], but the details of the kinetics of Sb segregation and diffusion have not been revealed yet.

In our previous work [3] we investigated the transformations in amorphous $Si_{1-x}Sb_x$ mono-, $Si/Si_{1-x}Sb_x/Si$ tri- and $Si/Si_{1-x}Sb_x$ multilayers of different compositions (x=13-26 at%) under different hydrostatic pressures and vacuum by Transmission Electron Microscope (TEM). In this study, in contrast to [3], where only qualitative indications on the composition wave formation were presented, we investigate the distribution of the components by means of Secondary Neutral Mass Spectrometry (SNMS) technique. Our new results confirmed that in samples with concentration 18 and 24 at% Sb the first detectable process is the segregation of Sb at the interfaces including the segregation at the free surface as well. The SNMS investigations revealed that asymmetrical composition maxima developed at the original Si/SiSb and SiSb/Si interfaces and that a segregated Sb-rich thin layer is formed at the topmost surface. Considering that in our system phase separation tendencies are expected, spinodal decomposition may result similar Sb concentration profiles as observed experimentally. The initial segregation may initiate crystallization near the interfaces, the formation of nano-size crystalline grains increas the segregated amount of Sb. Though we could not detect crystallization, such process can not be ruled out, since the amorphous-nanocrystalline transformation can hardly be revealed by X-ray diffraction. Our experimental finding that the decomposition was never observed in vacuum, could qualitatively be interpreted supposing that the pressure may enhance the crystallization [3]. This supposition is supported by the density data of the amorphous and crystalline phases: the crystalline phase has lower density than the amorphous one.

The number of the composition peaks depends on the thickness of the slab, the segregation behavior, solubility limits, etc. In order to find experimental evidence to support the spinodal-like decomposition we should investigate how the concentration profiles are affected by the thickness and the composition of the SiSb layer. These experimental investigations and theoretical simulations are in progress.

Acknowledgements This work was supported by OTKA Grant No. D-048594, T-043464, T-038125, F-043372 and "Bolyai János" scholarship (Z. Erdélyi).

a) Department of Solid State Physics, University of Debrecen, P.O. Box 2, H-4010 Debrecen, Hungary

[1] C.N. McKinty, A.K. Kewell, J.S. Sharpe, M.A. Lourenco, T.M. Butler, R. Valizadeh, J.S. Colligon, K.P. Homewood, Nucl. Inst. and Methods B 161-163 (2000) 922.

[2] J.R.A. Carlsson, J.E. Sundgren, L.D. Madsen, H.T.G. Hentzell, X.H. Li, Thin Solid Film 300 (1997) 51.

[3] Z.M. Papp, A. Csik, G. Erdelyi, G.A. Langer, D.L. Beke, L. Daroczi, A. Simon, K. Kapta, Vacuum 71 (2003) 273.

5.2 Stimulated transformation in nano-layered composites with $Se_{0.6}Te_{0.4}$

M. Malyovanik[a)], M. Shipljak[a)], V. Cheresnya[a)], I. Ivan[c)], S. Kokenyesi[a,b)], A. Csik[c)]

The main types of the photo-induced structural transformations (PST) in chalcogenide glasses and amorphous layers can be systematized as i) structural transformations within amorphous phase, ii) photo-induced crystallization or amorphyzation, iii) photo-induced mass transport. These main known types of PST can be further detailed, for example concerning photo-induced anisotropy, photobleaching, etc., and are widely investigated [1-2]. But the fundamentals of these effects even in the most known compositions like AsSe, As_2S_3 are not clear, especially for the nanostructures, where the possible cluster formation, size restrictions and interface conditions may essentially influence the parameters of the material. Furthermore, the basic applied problem related to the PST consists of the possibility of digital or analog optical information storage, phase change memory, fabrication of elements for optics and photonics. These applications require determined spectral and temperature range of functioning, increased sensitivity, transformation rates and stability of the memory at the same time. The realization of such requirements can be expected in nanosized objects made of chalcogenides due to the suitable change of thermodynamical parameters, conductivity, optical and other characteristics.

The establishment of correlations between the compositional modulation at nanoscale-dimensions (3-10 nm) in $Se_{0.6}Te_{0.4}$ and the changes of the optical and electrical parameters as well as the possible improvement of optical recording process in comparison with homogeneous $Se_{0.6}Te_{0.4}$ films were the aims of the present work. Two types of nano-multilayers, namely $Se_{0.6}Te_{0.4}/SiO_x$ and $Se_{0.6}Te_{0.4}/As_2S_3$ were investigated with respect to the thermo- or light-stimulated structural transformations, since they strongly differ by the possibility of intermixing or crystallization in a steady-state process of heating or laser illumination. Photo- and thermo-stimulated crystallization of nanometer thick $Se_{0.6}Te_{0.4}$ films embedded into SiO_x matrix in the form of nano-multilayer structure were measured with optical transmission and electrical conductivity change. It was found, that the as-prepared $Se_{0.6}Te_{0.4}/SiO_x$ structure contains crystallites which in a considerable extent determine the transformation due to the grain growth limited process. Illumination essentially enhances crystallization both in the single $Se_{0.6}Te_{0.4}$ layer and in the $Se_{0.6}Te_{0.4}/SiO_x$ structure, making the process more nucleation-dependent and fast what results in the higher efficiency of the stimulated transformation and optical recording in such a nano-layered structure.

Photo- and thermo-stimulated interdiffusion prevail in $Se_{0.6}Te_{0.4}/As_2S_3$ nano-layered structure what results in efficient intermixing of the adjacent nanometer thick layers, in photo- and thermally induced bleaching and in the change of electrical conductivity due to the formation of the solid solution of chalcogenide components.

Acknowledgements This work was supported by Hungarian-Ukrainian Cooperation Grant UK-2/02 and by Hungarian OTKA Grants T046758, D048594.

a) Uzhgorod National University, Uzhgorod, Pidhirna str.46, Ukraine

b) Department of Experimental Physics, University of Debrecen, P.O. Box 2, H-4010 Debrecen, Hungary

c) Institute of Nuclear Research, Hungarian Academy of Sciences, H-4001 Debrecen, P.O.Box 51, Hungary

[1] H. Jain, J. Optoelectron. Adv. Mater. 5 (2003) 5.

[2] K. Shimakawa, A. Kolobov, S. R. Elliott, Adv. in Physics 44 (1995) 475.

5.3 Kinematical simulation of XRD spectra of Co/Ru multilayers

M. Kis-Varga

Recently, it was shown by computer simulation, and also observed experimentally [1,2,3] that in multilayers where the diffusion coefficient has strong concentration dependence, an initially sharp A/B interface remains sharp during diffusion: i.e. if the diffusion in B is faster, the sharp interface shifts to A direction and the pure B layer fills up with A material (case *a*). For systems with composition independent diffusion coefficients the Fick I low predicts a gradual decay of abrupt concentration profile (case *b*).

To study the diffusion profile on nanoscale in multilayers, the X-ray diffraction is one of the most powerful undestructive technique. In order to compare the evolution of XRD patterns for the two cases described above, kinematical modeling of the first order high angle symmetric scans of hypothetical hcp (0001) Co/Ru multilayer structures (25 bilayer with 3:2 ratio of Co:Ru atomic plane numbers in each) has been carried out by using the SUPREX v9.0 code [4] for CuK_α X-ray source. The magnetic anisotropy exhibited by Co/Ru multilayer is interesting for fundamental research and for applications to recording media in high density magnetic storage devices, too.

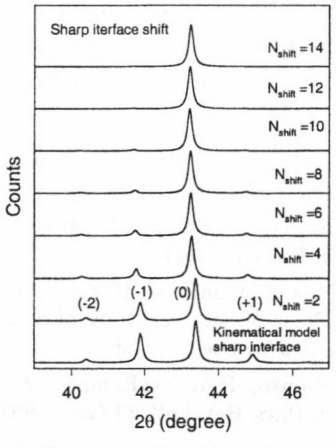

Figure 1. Simulated XRD patterns of Co/Ru multilayer as a function of sharp interface shift (case *a*).

As an example the evolution of XRD patterns for case *a*, starting with a sharp interface and shifting it by two successive atomic planes with simultaneous dissolution of Ru in Co layer is shown in Fig. 1. A rapid decrease of satellite intensities compared to the (0) order one can be seen. Similar but a moderate change of intensity ratios has been obtained for case *b*, too.

One of the most interesting result of this study is that the intensity ratio of (+1)/(-2) satellites changes in opposite direction for the two cases as seen in Fig. 2. This provides a simple experimental way to distinguish the two processes of intermixing and can help to choose the appropriate model and to set the input parameters for structural refinement fitting procedure which then gives the correct interlayer structure of the multilayer.

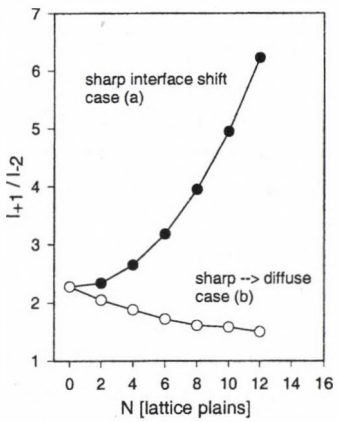

Figure 2. Intensity ratio of (+1)/(-2) satellites for sharp interface shift (case *a*) and for flattening interfaces (case *b*).

[1] Z. Erdélyi, D.L. Beke, P. Nemes, G.A. Langer, Philos. Mag. A79 (1999) 1757

[2] Z. Erdélyi *et al.*, Surf. Sci. 496 (2002) 129

[3] A. Csik *et al.*, J. Appl. Phys. 89 (2001) 804

[4] E.E. Fullerton, I.K. Schuller, H. Vanderstraeten, Y. Bruynseraede, Phys. Rev. B 45 (1992) 9292

5.4 High lateral resolution 2D mapping of the B/C ratio in a boron carbide film formed by femtosecond pulsed laser deposition

A. Simon, T. Csákó[a)], C. Jeynes[b)], T. Szörényi[c)]

Boron carbide, B_4C, is the third hardest material known behind diamond and cubic boron nitride. The high melting point, low density, high chemical resistivity and high neutron absorption cross-section make it attractive for specific electronic and nuclear applications. Although fabrication of boron carbide in thin film form is still a challenge, Pulsed Laser Deposition seems to be a perspective technique for this task.

Boron carbide films with a thickness of up to 550 nm and deposit size of 40 mm × 30 mm were prepared by ablating a B_4C target in high vacuum by pulses of 700 fs duration at 248 nm. The optical characterisation of the films with spectroscopic ellipsometry showed unusually high changes in the refractive index depending on the lateral position. For the interpretation of these results a non-destructive and absolute technique able to determine the distribution of the elements and the film thickness with high lateral resolution was needed. Rutherford backscattering spectrometry with a focussed ion beam is an excellent candidate for this task.

In order to map the layer thickness, the boron carbide film was measured every 2 mm along both of its main axes. Absolute light element contents were extracted from the fits and integrated to get the total layer thickness profiles along the main axes of the deposit. From the striking change of the optical properties of the film arises the question: whether stoichiometry varies as a function of lateral position as well as the film thickness. Thus, carbon, oxygen and total boron were plotted to investigate a possible correlation with layer thickness.

In Fig. 1 it is seen that the elemental composition is indeed highly non-uniform. The B/C ratio has a maximum at the centre with elemental contents of oxygen: 8±3 $\mu g/cm^2$; carbon: 16±2 $\mu g/cm^2$ and total boron: 50±5 $\mu g/cm^2$ (where the uncertainties are given by counting statistics). The B/C∼1 ratio measured at the edge of the deposit increases up to ∼3 toward the centre whereas the target composition was B_4C. From this it follows that while ablation with sub-ps pulses results in significant improvement in the surface morphology of the films by avoiding droplet formation, it cannot ensure stoichiometric material transfer.

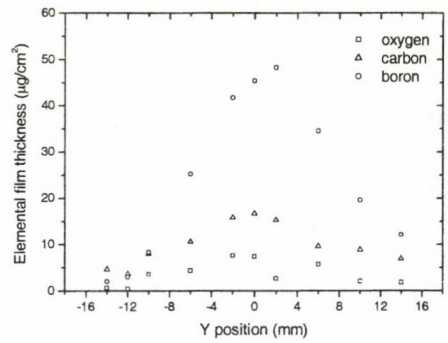

Figure 1. Individual elemental film thickness profiles of boron, carbon and oxygen along the Y axis.

Though, the experimental conditions were not optimized for quantitative determination of the abundance of ^{10}B and ^{11}B isotopes such results are also extracted from the RBS data. Our results confirm the observation of Pronko et al. [1] for boron nitride films; i.e. there is an enrichment of the light boron isotope at the centre of the deposit. Further details can be found in [2].

a) Dept. of Optics and Quantum Electronics, Univ. of Szeged, P.O. Box 406, H-6701 Szeged, Hungary

b) Univ. of Surrey Ion Beam Centre, Guildford GU2 7XH, United Kingdom

c) Research Group on Laser Physics of the Hungarian Academy of Sciences, Univ. of Szeged, P.O. Box 406, H-6701 Szeged, Hungary

[1] P.P. Pronko, P.A. VanRompay, Z. Zhang, J.A. Nees, Phys. Rev. Lett. 83 (13) (1999) 2596.

[2] A. Simon, T. Csákó, C. Jeynes, T. Szörényi: High lateral resolution 2D mapping of B/C ratio in boron carbide films, Nucl. Instr. and Meth. B, in press

5.5 Comparison of the minimum detectable concentration of Si by AES and XAES

J. Tóth, L. Kövér, D. Varga, I. Cserny

In surface analysis the electron excited Auger electron spectroscopy (e-AES) and X-ray excited AES (XAES) techniques are very popular. For analysts the minimum detectable quantities of different elements are crucial importance. In the present paper it is shown how can be increased the detection limit in the case of Si KLL Auger line detection [1]. For the detection limit the peak intensity (P) and the background (BG) are studied. The signal (S) is calculated as the difference of the peak (P) and the background (BG). The detection limit is determined by the ratio of signal to the square root of background (S/SQRT (BG)). On the detection limit there are more details in [2]. In this paper detection limit studies are made for amorphous Si (bulk) and SiOx (100 nm) specimens by the help of Si KLL Auger-line measurements.

The Si KLL Auger lines were measured by using the ATOMKI home-made ESA-31 electron spectrometer [3] equipped with home-made X-ray excitation sources [4] and with an electron source of type LEG62 (VG-Microtech, UK).

The electron spectrometer based on a hemispherical analyzer with energy resolution of $5{\cdot}10^{-3}$. In fixed retardation ratio mode (FRR) using a retardation ratio of k=16, the $5{\cdot}10^{-3}$ relative energy resolution was increased to $3{\cdot}10^{-4}$ (analyzer pass energy relative to the kinetic energy of the electrons at the entrance slit of the spectrometer lens system). For XAES Mo anode X-ray source was used at a power of 225 W (15 kV×15 mA). For e-AES electron beam was used at 5 keV energy, 10 nA beam current and about 2 mm beam diameter. During the measurements of the Auger lines the vacuum level was about $2.5{\cdot}10^{-9}$ mbar in the measurement chamber. For cleaning of the specimen surfaces Ar^+ ion etching was used with the beam of 2 keV energy, 40 degree incidence angle related to the specimen surface normal and a current density of about 20 $\mu A/cm^2$.

It was shown that using Mo XAES technique the minimum detectable quantity of Si can be decreased about by a factor of 40 related to the e-AES technique by the help of Si KLL Auger line.

This can be used as a powerful analytical tool and it is interesting for revealing the low intensity lines of the KLL Auger line group for atomic physics and solid state physics, and it is important in the determination of intrinsic and extrinsic line components with a relatively simple and cheap instrumentation in a shorter measurement time than with a conventional AES and XPS instrument. On the other hand the chemical state assignments are more reliable when we combine the conventional AES-XPS-XAES with the measurements which are shown here.

Acknowledgements

The authors are indebted for the financial Support to the Hungarian Science Foundation of OTKA: TO38016.

[1] L. Kövér *et al.*, Surf. Interf. Anal. 20 (1993) 659.

[2] J.C. Cazaux, Appl. Surf. Sci. 10 (1982) 124.

[3] L. Kövér *et al.*, Surf. Interf. Anal. 19 (1992) 9. (ECASIA-1991 Proc., Budapest)

[4] J. Tóth *et al.*, Book of Abstracts p. 293. (ECASIA-2001, Avignon).

Note: The paper was presented (by J.T.) at ECASIA-2005, Sep20-25, Vienna.

5.6 Experimental determination of the inelastic mean free path (IMFP) of electrons in SiO_2 applying surface excitation correction

G. Gergely[a)], S. Gurbán[a)], M. Menyhárd[a)], A. Sulyok[a)], J. Tóth, D. Varga and A. Jablonski[b)]

The inelastic mean free path (IMFP) [1] of electrons was determined applying elastic peak electron spectroscopy (EPES) [2] with Cu and Si reference samples. The IMFP was deduced from the integrated elastic peak ratio of sample and reference. Experiments were evaluated applying Monte Carlo (MC) simulation based on the NIST SRD 64 database and using the EPESWIN software of Jablonski [3]. Surface excitation correction (SEP) of the IMFP and the material parameter of SiO_2 were determined using the procedure described in [4] and REELS. The SiO_2 layer is an insulator. Its surface potential was determined by the energy shift of the oxygen O KLL Auger-peak. The energy shift was around 1-3 eV in the case of the AES O KLL peaks, the energy scale was calibrated by XPS C 1s line of surface hydrocarbon contamination and the XAES O KLL peak. The SEP factor of SiO_2 is low [5-7]. Our experiments resulted in similar material parameter values to those published in [5, 6].

Acknowledgements

The authors (J.T., D.V.) are indebted for the financial support to the Hungarian Science Foundation of OTKA: TO38016.

a) Research Institute for Technical Physics and Materials Science, Hungarian Academy of Sciences, P.O. Box 49 , H-1525 Budapest, Hungary

b) Institute of Physical Chemistry, Polish Academy of Sciences, Kasprzaka 44/52, 01-224 Warsaw, Poland

[1] C.J. Powell and A. Jablonski, J. Chem. Phys. Ref. Data 28 (1999) 19

[2] G. Gergely, Progr. Surf. Sci. 71 (2002) 31

[3] A. Jablonski, Software EPESWIN, jablo@ichf.edu.pl

[4] G. Gergely *et al.*, Surf. Interf. Anal. 36 (2004) 1098

[5] C.M. Kwei *et al.*, Surf. Interf. Anal. 26 (1998) 682

[6] R. Jung *et al.*, Surf. Sci. 543 (2003) 153

[7] F. Yubero *et al.*, Surf. Interf. Anal. 20 (1993) 719

Note: The paper was presented (by M.M.) at ECASIA-2005, Sep. 20-25, Vienna (to be published in Surf. Interf. Anal.).

5.7 Experimental determination of the inelastic mean free path (IMFP) of polyaniline and polyacetylene polymer samples applying elastic peak electron spectroscopy (EPES) and the NIST SRD64 version 3.1 database

B. Lesiak[a)], A. Jabłoński[a)], A. Kosiński[a)], G. Gergely[b)], M. Menyhárd[b)], A. Sulyok[b)], J. Tóth, D. Varga and R. Nowakowski[a)]

The inelastic mean free path (IMFP) has been determined experimentally on selected polyaniline and polyacetylene samples applying the elastic peak electron spectroscopy (EPES). The Ag and Ni reference samples were used [1]. The preparation of the samples has been described elsewhere [2]. Their surface composition was determined by XPS, their density by helium pycnometry. The hemispherical (HSA) spectrometer ESA-31 (ATOMKI) was used and the measurements were made in the energy range E = 0.2 – 5.0 keV. The integrated elastic peak intensity ratios for sample and reference have been evaluated using Monte Carlo (MC) simulation based on the electron elastic scattering cross-sections database NIST SRD64 version 3.1 and the EPESWIN software of Jabłoński [3]. For the IMFPs of the reference samples the TPP-2M [1] and the G1 of Gries [1] formulae were applied for polymers. Surface excitation corrections and material parameters for polymers were determined [4] based on the model of Chen [5]. The elastic peak of hydrogen was simulated by MC and detected by the EPES and recoil shift [6]. The application of SRD64 (version 3.1) resulted in a better approach of calculated data.

Acknowledgements

The authors (J.T.,D.V.) are indebted for the financial support to the Hungarian Science Foundation of OTKA: TO38016.

a) Institute of Physical Chemistry, Polish Academy of Sciences, Kasprzaka 44/52, 01-224 Warsaw, Poland

b) Research Institute for Technical Physics and Materials Science, Hungarian Academy of Sciences, P.O. Box 49 , H-1525 Budapest, Hungary

[1] C.J. Powell and A. Jabłoński, J. Chem. Phys. Ref. Data 28 (1999) 19

[2] B. Lesiak *et al.*, Surf. Interf. Anal. 29 (2000) 614; and Polish J. Chem. 74 (2000) 847

[3] A. Jabłoński, EPESWIN12 (2004), jablo@ichf.edu.pl

[4] G. Gergely *et al.*, Surf. Interf. Anal. 36 (2004) 1098

[5] Y.F. Chen, Surf. Sci. 519 (2002) 212

[6] G.T. Orosz *et al.*, Surf. Sci. 566 (2003) 544

Note: The paper was presented (by J.T.) at ECASIA-2005, Sep. 20-25, Vienna.

5.8 XPS Study of Graphite – Polymer Interfaces of Polyacrylate Composites

T. Károly[a)], *I.P. Nagy*[a)], *J. Tóth*

Polyacrylate – acrylamide – graphite composite samples were prepared via frontal polymerization. Three different types of acrylate monomers were used to prepare samples and eight different samples were prepared with each type of acrylate monomers. The acrylate/acrylamide monomer ratio was varied between 0.1 and 7.5. The graphite concentration was constant in all samples. To verify or disprove polymer – graphite interactions in the composites, the composite – graphite interfaces were studied by Al K-alpha excited XPS, using a custom made high energy resolution electron spectrometer in fixed retardation mode. Primary spectra showed by 2-4 shouldered structures in the C 1s. O 1s peaks were also studied, however less structured peaks and shoulders were found than in the cases of C 1s. On the basis of literature, a typical bound energy was assign to the C and O atoms in different chemical bond states. On the basis of these facts, the C 1s and O 1s photopeaks were decomposed according to different chemical bond states. Thus an ambiguous connection has been found between the acrylate/acrylamide molar ratio and peak ratio. The chemical bound formed between the polymer and graphite in the composites has also been verified.

Acknowledgements

The authors are indebted for the financial support to the Hungarian Science Foundation of OTKA: (T.K. and I.P.N.) for T008078 and (J.T.) for T038016.

a) University of Debrecen, Hungary

Note: The paper was presented (by T.K.) at EUROMAT-2005, Sep 5-8, Prague.

5.9 SNMS and XPS analysis of thin layers containing SiC

Z. Berényi, J. Tóth, G.L. Katona and K. Vad

Feasibility studies were carried out in the composition depth profiling of thin semiconductor films containing SiC by quantitative X-ray Photoelectron Spectroscopy (XPS) and Secondary Neutral Mass Spectroscopy (SNMS) measurements. Samples were prepared at the KFKI-MFA by d.c. magnetron sputtering of Si in CO_2 gas background using three different sputtering conditions and gas pressures.

Prior to SNMS examinations quantitative XPS measurements were performed using our home-built ESA-31 electron spectrometer in order to determine the surface chemical composition of the samples. XPS - contrary to mass spectroscopy techniques - has the advantage of revealing surface chemical states of the elements in a non-destructive way. It is also very useful for the quick and non-destructive determination of the major elemental components of the sample to be recorded by SNMS. Accessible in-depth information is determined by the inelastic mean free path of the detected electrons in the sample, which can be varied using different excitation sources.

In the present study Al Kα x-rays were used as excitation. The main components of the samples were determined to be C, O and Si. Signals involving O 1s, Si 2p, C 1s and Ar 2p levels were used for quantification.

The evaluation of the chemical shifts showed that in the case of the surface regions of Sample# 1 and Sample# 3 Si and O are in the form of SiO_2 and C was in the form of C-C binding and was not bound to Si atoms. In the case of Sample# 2, however, three different chemical states of C and two of Si could be observed in the surface region. From the chemical shifts it was concluded that the majority (83%) of the Si atoms were in the form of SiC, while the minor part (17%) was present as SiO_2. Carbon atoms were present in SiC, hydro-carbon or graphite and $C_xH_yO_z$ forms. From the XPS measurements we concluded that probably Sample# 2 contains SiC in the surface region (about 5-7 nm).

SNMS measurements were performed at the INA-X SIMS/SNMS system. Each sample was examined using Ar and Kr sputtering in order to monitor sputtering artifacts during depth profiling. Kr sputtering had the advantage of allowing us to detect SiC clusters (at mass 40), as well.

SNMS profile of Sample# 1 did not exclude the presence of SiC at the surface region, however it was successfully refuted by XPS. Sample# 2 showed roughly constant stoichiometry up to the substrate, which - combined with the information from XPS - consisted of SiC in about 70 atomic percent. Sample# 3 could be suspected to contain a buried SiC (mixed with SiO_2) layer between the surface layer (mostly SiO_2) and the substrate (Fig. 1.). The latter information, however, was not confirmed regarding to chemical composition.

These measurements let us to conclude that in those cases when the quantitative depth profiling of composites is targeted it is necessary to apply other standard analytical techniques such as XPS, providing complementary information not only about stoichiometry but chemical state, as well.

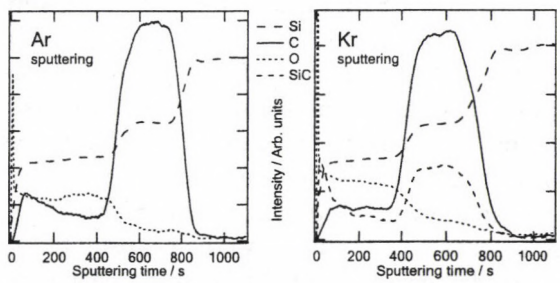

Figure 1. SNMS profiles of Sample# 3 using Ar and Kr sputtering

Acknowledgements

The authors are indepted to Dr. G. Battistig and Ms. A. Pongrácz (Research Institute for Technical Physics and Materials Science of the Hungarian Academy of Sciences – KFKI-MFA) for the test samples.

5.10 Determination of Ni grain boundary and volume diffusion coefficients in W using SNMS and tracer depth profiling

G.L. Katona, G. Erdélyi[a)], A. Csik[a)], G.A. Langer[a)], Z. Berényi, K. Vad, D.L. Beke[a)]

Diffusion of nickel in tungsten is important in a number of structural applications involving W alloys. One of the technologically important examples is the well known activated sintering of tungsten powder due to small additions of transition metals, which allows the reduction of its sintering temperature to the range of 1500 K. The enhanced sinterability of W is accounted for the promoted diffusion processes along grain boundaries in the presence of these transition metals. One example is that the grain boundary self diffusion in W is increased in the presence of Ni in the grain boundaries. In spite of their technological importance very few investigations on these problems have been published.

In this report we present our preliminary results on Ni diffusion in W using Secondary Neutral Mass Spectrometry (SNMS) and tracer depth profiling technique. The tracer technique is used to measure the grain boundary diffusion coefficient. However, the evaluation of the tracer measurements requires data on the volume diffusion coefficient. Since it is not available in the literature we planned to determine it by SNMS depth profiling.

Both SNMS and tracer measurements were carried out using tungsten polycrystalline substrates with grain size of ca. 40 μm. The substrates were prepared by mechanical polishing prior to electrodeposition of Ni for tracer measurements, and deposition of 100 nm Ni by DC magnetron sputtering [1] for SNMS measurements. The samples were encapsulated in quartz tubes filled with Ar for heat treatments. The tubes also contained a piece of Ti to reduce oxidation. The tungsten sputtering rate for the SNMS depth profile was determined by weight difference measurement of a tungsten reference before and after a long time sputtering. This yielded a sputter rate of 0.21 nm/s.

Two samples for the SNMS measurements were prepared by annealing at a temperature of 1403 K, but with different annealing times. One was annealed for 16.5 hours, while the other was annealed for 60 hours.

SNMS time profiles of Ni-58, W-184 and Cu_2 (mass: 128 amu, from the sample holder) were recorded. The Cu_2 signal was used to normalize the obtained intensities in order to remove fluctuations of the total sputtering yield.

Figure 1 shows the depth profile of the sample annealed for 16.5 hours. Because the W substrate is polycrystalline, we have to take into account grain boundary diffusion, as well. Considering, that at the choosen temperature the volume penetration depth is about 200 nm for the shorter, and about 400 nm for the longer annealing, the effect of the grain boundaries is small.

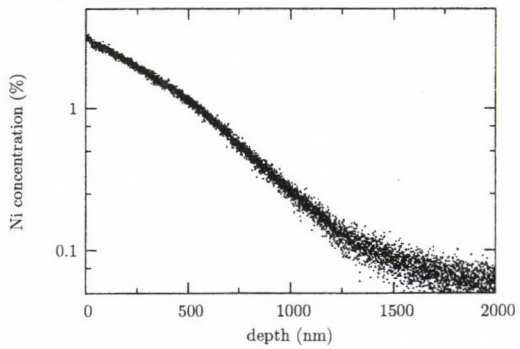

Figure 1. Depth profile of the sample annealed for 16.5 hours at 1403 K

Using the solution of Fick's second law for volume diffusion from instantenous source [2] for the region between 300 and 900 nm we have obtained $D_v = 3 \times 10^{-18}$ m^2/s. Approximately the same value was obtained from the longer annealed sample, which shows, that the method is well applicable to (volume) diffusion measurements.

Acknowledgements

This work was supported by OTKA Grant No. T038128.

a) Dept. of Solid State Physics, Univ. of Debrecen

[1] D.L. Beke *et al.* Vacuum **50/3-4** 373-383 (1998)

[2] D.L. Beke, General introduction, pp. 1-1 – 1-23, Landolt-Börnstein New Series Vol. III-33a "Diffusion in Semiconductors" (1998)

5.11 Fragmentation of kidney stones

K. Kovács[a)], *F. Kun*[a)] *and T. Vertse*

Fragmentation, *i.e.* the breaking of particulate materials into smaller pieces is abundant in nature and underlies several industrial processes, which attracted a continuous interest in scientific and engineering research over the past decades [1]. In industrial applications, fragmentation processes are mostly used for the comminution of ores in various types of mills.

Kidney stone is a well known human disease which embitters the life of many people (in a country like the USA about 10^6 cases are registered yearly). In order to extract large kidney stones (diameter $\geq$ 1 cm) from the human body without operation, one of the most efficient treatment is the fragmentation of kidney stones by the so-called extracorporal shock wave lithography method: a shock wave penetrating the human body is generated by an electric pulse. The repeated application of the shock wave gradually fragments the stones into pieces of size $\leq$ 2 mm which then leave the body through the urine system. Recently, a novel type of lithographic method has been suggested by using widely focused shock waves which fragment the stones by a squeezing mechanism. Laboratory experiments showed that the widely focused squeezing waves achieve a higher fragmentation efficiency than the frequently used shock waves of sharp focus. Based on this method a novel medical treatment can be introduced which is less demanding for the patients [2].

Before the application of the method in the clinical practice a detailed understanding of the fragmentation mechanism of kidney stones due to shock waves is required. Since analytic theoretical methods have serious limitations in this field, we develop a realistic model of the mechanical behavior of kidney stones and a simulation code which makes possible to study the mechanism of breakup under various external conditions. Computer simulations in two dimensions have revealed a peculiar way of crack formation, *i.e.* the crack which finally breaks the stone gradually grows as a result of the interference of relatively low amplitude shock waves, see Fig. 1. In the framework of the model we can find the optimal set of parameters which provide the highest fragmentation efficiency (less number of pulses) in order to minimize the difficulties of clinical tests [3]. The three-dimensional version of the model and the implementation of the simulation code is in progress.

a) Dept. of Theor. Phys. Univ. of Debrecen

[1] F. Kun, et al. Phys. Rev. Lett. **96**, 025504 (2006).

[2] W. Eisenmenger, Ultrasound in Med. & Biol. **27**, 683 (2001).

[3] K. Kovács, F. Kun, W. Eisenmenger, T. Vertse, preprint.

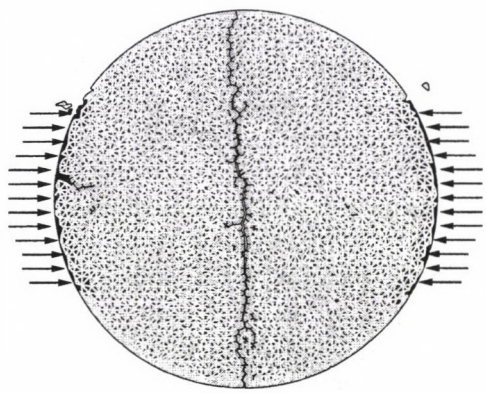

Figure 1. A disc shaped two-dimensional kidney stone was periodically hit along a surface region as it is indicated by the arrows. In agreement with the experiments, the crack is formed perpendicular to the direction of the shock wave.

6.1 Elemental concentrations of PM10 and PM2.5 aerosol in Debrecen

I. Borbély-Kiss, E. Dobos, Zs. Kertész, E. Koltay, Gy. Szabó

The aim of this work was to follow the variation of the elemental concentration both in PM10 (coarse mode) and PM2.5 (fine mode) aerosol fractions. For the qualification of local air at a given region the total particulate mass and its elemental composition are usually used.

Aerosol samples were collected in Debrecen twice a week with a two-stage "GENT" SFU (stacked filter unit) sampler. Total airborne particulate mass (PM10 and PM2.5) was measured using a Sartorius microbalance. The black carbon (BC) content of fine aerosol was determined by a Smokestain reflectometer. Fig.1.*a* shows the data, measured from Aug. 2004 to Sept. 2005. Samples were analyzed by PIXE and elemental concentrations of Al, Si, P, S, Cl, K, Ca, Ti, V, Cr, Mn, Fe, Ni, Cu, Zn, As, Br, Pb were calculated.

Monthly average concentrations and enrichment factors of the above elements were calculated from the database obtained by the analyses. From the variation of the monthly average concentrations conclusions were drawn on the seasonal behaviour of the elements. Concentrations of S, Cl, K, V, Ni, Zn, and Pb elements, derived mainly from anthropogenic sources, both in fine and coarse mode have their maximum in winter. Concentrations of Si, Ca, Ti, Mn, Fe elements derived mainly from natural sources have their maximum in summer. Fig.1.*b* illustrates the variation of concentrations of a few elements originating from anthropogenic sources in the fine mode aerosol during the investigated time interval.

The origination of an element can be defined by the E_f enrichment factors:

$E_f = (C_x/C_{Ti})_{aerosol}/(C_x/C_{Ti})_{Earthcrust}$

where C_x is the concentration of the element in question, C_{Ti} is the concentration of Ti. $E_f \approx 1$ values mean natural (crustal) origin, and $E_f \geq 10$ values imply anthropogenic origin. Fig.1.*c* shows the monthly averages of enrichment factors of some elements in the fine mode aerosol. The enrichment of K and V in winter is the result of domestic heating and oil-firing, respectively.

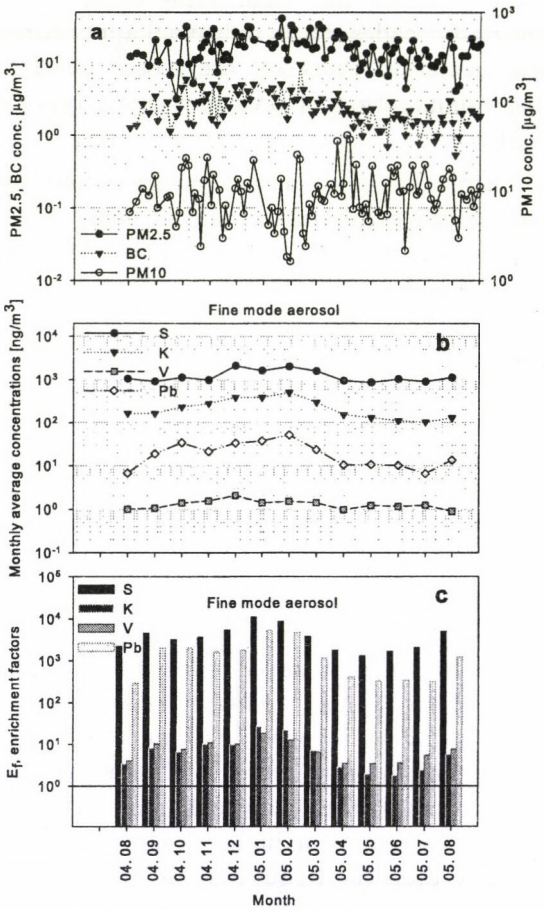

Figure 1. Part *a* shows the mass concentrations of PM10, PM2.5, BC, and part *b* the monthly average concentrations of S, K, V, Pb in the fine mode aerosol; part *c*: illustrates the monthly averages of enrichment factors of some elements in the fine mode aerosol.

Acknowledgements

This work was supported by the National Research and Development Program (NRDP 3A/089/2004).

6.2 Far-field hydrogeological model of Paks NPP

É. Svingor, K. Bérczi[a)], *L. Köves*[b)]

The settlements in the vicinity of Paks NPP gain the drinking water from the lower Pannonian aquifers. Uncontrolled releases from the NPP enter into the shallow groundwater and they are transported to the Danube in the Quaternary alluvial sandy gravel layer. The hydraulic potential in the area increases with the depth, so leakage from the upper gravel layer to the lower aquifer is not possible in undisturbed circumstances. The question is that an overexploitation of drinking water can change the pressure conditions so that the contaminated water can enter from the upper gravel layer into the lower aquifer.

To answer this question the Visual MODFLOW program was used to simulate the groundwater flow, providing quantitative estimates of flow rates, flow paths and travel times. The simulation was designed to represent average steady-state flow conditions.

A mathematical model is a representation of a real system or process. The subsurface environment constitutes a complex, three-dimensional, heterogeneous hydrogeologic setting, which strongly influences groundwater flow and transport, and it can be described through careful hydrogeologic practice in the field. The conceptual model of the hydrogeological system in the surroundings of Paks NPP was constructed from the available geologic, hydrogeological, geographical and meteorological data [1].

To obtain a unique solution of a generic model corresponding to a given area, additional information about the physical state of the system is required (boundary and initial conditions). The model was constructed on a 20km x 22km area, its eastern boundary is Danube, the others are defined as no flow boundaries.

The model consists of 5 main layers: upper sequences of Pleistocene alluvial sediments (sandy layer, $K_{x,y}=10^{-4}$m/s); lower sequences of Pleistocene alluvial sediments (gravel, $K_{x,y}=10^{-3}$m/s); upper Pannonian sediments of restricted transmissivity ($K_{x,y}=5{\cdot}10^{-6}$m/s); Pannonian aquifer ($K_{x,y}=10^{-4}$m/s); lower Pannonian aquitard ($K_{x,y}=10^{-7}$m/s). The anisotropy factor for every layer was $K_{x,y}/K_z=10$.

Assuming average precipitation of 600 - 650 mm/y, a recharge rate of 10% (65 mm/y) and average water level in the Danube we found:

- The groundwater in the Danube-valley is continuous and is recharged by precipitation in the higher elevations in Mezőföld.
- The groundwater flows from the northwest to the south-east toward the Danube.
- The mean residence time of groundwater in the lower Pannonian aquifer is 230 - 260 ys.
- The contamination released from the NPP enters into the gravel and the groundwater transports it to the Danube. The water level of the Danube has little influence to the flow direction, but the travel times are shortened by low and increased by high water level.
- The pressure conditions dont let the shallow groundwater and so the contamination flow down to the Pannonian aquifer, rather an upwelling can be expected.
- An increasing water production from the Pannonian aquifer can change the hydraulic heads and an overexploitation may alter the whole flow system. In the present climatic conditions the enhancement of water production by a factor of four may change the basic flow directions, and the contaminated water may get into the Pannonian aquifer. A permanent drought increases the vulnerability of the aquifer: because of the insufficient precipitation the recharge decreases, the hydraulic heads are depressed, and the flow directions may reverse even in the case of restricted water production.

a) ETV ERŐTERV. Budapest, Hungary

b) Paks Nuclear Power Plant, Paks, Hungary

[1] Jelentés a Paksi Atomerőmű telephely-jellemzési programjának keretében a tágabb környezetre vonatkozó hidrogeológiai modell elkészítéséről. ETV-ERŐTERV Rt. Budapest, 2005. augusztus

6.3 Monitoring system with automatic sampling units around Paks NPP

L. Palcsu, M. Molnár, M. Veres[a)], T. Pintér[b)], L. Köves[b)], É. Svingor

Continuous monitoring of the uncontrolled tritium emission from Paks NPP has been carried out since the starting of the NPP. To control the release of fission and corrosion products automatic samplers were designed and installed into 20 observation wells in the vicinity of the reactor blocks. The automatic samplers contain two columns filled with anion and kation exchange resins and they are equipped with filters for trapping the chelating agents. The samplers are working two meters below the groundwater level. Water pumps fed by accumulator ensure the water sampling through the ion-exchange columns. The conductivity, flow-rate and the volume of the water passed the columns are continuously registered. If the conductivity of the passed water exceeds a prescribed limit (the resins have became saturated), the pump is automatically stopped. After a two-month working period the trapped ions are eluted from the resins. The activity of the gamma-emitters, ^{14}C, ^{90}S and transuranic elements are measured in the dried elute, the tritium activity is measured in the collected water.

The automatic samplers have been working for five years at Paks NPP. The experiences are the following:

- After a volume of 30 - 60 liters of the water passed the columns the resin became saturated.
- The efficiency of the chemical digestion was typically 50 - 80 %.
- The total gamma activities in the observation wells were less than 1 Bq/L and they were emitted mainly by natural isotopes, first of all ^{40}K. There were no fission products above the detection limit (1E-04 Bq for ^{137}Cs), and we found 1 - 2E-03 Bq/L of corrosion product ^{60}Co only three times in two wells near the main building of blocks 1-2.
- The activity concentration of ^{90}Sr was at the detection limit ($\approx$1E-04 Bq/L, Tri-Carb 3170 TR/SL LSC).
- There was no plutonium or any other transuranic isotopes above of the detection limit of 1E-05 Bq/L.
- The activity concentration of ^{14}C was measured on the carbonate content of the water in a low-level gas proportional counter in the form of CO_2. In the most of the wells the activity concentration of ^{14}C was 80 - 90 pmC %, typical for shallow groundwaters (100 pmC = 0.226 Bq/g C). In a few wells the activity was a bit higher, and in one well it was regularly well above the background. Although the ^{14}C activity concentration of the water in these wells was less than 0.2 Bq/L, it indicates a ^{14}C release from the plant.
- The tritium content was above the background only in several wells near the reactor blocks, and it fluctuated in these wells. It seems that there is a tritium cloud under the plant, and its extension is controlled by the water level of Danube.

a) Isotoptech Co. Ltd. Debrecen, Hungary

b) Paks Nuclear Power Plant, Paks, Hungary

6.4 Late Holocene environmental changes recorded at Gheţarul de la Focul Viu, Bihor Mts, Romania

L. Palcsu, M. Molnár, I. Futó, L. Rinyu, Zs. Szántó, Z. Kern[a)], *I. Fórizs*[b)], *B. Nagy*[a)], *M. Kázmér*[c)], *A. Gál*[d)]

A significant number of ice caves in temperate climatic region contain ice and wood remnants from same site and probably same time span. Gheţarul de la Focul Viu is located in the Bihor Mts. (46.27° N , 22.68° E) approximately 50 kilometres far from Cluj (Romania). A 772 cm long ice core was extracted in November 2001 from the ice floor of the Main Chamber. At the depth of 6.67 meters of the ice core a piece of wood appeared. In addition, a branch outcropping from the ice block at its sidewall at 11.1 meters depth was also sampled. Both wood remnants were undergone radiocarbon age determination. In February of 2002 we have collected ice samples for tritium measurements.

This paper synthesizes the isotope and tree-ring data gathered at Focul Viu Ice Cave. The oxygen isotope compositions were analysed in the Institute for Geochemical Research, Hungarian Academy of Sciences (Budapest). Radiocarbon dates of wood samples were determined by gas proportional counting and the tritium content of the water samples were determined by the ^{3}He-ingrowth method in the Institute of the Nuclear Research of the Hungarian Academy of Sciences (Debrecen).

We have found a correspondence between the impurity layers of the ice block, δ^{18}O data of the shallow ice core and standardized ring width curve of a conifer species. The 850 $\pm$ 50 year BP radiocarbon age (1160-1260 cal AD) from 6.67 m depth of ice indicate, that the stable isotope data of the 7 metres long ice core origin approx. from the past 800-900 years. However, melt events introduce obvious hiatuses in the sequence. The response function analysis revealed that main growth influencing climate factors for *Abies alba* are June mean temperature and early summer water supply. The sufficiently represented part of the 420 year long tree-ring index curve suggests particular periods unfavourable to annual increment of the firs. Decades unfavourable for fir growth are 2000-1980, 1940-1920, 1890-1870, 1860-1820, while the favourable periods are 1980-1940, 1920-1890, 1870-1860.

The fit between the growth favourable decades and the muddy layer concentrations seems to be a promising dating method of the ancient melting events and fragmentally remained ice bands. Previously negative intervals of Easton coefficient time series were fitted to ice accumulating periods. The independent dating methods - Easton coefficient and fir index - show similarity back to 1730 for ice accumulation and melting periods.

a) Eötvös Loránd University, Department of Physical Geography, Budapest, Hungary

b) Institute for Geochemical Research, Hungarian Academy of Sciences, Budapest, Hungary

c) Eötvös Loránd University, Department of Paleontology, Budapest, Hungary

d) University Babeş-Bolyai, Faculty of Geography, Depertment of Physical Geography, Cluj, Romania

6.5 Study of gas generation in drum L/ILW packages using hermetic containers

M. Molnár, L. Palcsu, É. Svingor, I. Futó, Z. Major, F. Frigyesi[a)], *P. Ormai*[a)], *I. Barnabás*[a)], *A. Fritz*[a)], *M. Veres*[b)]

During the storage of low and intermediate level radioactive waste (L/ILW) significant quantities of gas may be produced. It is likely that a small proportion of the generated gas will be radioactive as a result of the incorporation of the isotopes ^{3}H and ^{14}C that are present within the waste.

To obtain reliable estimates of the quantities and rates of the gas production in L/ILW a series of measurements was carried out of waste packages produced and temporarily stored at the site of Paks Nuclear Power Plant (NPP). Ten drums filled with selected original L/ILW were placed into hermetic containers equipped with sampling valves for repeated sampling. These hermetic containers were stored at the same site where the L/ILW is stored primarily in the Paks NPP.

The pressure and the temperature of the headspace gas in the containers were monitored continuously. Qualitative gas component analyses of headspace gases of drums and their containers were executed by quadrupole mass spectrometer. The gas generation rate in the stored L/ILW was calculated by the measured state parameters and the composition variation of the gas in the closed containers.

Stable isotope measurements were executed from the CO_2, CH_4 and N_2 fractions by stable isotope ratio mass spectrometer. Helium measurements were done by noble gas mass spectrometer. The tritium content of the vapour, H_2 and CH_4 fractions was measured by a low background liquid scintillation counter. ^{14}C content of the CO_2 and CH_4 fractions was measured by a low background gas proportional counter system (ATOMKI).

Our results showed that the main generated gases in L/ILW are carbon dioxide, methane, hydrogen and nitrogen. The typical rates were 0.05-0.2 normal litre gas/day for CO_2 and CH_4 generation, and less than 0.02 normal litre gas/day for H_2. Because of the typical vanishing of the O_2 from the headspace gases no explosive gas mixture was indicated in the L/ILW drums during the investigated storage period.

The stable carbon isotope results show that the main source of the CO_2 gas is the degradation of organic matter in the waste. The low ^{13}C content indicates microbial degradation processes as the main sources of CH_4 gas. The He isotope ratios represent ^{3}He enrichment in the headspace gases produced by tritium decay in the waste.

Significant variation of tritium content in individual drums with time was typical. The maximal value was more than 20 Bq ^{3}H/litre. The typical tritium activity concentrations were between 0.1 and 10 Bq ^{3}H/litre. The main tritium content always was related to the vapour fraction, but when the methane became main component in the headspace gas it also could contain significant amount of ^{3}H.

The radioactivity of the carbon in the gas phase of the L/ILW drums are always significantly higher (10 or 100 times) than in the air. This ^{14}C enrichment also appears in the methane fraction if it became main component in the headspace gas. Maximal measured radiocarbon activity was about 3.0 Bq/litre. Typical ^{14}C activity values of the headspace gases were between 0.1 and 2.0 Bq/litre.

a) Public Agency for Radioactive Waste Management (PURAM), Paks, Hungary

b) Isotoptech Co. Ltd., Debrecen, Hungary.

6.6 Investigation of dissolved gases in the coolant of the cooling ponds and service pool No.1 of reactor No.2 of Paks Nuclear Power Plant

M. Molnár, L. Palcsu, Z. Major, É. Svingor, M. Veres[a)], T. Pintér[b)], P. Tilky[b)],

Changes of the composition or content of the dissolved gas in the coolant, especially of the noble gases and the hydrogen, are really significant indicators of the alterations in state parameters of the nuclear reactors during the working or the shutdown periods. The aim of this work was the investigation of the effect of nuclear fuel rods to the composition of the dissolved gas in the cooling water of the cooling ponds and service pool No.1 of reactor No. 2 of Paks Nuclear Power Plant (Paks NPP). The dissolved gases in coolant were measured for surveying the kilter of the nuclear fuel remained in service pool No.1 after the incident in April of 2003.

For dissolved gas measurements the gas must be representatively retrieved from the coolant of the cooling ponds and service pool No. 1. Two different experimental ways were applied in parallel for ensuring the better reliability of the results. The basis of the first method is gas sampling with degassing of the coolant on the site and the measurements are carried out later from this gas samples in the lab. The other way means in-situ measurement of the dissolved gas directly from the coolant with membrane inlet quadrupole mass spectrometer on the site. Noble gas isotope measurements were carried out by a noble gas mass spectrometer from the gas in ampoules. Gamma activity of the gas samples in the ampoules was measured by HPGe detector.

The concentration of the total dissolved gas is similar in the coolant of all the investigated cooling ponds and service pool No. 1. On the other hand the compositions of the dissolved gas in the systems of reactor No. 2 and in the other cooling ponds were completely different. In the cooling ponds of reactors No. 1, 3 and 4 the dissolved gas in the coolant is air, with only little H_2 and CO_2 surplus, and these values were relatively stable during the whole sampling period. The composition of the dissolved gas in the cooling pond and service pool No. 1 of reactor No. 2 differs from the air and strongly varied during the sampling period. The hydrogen content of the coolant of the service pool No.1 continuously increased till the fifth sampling in 2004, and reached a value of 2,4 cm^3 H_2 /litre coolant. That time the portion of CO_2 was also significantly higher than in the other investigated coolants. But before the H_2 concentration increased over the 1 cm^3/litre value, the oxygen content in the coolant drastically decreased (fourth sampling in 2004 of the service pool).

In the samples from the cooling ponds of reactors No. 1, 3 and 4 the noble gas contents were very similar to each other and to the dissolved air. Noble gas content in these systems was varying and a little bit lower than the typical values of the water saturated with air. In the cooling water of service pool No. 1 of reactor No. 2 the amount of dissolved Xe and Kr is significantly higher than in the other investigated cooling ponds. This difference is two or three orders of magnitude. In the cooling pond of reactor No. 2 the Xe content was also ten times higher than in the others of Paks NPP.

The gamma analytical results from the degassed samples showed that only ^{85}Kr isotopes gave measurable activity and only for the samples from reactor No. 2. All the other samples had no detectable radioactivity. The measured ^{85}Kr activities showed similar trends in time, but the values were 10-100 times higher in the case of the service pool. At the time of the last sampling in 2004 the ^{85}Kr activity was more than 10 kBq/litre for the coolant of the cooling pond and more than 1000 kBq/litre in the case of service pool No. 1.

a) Isotoptech Co. Ltd., Debrecen, Hungary

b) Paks Nuclear Power Plant Co. Ltd., Paks, Hungary

6.7 Examination of the effect of particle-size on the radionuclide-content of soils

Á. Bihari and Z. Dezső[a)]

The size of soil and rock particles affects directly the intensity and possibility of soil erosion. The processes involved are known to remove and transport finer particles with larger efficiency. Fallout radionuclides (e.g. ^{137}Cs) are rapidly and strongly adsorbed to soil particles, therefore, the understanding of their distribution between different size fractions is important for their use as tracers in soil transport. On the other hand, the cation exchange properties of particles depend also on particle size. This dependence is due to the fact that mainly a surface layer (or the inner surfaces of the pores of a porous particle), and not the whole particle mass, is participating in the exchange of radionuclides.

A particle with a smaller diameter has larger surface for sorption than a larger one relative to its mass. Thus, the same amount of finer particle is assumed to have a higher radionuclide-content than a coarse one if the source of the adsorbed radionuclide is the same. Consequently, changes in radiotracer-content at a landscape-point compared to the reference value could be related to different rate of erosion in case of different particle-size distribution.

The aim of this work was to obtain information on this kind of particle-size – radionuclide-content distribution regarding the reference site defined in our previous report [1]. To this, the soil samples from the upper five sections (0-10 cm) of "Plateau NE" have been mixed carefully (sum: $\sim$ 5.5 kg) and then separated by size with different techniques and analyzed for radionuclide concentration.

After an initial dry-sieving, separation was completed with multiple wet sieving (washed with ion-exchanged water). The number of cleaning steps for each fraction was dependent on the magnitude of changes in the activity concentration (AC) of the different radionuclides (^{40}K, ^{137}Cs and ^{232}Th). The <36 μm fraction from each cleaning step has been collected into one mass. In the course of the sieving process, the mass distribution compared to that obtained after dry-sieving has dramatically changed.

Table 1. shows the main results of the analyses: the first column defines the theoretical boundaries of fractions, the second and the third contain the results of the first and last cleaning steps, respectively. In each data-cell, the first row shows the total mass of the fraction (g), the second and the third one give the AC of ^{137}Cs and (Bq/kg) with 1σ random error inc. counting and geometric errors, respectively.

Table 1. Mass and radionuclide concentrations for the different size-fractions obtained in wet-sieving.

Fraction [μm]	First wet-sieving	Last wet-sieving
5000-10000	790.0 4.5±0.8 15.5±2.0	744.4 3.7±0.4 15.7±0.2
2000-5000	727.0 7.8±1.0 21.8±1.0	687.1 6.8±0.6 19.3±0.6
1000-2000	299.6 11.6±0.8 26.3±2.2	210.2 12.4±0.8 27.5±1.4
500-1000	127.4 10.9±1.0 85.2±2.0	136.6 10.9±1.0 66.8±3.2
200-500	189.1 12.6±1.0 132.9±4.2	166.9 10.4±0.8 139.0±2.2
125-200	314.3 8.6±1.0 107.8±2.0	129.6 8.2±0.8 135.8±4.8
80-125	393.1 11.0±0.6 62.7±1.0	428.8 6.9±0.8 72.9±1.4
63-80	109.2 11.3±1.2 50.9±2.0	174.2 7.0±0.6 51.9±1.2
45-63	200.5 14.3±1.0 46.5±1.0	158.1 6.4±0.6 39.9±1.8
36-45	108.7 6.9±1.0 33.6±1.0	102.0 5.8±0.6 34.4±0.6
<36	2840 29.3±0.6 58.2±4.0	

The results show a general decrease in the AC(^{137}Cs) of the >36 μm fractions throughout the whole cleaning procedure, some of which was quite spectacular, especially in the range of 45-125 μm. The final picture of AC(^{137}Cs) distribution can be divided into three parts: a relatively rapid inclination at the coarser fractions up to 1000-2000 μm, then a slow but steady decline towards the finer fractions. The <36 μm fraction shows a relatively high caesium value. This trend is completely opposite to the theory. We assume that fractions under 200 μm contain more quartz fragments with smooth surface compared to those between 2000-200 μm which, in contrary, contain more rock fragments with serrated surface. It is highly possible that clay could be trapped in the "holes" created by this serration despite of washing. The difference in rock and mineral composition can also be deduced from the distribution of thorium content of the different fractions. High thorium can be related to volcanic rocks while the majority of the parent material is quartzite. The AC of ^{40}K has also been measured: it ranges from 200 to 350 Bq/kg and shows an inclination with decreasing particle-size.

To remove the remaining clay traces from the above-mentioned "holes", wet sieving has been enhanced with the application of an ultrasonic shaker. Fractions larger than 2 mm have been excluded from these further experiments. In these cleaning procedures some boundaries between fractions had to be changed because of minimum mass requirement of the gamma-spectrometric measurement. During each cleaning step, fractions were shaken at least 12 times for 8 minutes each, carefully wet-sieved in between. The new results obtained are shown in Table 2. which has the same layout as Table 1.

Examining the dataset and comparing it with that in Table 1., it can be seen that this time the biggest changes in AC(^{137}Cs) have been taken place in the coarse fractions. This seems to give evidence to the possibility of the presence of "trapped" clay-particles. At the end of the whole cleaning process, AC(^{137}Cs) shows an almost uniform distribution throughout the fractions. If the values are taken with 2σ error, their average will be approx. 6 Bq/kg. The AC(^{137}Cs) in the <36 μm fraction is 5 times larger than this value. The <36 μm fraction comprises 70% percent of total mass and 90% of total ^{137}Cs activity, which makes it useable as tracer at the particular area. Furthermore, AC(^{232}Th) shows a sharp maximum in the 200-500 μm fraction and an asymmetric distribution. This hints that thorium is attributed to a certain mineral in this particular size range. The "tail" may be the result of in-site weathering of the thorium-mineral bearing bedrock. The further separation of the finer particles and the search for the thorium-mineral is in progress.

Table 2. Mass and ACs for the different size-fractions obtained in ultrasonic assisted wet-sieving.

Fraction [μm]	**1st wet-sieving with ultrasonic**	**2nd wet-sieving with ultrasonic**
1000-2000	156.0 8.3±0.6 20.2±0.2	135.8 5.9±0.6 14.7±1.0
500-1000	118.6 7.0±0.6 67.9±1.6	102.9 5.5±0.6 64.0±1.8
200-500	155.9 7.5±0.8 157.5±6.4	142.4 7.0±0.8 152.7±5.0
100-200	447.2 4.3±0.4 87.1±1.8	457.0 4.7±0.2 88.4±1.0
63-100	222.8 6.3±0.6 43.3±1.6	233.8 6.0±0.6 46.7±0.8
45-63	156.0 4.9±0.4 37.8±0.8	157.4 6.0±0.4 37.5±1.2
36-45	91.0 4.8±0.8 35.4±0.8	88.4 4.6±0.8 35.3±2.6

a) Univ. of Debrecen, Dept of Environmental Physics

[1] Z. Dezső *et al.*, Atomki Ann. Rep. 2003 (2004) 57.

7.1 Radioisotope Tracer Study of Co-reactions of Methanol with Ethanol Using ^{11}C-labelled methanol over Alumina and H-ZSM-5

É. Sarkadi-Pribóczki, N. Kumar[a)], T. Salmi[a)], D.Yu. Murzin[a)], Z. Kovács

The transformation of methanol has been investigated over alumina and H-ZSM-5 in our previous experiments by ^{11}C-radioisotope tracing [1]. The main product in methanol conversion over alumina was dimethyl ether due to Lewis acid sites while over H-ZSM-5 mostly hydrocarbons were formed due to both Lewis and Brřnsted acid sites. With increasing temperature first the ethanol was dehydrated to diethyl ether followed by ethene formation over alumina and H-ZSM-5.

In this work, ^{11}C-labelled methanol as radioisotope tracer was added to non-radioactive methanol for investigation of co-reaction with non-radioactive ethanol over alumina and H-ZSM-5. The ^{11}C-methanol tracer was used to distinguish the methanol derivates and co-reaction derivates of methanol with ethanol against non-radioactive ethanol derivates. The yield of methyl ethyl ether as mixed ether and the influence of ethanol for the yields of C_1-C_5 hydrocarbons were studied as a function of reaction temperature and contact time.

The ^{11}C-methanol was formed by a radiochemical process from $^{11}CO_2$ produced at cyclotron. The mixture of methanol and ethanol was added to ^{11}C-methanol and injected to the catalyst. The catalysis was carried out in a glass tube fixed-bed reactor after its pretreatment. The derivates were analyzed by radio-gas chromatography (gas chromatograph with thermal conductivity detector coupled on-line with a radioactivity detector). The comparative analysis of yields of radioactive and non-radioactive products as a function of reaction temperature gives information about the reaction pathways. Over alumina the yields of dimethyl ether and methyl ethyl ether (co-product) as radioactive and diethyl ether with ethene as non-radioactive main products were monitored as a function of reaction temperature and reaction time in the range of 513-593 K. Alongside ethanol derivates the ethene turns into main product in contrast with methyl ethyl ether and diethyl ether at higher temperature.

In co-reaction over H-modified ZSM-5, while the ethanol was transformed to an olefin (ethene) at lower temperature, methanol reacted to hydrocarbons at higher temperature. Above 553 K, dimethyl ether and lower amounts of methyl ethyl ether were formed compared to these products over alumina, while higher yields of C_3-C_6 hydrocarbons were obtained in comparison with single methanol conversion. This result proves the influence of ethanol (reacting immediately to ethene) in the co-reaction to produce higher yields of C_3-C_5 olefins [2].

It can be concluded that the single methanol transformation was modified by ethanol reactant producing new derivates i.e. mixed ether over alumina and also C_3-C_5 hydrocarbon co-products over H-ZSM-5.

Acknowledgements

This work was financially supported by the Hungarian Scientific Research Fund No. T 048345.

a) Laboratory of Industrial Chemistry, Process Chemistry Centre, Åbo Akademi University, FIN-20500 Åbo / Turku, Finland

[1] É. Sarkadi-Pribóczki, N. Kumar, T. Salmi, Z. Kovács, D.Yu. Murzin, Catalysis Letters 93. (2004) 101, Catalysis Today 100 (2005) 379.

[2] S. Svelle, P.O. Ronning, S. Kolboe, J.Cat. 224 (2004) 115.

7.2 Nuclear microprobe study of heavy metal uptake and transport in aquatic plant species

Zs. Kertész, I. Kocsár, Z. Szikszai and Gy. Lakatos[a)]

In aquatic ecosystems water contamination by trace metals is one of the main types of pollution that may stress the biotic community. Although some metals are needed as micronutrients for autotrophic organisms, they can have toxic effects at higher concentration.

Aquatic plants can take up large quantities of nutrients and metals from the environment, they can live under extreme environmental conditions therefore they are being increasingly used in remediation processes to reduce contamination.

Besides the usually applied bulk analytical techniques quantitative micro-PIXE investigation of the macro, micro and trace element distribution within the root can lead to a better understanding of the heavy metal uptake, transport and detoxification mechanisms of the plants and thus helps to select the proper species for the remedial activity, or possibly to increase the efficiency of the remediation.

In this work we determined the elemental distributions in root cross sections and along the roots of reed (*Phragmaties australis*), bulrush (*Typha angustifolia*) and sea club-rush (*Bolboschoemus maritimus*) using the Debrecen nuclear microprobe. The plants originate from the dried units of the wastewater sedimentation pond system of the tannery of Kunszentmárton. 1500 m^3 waste water containing lime, sodium-salts, ammonium-salts, chromium-salts, sodium, chlorine and magnesium ions, sulphur and organic material was released to the pond system every day till 1988. The chosen species are the dominant species of the area, composing 85-90% of the green plant covering. This heavily contaminated area has been regularly monitored by the colleagues of the Dept. of Applied Ecology of the Univ. of Debrecen since 1998. They focused their work the potentially toxic heavy metal chromium.

In order to conserve the samples in the living state, the roots were frozen in liquid nitrogen. 16-20 μm thick cross sections were made with cryo-microtome, and all the samples were freeze-dried. A proton beam of 2MeV energy and of 100 pA current focused down to 2.5μm×2.5μm was used for the nuclear microprobe measurement. Off-axis STIM and PIXE-PIXE ion beam analytical methods were used simultaneously to determine quantitative elemental concentrations and distributions.

The essential macro-elements like P, K, S, Cl, Si, Na, Ca, Mg were found to be equally distributed along and within the roots, while most of the metals (Fe, Mn, Cu, Zn, Al, Ni, As, Ti, Sc, Hg and Cr) were found in much higher concentrations in the epidermis than in the inner tissues. Furthermore the concentration of metals showed strong positive correlation with the concentration of iron.

Iron plaques were observed on the roots of the bulrush and sea club-rush, while on the root of the examined reed there were no such plaque. In accordance with this observation the iron content of the reed root was 20 times lower than of the other two species, and the concentrations of the non essential elements were an order of magnitude lower in the reed roots too.

Such plaque formation is a known phenomenon. Field observations have shown that wetland plants which can survive in metal-contaminated soils frequently have iron plaque on their root. The uptake of the non-essential and the potentially toxic elements seems to be bound to the presence of these iron plaques.

Although neither of the investigated species is hyperaccumulator, they show high capability to accumulate trace metals in the roots, thus appear to be good monitor of lake contamination.

Ion microscopy study, providing elemental concentrations in a micrometer scale, is proved to be a useful complementation to the bulk analytical techniques in understanding the elemental uptake and transport processes, and heavy metal resistance of these plant species.

a) Dept. of Applied Ecology, Univ. of Debrecen

8.1 Status Report on Cyclotron Operation

Z. Kormány, P. Kovács, I. Szűcs, I. Ander, F. Tárkányi

The operation of the cyclotron in 2005 was concentrated to the usual 9 months; January, July and August were reserved for maintenance and holidays. The overall working time of the accelerator was 3302 hours; the time used for systematic maintenance was 418 hours. The breakdown periods amounted to 42 hours last year. The cyclotron was available for users during 2842 hours. The effectively used beam-on-target time is summarized in Table 1.

Table 1. Statistics of the irradiation time (beam-on-target) for different research groups

Projects	**Hours**	**%**
Nuclear spectroscopy	378	28.0
Nuclear astrophysics	489	36.1
Radiation tolerance test	34	2.5
Nuclear reaction data	95	7.0
Medical isotope production	260	19.2
This layer activation (TLA)	97	7.2
Total	**1353**	**100**

During the summer shutdown period the Cobalt-60 source was moved from vault Nr.6 to vault Nr.3 to make space for the installation of a mass separator transferred from Sweden (OSIRIS). The beam lines used for transporting beams to target stations in vault Nr.3 were dismantled. Using part of the dismantled elements a new beam line for in-beam nuclear spectroscopy on analyzed beam was built in vault Nr.4. Another part of the elements will be used to build a new transport line for the mass separator. Ion-optical calculations for this new beam line have been carried out. Based on their results the design of the line to vault Nr.6 has been started.

8.2 Activities at the Van de Graaff Accelerator Laboratory

L. Bartha

During 2005 the beam time of the VdG-1 machine amounted to 296 hours. The accelerator delivered He^+ and C^+ beams used for low energy atomic physics experiments. The beam time of the hollow cathode ion source – which is also operated on the beam transport of VdG-1 accelerator – is excluded.

The 5 MV Van de Graaff machine was operating for 2025 hours during this period. Proton (38.82 %), D^+ (13.78 %), $^3He^+$ (32.54 %) and $^4He^+$ (14.86 %) particles were accelerated. The beam time was distributed among different research subjects as shown in Table 1.

Table 1. Time distribution among different research activities at VdG-5

Field	Sign	Hours	%
Atomic physics	AP	409	20.20
Nuclear physics	NP	447	22.07
Nuclear astrophysics	NAP	95	4.69
Analytical studies	IBA	967	47.75
Micromachining	MM	95	4.69
Machine tests	MT	12	0.60
Total		**2025**	**100**

Improvements:

During the last months of the year a reconstruction work on the 5 MV VdG machine has been started relating to an EU co-funded Economic Competitiveness Operative Programme (GVOP) won by the institute. Till the end of the year the following improvements on the accelarator have been carried out:

- By means of an earlier designed and fabricated high pressure bellows the plain angle error of the bottom of the vessel has been compensated, and a newly built-in acceleration tube has been adjusted to exactly vertical position

- The column structure of the accelerator has also been aligned to the tube, and the supporting legs of the highest level have been changed to new ones

- In order to improve conductance of the new tube, the pumping cross section of the electron suppressor electrodes has been increased by a factor of three. Due to this modification, for the conductance cacc of the tube the following values have been measured:

for nitrogen: $c_{acc.N} \geq 35$ l/s

for hydrogen: $c_{acc.H} \geq 51$ l/s

In the frame of the GVOP programme the complete vacuum-system of the laboratory will be replaced by oil-free vacuum pumps consisting of piston/scroll fore-vacuum pumps and turbopumps, and all the Wilson type vacuum sealings will be changed for edge welded vacuum bellows parts. Except of a few Viton-sealed connection, everywhere metal gaskets will be applied. Certain beam-lines will be separated off by differentially pumped section from the high purity, carbon free vacuum system.

Till the end of the year 8 fore-vacuum pumps, 6 turbomolecular pumps and their accessories arrived to the laboratory. The fabrication of some other parts of the vacuum system has been started in the workshop of the institute.

8.3 Installation of an isotope separator in Debrecen

Z. Gácsi, J. Gulyás, A. Vitéz, L. Csige, A. Krasznahorkay

An isotope separator named OSIRIS [1,2] was decommissioned in Studsvik, Sweden last July. Researchers there offered this equipment to us for dismantling and moving it over to ATOMKI in Debrecen for installation at the cyclotron lab and save and use it in nuclear physics and other sciences where stable and radioactive isotopes are used extensively for fundamental and applied research.

Since the separator was used to separate radioactive isotopes, the ion source with its beam extracting, shaping, and transporting accessories, as well as the lining inside the bending magnet, furthermore the beam diagnostic and shaping elements in the "switchyard" part of the separator had to stay in Studsvik because of the high radioactive contamination. In order to operate this equipment, first we have to design and manufacture these parts together with a new endstation for the collection and handling of the separated isotopes.

Parallel with the installation, we also concentrate on different applications of an isotope separator, including separation of stable isotopes for labelling special compounds used in many branches of sciences, medical care, and industry, and on studying single ion implantation possibilities, as well as on the production of special targets for nuclear physics research. First we want to separate stable isotopes, and then, when we overcome all technical pitfalls, we will consider using this equipment to separate radioactive isotopes as well.

Our intention is to have this equipment available to anyone at ATOMKI and elsewhere interested in using its capabilities in their own research fields. Consequently, all comments, suggestion, and ideas are welcome now and continuously, since the design and manufacture of parts can then be oriented by taking into account all the suggestions as much as possible.

[1] L. Jacobsson et al., Nucl. Instrum. Methods B26 (1987) 223 and references therein.

[2] B. Fogelberg et al., Nucl. Instrum. Methods B70 (1992) 137 and references tehrein.

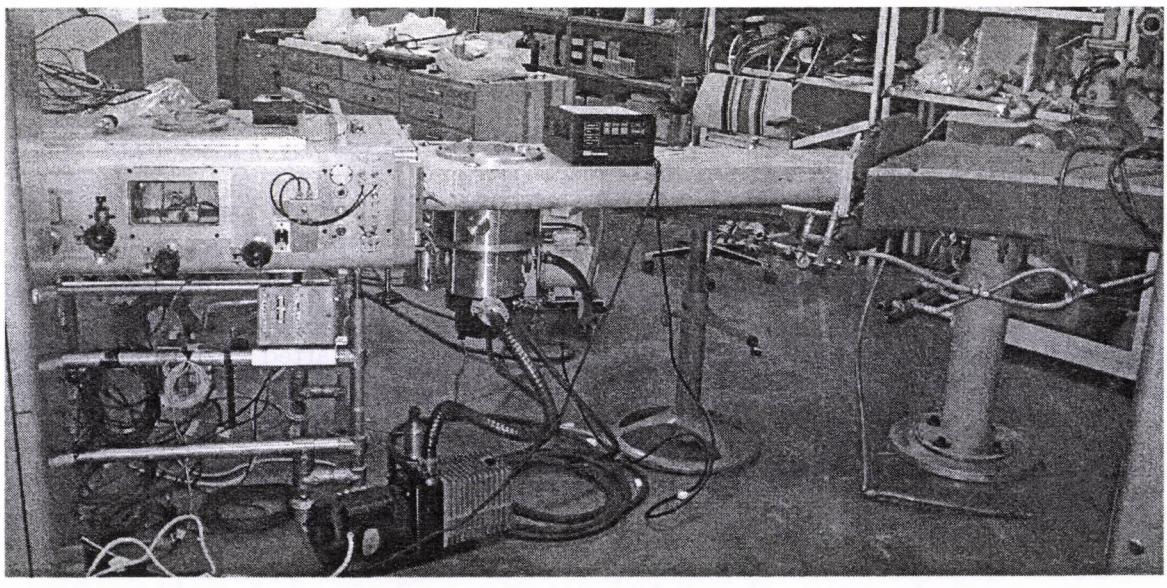

Figure 1. Present status of installation of the separator in the cyclotron lab

8.4 Further investigations of fullerene plasmas

E. Fekete, S. Biri, I. Iván, A. Jánossy[a], J. Pálinkás[b], A. Kitagawa[c], M. Muramatsu[c]

The electron cyclotron resonance (ECR) ion source (ECRIS) of ATOMKI was originally designed for the production of multiply charged heavy ions, but it is suitable to form unusual plasmas, too (e.g. fullerene and it's derivatives)[1]. One of our research goals is to obtain high intensity beams of single and multiply charged fullerenes. Another topic is the research of fullerene modifications in the plasma of the ion source. Last year we concentrated on fullerene and iron mixture plasmas (see below).

To evaporate the fullerene into the plasma in 2005 we used a RIKEN micro oven [2]. The result was a cleaner, more stable plasma. Due to it's small size we could move on-line the oven inside the ECRIS. We achieved record beams of C_{60}^{+} and C_{60}^{2+} ($600nA$ of C_{60}^{+} and $1500nA$ of C_{60}^{2+} at $500V$ and $1kV$ extracting voltage, respectively) by moving the oven deeply into the plasma chamber. The optimal oven distance from the resonant zone was only a few millimeters. These high beam currents were reproducible and the fullerene powder consumption was lower than in earlier experiments, in spite of the applied higher oven power. These results are encouraging especially regarding the research of fullerene modifications, as the beam intensity of the fullerene derivatives is orders of magnitude lower.

Many times we found C_{62} in the mass spectra. Budyka et al.[3] found C_{62} in time-of-flight mass spectrometer with laser desorption, but the peak was wide, showing that the molecule was decomposing during the flight. In our ECRIS the C_{62} peak is sharp, showing that C_2 not only 'flies together' with C_{60}, but is really 'ingested' by the C_{60}.

For the study of iron and fullerene mixture plasmas we used the above mentioned fullerene-oven and a simple filament Fe-oven[4] for obtaining the iron component. In the Fe-oven we tested BN and Al_2O_3 insulators and the Al_2O_3 proved to be better, with less impurities. The iron-oven was fixed, the fullerene-oven was movable. During the experiments we concentrated on smaller fullerenes (with less than 60 carbon atoms), because the smaller fullerenes are less stable, so they are more likely to form compounds. We could not find FeC_{60}, but we found two stable, sharp, reproducible peaks at $m/q = 752$ and $m/q = 376$. We carefully analyzed many beam spectras (at different settings of the ion source, different oven temperatures) and we concluded that these peaks have to be $(FeC_{58})^{+}$ and $(FeC_{58})^{2+}$.

With a little tuning of the plasma we could form a special plasma where both C_{62} and FeC_{58} were present in the mass spectras.

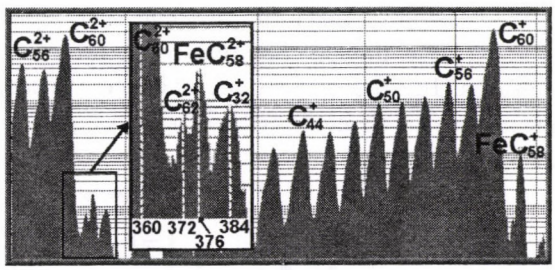

Figure 1. A spectrum where both C_{62} and FeC_{58} are present (1+ and 2+).

In the near future we plan to guide the ion beam onto a foil and analyze the deposited material by off-line methods.

a) University of Technology and Economics, Budapest, Hungary

b) University of Debrecen, Debrecen, Hungary

c) Nat. Inst. Rad. Sci. (NIRS), Chiba, Japan

[1] S. Biri et al., Rev Sci. Instrum. 73 (2002) 881-883.

[2] M. Kidera et al., Proc. 15^{th} Int. Workshop on ECR Ion Sources, Jyväskylä, Finland, 2002

[3] M. F. Budyka et al., Chemical Physics Letters 354 (2002) 93-99

[4] Y. Kato, M. Tomida, S. Ishii, Rev Sci. Instrum. 75 (2004) 1919-1921

8.5 An evaluation of X-ray microanalytical techniques using reference materials

A. Simon, Á.Z. Kiss, I. Gomez-Morilla[a], R. Simon[b], C.T. Williams[c], G.W. Grime[d]

Techniques for microanalysis using X-ray emission spectrometry are growing in importance as the technological development moves from the micro to the nano scale. It will be increasingly important to be able to make comparable measurements on this scale using a variety of X-ray excitation methods. A number of standards were investigated for suitability, but BCR 126A glass standard proved to be the best option. For the inter-comparison measurements the following X-ray microanalysis techniques were employed: Particle Induced X-ray Emission (PIXE); Synchrotron X-ray Fluorescence Microanalysis (μ-SRXRF) and Wavelength Dispersive X-ray Spectrometry (WDS).

Series of sequential analyses at the same spot on the glass were carried out to measure the precision of the four different x-ray spectrometry techniques. The relative standard deviations (RSD) of the elemental concentrations measured for elements with Z > 13 are plotted in Figure 1.

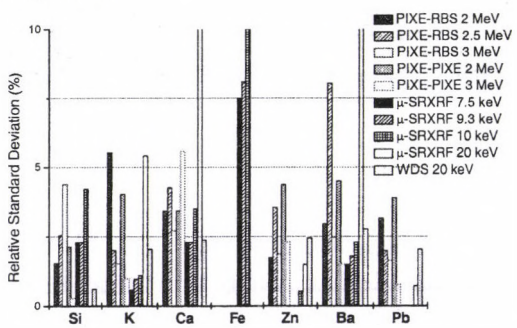

Figure 1. Relative Standard Deviation of the elemental concentrations (Z > 13).

The precision of the techniques is generally better than 5%, with mean values over the four techniques of 2.3% for Si, 2.5% for K, 5% for Ca, 2.3% for Zn, 5% Ba, and 2% for Pb. Fe, which is present in this glass in a very low concentration (0.004 % wt), is only detected and quantified with μ-SXRF at low energies (up to 10.0 keV), with an average precision of 11%.

With a homogeneous sample, the deviation of the individual measurements from the certified values gives an estimation of the accuracy of the analytical technique. This has been investigated by analysing the glass at randomly selected spots with the different techniques and at different beam energies.

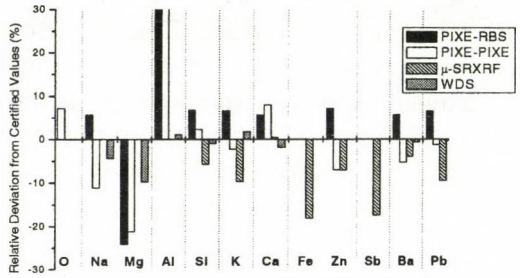

Figure 2. Relative deviations from the certified values of the elemental concentrations measured at random points on the sample.

Overall, the deviation from the certified values is well below 5% for elements such as Si (3.3%), K (3.5%), Zn (4.7%) Ba (4%) and Pb (3%). Other elements such as O, Na, Ca also present small deviations from the certified values (7%, 7% and 5% respectively). Conversely, Mg, Al and Fe deviate as expected. Further details on this work can be found in [1].

Acknowledgements

This work was implemented within the EU 5th Framework Programme (MICRO-XRF).

a) Advanced Technology Institute, Univ. of Surrey, Guildford GU2 7XH, U.K.

b) Institute for Synchrotron Radiation, Forschungszentrum Karlsruhe GmbH, Hermann von Helmholtz Platz 1, Eggenstein-Leopoldshafen D-76344, Germany

c) Dept. of Mineralogy, The Natural History Museum, London SW7 5BD, UK

d) Dept. of Physics, Univ. of Surrey, Guildford GU2 7XH, U.K.

[1] I. Gomez-Morilla, A. Simon, R. Simon, C. T. Williams, Á.Z. Kiss, G.W. Grime: An evaluation of reference materials for PIXE and other X-ray microanalysis techniques, Nucl. Instr. and Meth. B, in press

8.6 Study of advantages and limitations of Si pin diodes as radiation detectors

G. Kalinka M. Novák Á.Z. Kiss N. Skukan[a)], M. Jakšić[a)], A. Simon

A new research activity in collaboration with the Ion Beam Laboratory, Department of Experimental Physics, Ruđer Bošković Institute was started in 2005 within the framework of the Hungarian-Croatian Intergovernmental Science & Technology Cooperation Programme. The aim of our project is to characterise the spectroscopic features of Si pin photodiodes using nuclear microprobe techniques. The results of the characterisation will be used for the improvements of spectroscopic features as well as for the assessment of possible new applications of these simple devices, including various aspects of nuclear spectroscopy. Possibility to create radiation damage by selective irradiation using nuclear microprobe will be included in the investigation in order to extend application possibilities to position sensitive operation and particle identification.

In order to select the Si pin detector of the best quality for ion beam modification, electrical characterizations of three pin photodiodes (two Hamamatsu S5821-02 and one BPX 65 from Centrovision) were done. The measurement of the I-V and C-V characteristics was implemented in the Radiation Detector Laboratory of ATOMKI in the range of 0.0005V and 300V bias voltages. These measurements give information on the depth distribution of generation centers and ionized impurities, respectively. Noise measurement enables the separation of series (Johnson), parallel (shot), 1/f and dielectric loss noise components.

Our results show that Hamamatsu S5821-02 is the best candidate for further ion beam modification as the measured current at a given bias voltage is two orders of magnitude less than that of the other diodes. It means that both the electrical noise and impurity level is the smallest of this diode, i.e. it has the best quality for our purpose. Therefore we chose this diode for future high lateral resolution ion beam investigations. This will help us to minimize artefacts in the charged particle spectra and to separate different effects of radiation damage or structure modification we aim to create via ion implantation.

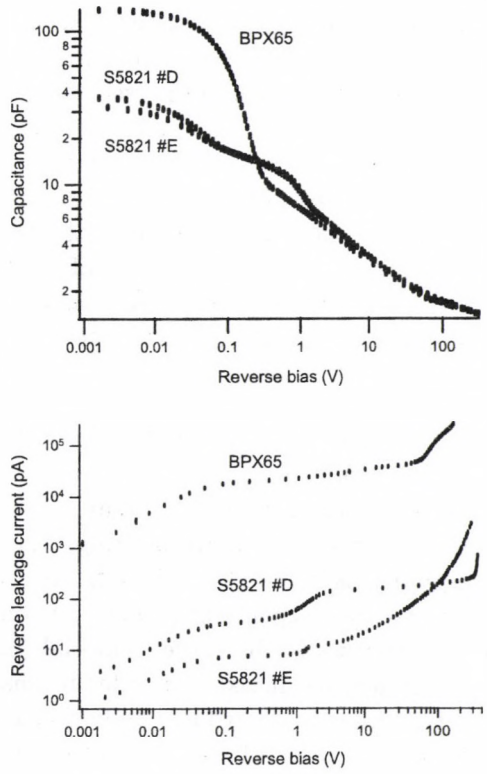

Figure 1. C-V and I-V curves of the different Si pin diodes.

Acknowledgements

This work was supported by the Hungarian Research and Technology Innovation Fund and the Croatian Ministry of Science, Education and Sports within the framework of the Hungarian-Croatian Intergovernmental Science & Technology Cooperation Programme (Project code: HR-31/2004).

a) Department of Experimental Physics, Ruđer Bošković Institute, P.O. Box 180, 10002 Zagreb, Croatia

8.7 Proton Beam Writing

I. Rajta, E. Baradács[a)], S.Z. Szilasi, I. Csige

Refractive index depth profile in PMMA due to proton irradiation

Proton Beam Writing has been successfully used to create buried channel waveguides in PMMA [1,2], which suggested that proton irradiation increases the refractive index. To investigate this effect, PMMA samples were irradiated by 1.7-2.1 MeV proton beam. Spectroscopic Ellipsometry has been used to investigate the depth profile of the refractive index. An increase of the refractive index was observed in the order of 0.01, which is approximately one order of magnitude higher than the detection limit. The highest increase of the refractive index occurs at the end of range, i.e. we found a good correlation with the Bragg curve of the energy loss.

Hardness changes in PMMA due to proton beam micromachining

As protons penetrate a target material and lose their energy according to the Bragg curve, the energy loss is different at different depths. This causes depth-dependent changes of some physical properties in the target material (e.g. refractive index, hardness). In order to characterize the changes of hardness and other mechanical properties as a function of beam penetration depth, systematic investigations have been performed on PMMA, the most common resist material used in proton beam micromachining.

Silicon check valve made by proton beam micromachining

The possible application of Proton Beam Micromachining (PBM) has been demonstrated by a few authors [3,4] for creating 3D Si microstructures. In this work we present alternative methods for the formation of a simple a non-return valve for microfluidic applications. Two different approaches have been applied, in both cases we exploited characteristic features of the PBM technique and the selective formation and dissolution of porous Si over the implantation damaged areas.

In the first case we implanted 10 μm thick cantilever-type membrane of the valve normally to the crystal surface and at 30-60 degrees to the sidewalls of the flow channel, which were also implanted at the same irradiation. During the porous Si formation we developed the sample 6-8 μm deeper than the implanting ion range damaged the crystal. Due to the isotropic nature of the porous Si etching, the thick sidewall blocks are still connected to the crystal while the thin membranes detached from the bottom, and they are only connected to one of the sidewalls.

The other construction utilized the goniometer facility mounted on the microbeam chamber, we implanted the samples at 40 degrees tilt, and developed the samples not as deep as the ion range. This way both the sidewalls and the membranes are attached to the bottom of the sample.

The SEM images of the samples showed that both of these types of valves can be actively working, however, the thickness of the moving membrane requires extremely large force according to the fluidic tests. In order to achieve a successful demonstration of the functionality, the membrane rigidity should be reduced by decreasing the wall thickness.

Reduction of optimal fluence by CO_2 treatment after exposure and vacuum effects in proton beam micromachining of CR-39

CR-39 has been shown to be a suitable material as a thick resist for Proton Beam Writing [5]. These samples are normally used to detect single alpha particles in normal air conditions. However, to use this material as proton or alpha micromachinable resists, we need to irradiate the samples in vacuum. In this work, we investigated the effects of vacuum on the micromachinable properties of CR-39. Our investigations proved that there were no drawbacks of the vacuum storage of the samples, so we concluded that CR-39 is a suitable material as

a PBM resist in this respect, too.

Another part of the current work concentrated on the effect of post-irradiaton CO_2 treatment of the samples. Such a treatment increased the radiation sensitivity of CR-39, i.e. decreased the necessary optimal ion fluence. We have found that approximately 60% of fluence that of not-treated samples was enough to fully develop the radiation damaged structures.

Proton beam micromachined channels in negative tone resist materials

Tilted structures are very interesting for various applications, such as photonic crystals and gas/liquid handling on chips. The fabrication of thick tilted structures is a challenging task for the conventional (optical and electron beam) lithographic technologies. X-ray lithography has been proved capable to produce tilted structures of very fine resolution but at a very high cost due to the required delicate mask. The use of proton beam irradiation has already been proved very successful to the patterning of thick resist films with very high aspect ratio and vertical sidewalls [6]. Proton Beam Writing (PBW) is promising for the fabrication of tilted structures due to the fact that the proton beam does not broaden significantly (e.g. a 2MeV proton beam allows the patterning of 50 μm thick resist films). PBW is a direct write method, i.e. it is a maskless process which is an obvious advantage for research applications. In the present work the Atomki microprobe facility [7] has been used to write long tilted structures by 2MeV protons. For the formation of the structures, two exposures have been carried out at $+20°$ and $-20°$ using a goniometer stage sample holder. The tilted structures were resolved in the negative tone resist materials SU-8 [8] and ADEPR (an aqueous base developable chemically amplified resist) [9]. The length of the microchannels was varied between 100 μm and 1000 μm, the wall thickness was 10 μm. By applying the developed methodology it was possible to resolve the desired layout through the whole length of the channel.

Acknowledgements

This project was supported by the Hungarian National Research Foundation OTKA (Grant Nos. A080, M041939, M36324 and F42474). One of the authors (I.R.) was a grantee of the Bolyai János Scholarship.

a) Univ. of Debrecen, Dept. of Environmental Physics

[1] T.C. Sum *et al.*, NIM B210 (2003) 266.

[2] A.A. Bettiol *et al.*, NIM B231 (2005) 364.

[3] P. Polesello *et al.*, NIM B158 (1999) 173.

[4] M.B.H. Breese *et al.*, NIM B231 (2005) 357.

[5] I. Rajta *et al.*, NIM B231 (2005) 384.

[6] F. Watt, NIM B158 (1999) 165.

[7] I. Rajta *et al.*, NIM B109 (1996) 148.

[8] C.N.B. Udalagama *et al.*, NIM B210 (2003) 256.

[9] I. Rajta *et al.*, NIM B231 (2005) 423.

8.8 Multiwire Proportional Counter (MWPC) for e^- e^+ angular correlation measurements

A. Vitéz, Z. Gácsi, J. Gulyás, A. Krasznahorkay

In a project of searching for a 9-MeV neutral boson we have got a breakthrough last year. We could observe, for the first time, e^- e^+ pairs from a 10.95 MeV $0^- \rightarrow 0^+$ strictly forbidden transition in ^{16}O [1]. In order to get a better signature for the existence of the new particle and to determine their mass more precisely, angular correlation measurements were planned.

Position sensitive detectors with low energy loss for the e^- e^+ pairs were needed. The most suitable choice for this purpose was turned out to be a gas filled MWPC detector. The MWPC consists of a set of thin, parallel anode wires stretched between two cathode planes. Electrons released by ionization in the working gas of the chamber drift towards the anode wires and experience ionizing collisions in the high electric field in the vicinity of the thin wires. Avalanche multiplication provides a large gain (10^5) to the charge signal.

The mechanical construction of the detectors is as follows: The cathode planes consisting of also wires (diameter: 0.1 mm, silver plated copper) stretched in one side in x and at the other side in y directions. The signals on those wires were used for getting the position of the hits. The anode wires (diameter: 10 μm, gold plated tungsten) are welded onto single-sided printed circuit boards. Between the anode and cathode planes, 7-mm gaps were applied. The whole system is encapsulated in an aluminum box for electrical shielding. This box has two windows covered with 10 μm mylar foil avoiding extra energy loss of the pairs. The counting gas is supplied via plugs in holes drilled in the aluminum box. The gas flow was regulated. The gas pressure was only slightly exceeded the atmospheric pressure. The usual P10 gas mixture of Ar(90%) + CH_4 (10%) was used for the first time, then we turned to a Ar(50%) + C_2H_6(50%) mixture in order to get a faster drift time for the electrons.

We did not read out all of the signal wires separately but we used resistive and delay readouts. In the first case the signal wires were interconnected by resistors. One end of the resistor chain was grounded and the other one was connected to usual charge sensitive preamplifier. The total charge was also collected with a preamplifier connected to the anode wires. Conventional spectroscopy amplifiers with shaping times of 2 μs was used to amplify the signals. After digitizing both signals separately for the x and y directions, their ratio supplied the position information for both directions. By using low noise preamplifiers this method could be used with relatively low gas multiplication factor (U = 3000 V) allowing stable working conditions. However, the large shaping time used in the amplifiers caused distortions of the spectra at higher counting rates and the capacitance of the wires caused nonlinearities in the position readout.

In order to get better linearities and higher counting rate capabilities we changed to delay line readout, when the signal wires were interconnected by delay lines (2 ns/tap). Fast, current sensitive preamplifiers were used at both ends of the delay line, which were connected to fast timing filter amplifiers and constant fraction discriminators. In this case the time difference measured at the ends of the delay lines supplied the position information. We had to use larger gas multiplication factor in this mode with high voltages close to the discharge voltage (U = 4000 V), but the performance of the detectors was definitely better compared to the resistive readout. We could reach a position resolution of 1 mm, which corresponded to <2 degrees in angle resolution.

[1] A. Krasznahorkay *et al.*, Atomki Ann. Rep. (2004); AIP proceedings **802** (2005) 236; Acta Phys. Pol.**B37** 239.

8.9 Determination of self absorption features in an ^{241}Am α-source

G. Kalinka and M. Novák

Radionuclide α-sources are convenient tools for the characterization of nuclear detectors. These thin sources are made by methods (evaporation, electro-deposition, implantation, etc.) which keep the energy loss of emerging alphas low. For delicate detector measurements an accurate knowledge of the energy loss inside the source is needed. A simple and commonly used method is to measure the energy of the α-particles as a function of the emission angle θ, relative to source surface normal, thus varying the effective thickness x=x/sin(θ) of the absorbing layer.

Recently we have been evaluating silicon pin diodes for their applicability as high quality particle- or x-ray detectors using a commercial ^{241}Am alpha source deposited on a stainless steel plate.

These diodes, if not collimated, exhibit rather complex spectra – in addition to the inherently complex alpha structure of ^{241}Am – due to the differing energy loss in specific parts of the diode: central region, electrode metallization, edge protection, etc. In order to unfold minute details of such spectra, a powerful fitting routine has been written. This program describes each line in the spectrum as a sum of a Gaussian, two exponential tails and a flat background component. This program was also used for the evaluation of angle dependent response of the source taken with a commercial photodiode. In addition to the normally sought peak position data, obtained as the center of gravity of the Gaussian plus the short exponential tail, the FWHM width of the Gaussian and the slope parameter of the short exponential are also shown here (for the central part of the diode). Using a linear fit, 7.5±0.5 keV is obtained for the energy loss, corresponding to ~40 nm Fe equivalent absorber thickness. Due to it's low activity, the active source layer is only about 0.2 nm thick, therefore significant self absorption in it can not be assumed.

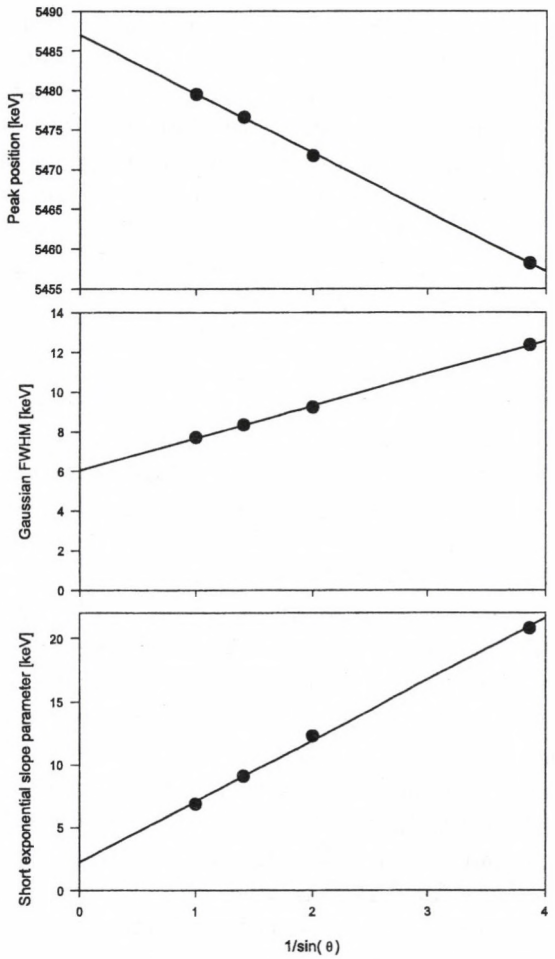

A surprising, hitherto unnoticed result is the major contribution of the alpha source to the slope parameter, and a minor one to the Gaussian width. The low (2.25 keV) intercept value in the former, and a larger one (6.04) in the latter are expected only to originate from the detector itself.

Complementary investigations of the angle dependent response of Si pin diodes are under way. The interpretation of those results must, however include detailed consideration of charge collection processes as well.

8.10 Cross-sections for deuteron induced γ-ray emission analysis of light elements

G.Á. Sziki, A. Simon, Z. Szikszai, Zs. Kertész, E. Dobos, I. Uzonyi, Á.Z. Kiss

With the aim of providing fundamental cross-section data for deuteron induced gamma ray emission analysis (DIGE), and eliminate the application of standards from routine analytical work, thin target gamma ray yields of the $^{6}Li(d,p\gamma)^{7}Li$, $^{9}Be(d,n\gamma)^{10}B$, $^{11}B(d,p\gamma)^{12}B$, $^{16}O(d,p\gamma)^{17}O$ and $^{19}F(d,p\gamma)^{20}F$ nuclear reactions were measured in the 0.6–2 MeV energy range with fine energy resolution.

The measurements were carried out on the 5 MV Van de Graaff accelerator of ATOMKI. Thin targets were made by vacuum evaporation or DC reactive magnetron sputtering [1]. The chemical and thickness analysis of the targets were performed with Rutherford backscattering spectrometry (RBS) both with 2 MeV H^+ and 2.5 MeV He^+ focussed ion beams.

Fitting an adequate function to the measured yields below 1 MeV, we extrapolated them to the 0–0.6 MeV energy range and then converted data into cross-sections through a novel procedure. Values were calculated for the most dominant 478 keV (Li), 718 keV (Be), 953 keV and 1674 keV (B), 871 keV (O) and 656 keV (F) gamma lines. Results for boron are shown in Fig. 1 for demonstration.

This kind of systematic and uniform cross-section data set for the accurate DIGE analysis of light elements has not been available in the literature in this extent. The presented cross-section curves are useful tools for the analysis of thin targets and serve as input parameters for the concentration calculus of thick and intermediate thick samples.

The paper containing the details and final results is under publication [2].

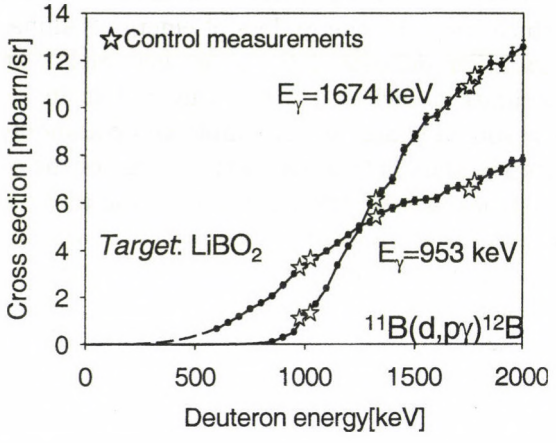

Figure 1. Gamma ray production cross-section curves of the $^{11}B(d,p\gamma)^{12}B$ nuclear reaction for the analytically most suitable 953 keV and 1674 keV γ-ray lines.

Acknowledgements

This work was supported by the International Atomic Energy Agency under the CRP contract No. 13261/R0.

[1] A. Csik, G. Langer, D.L. Beke, Z. Erdélyi, M. Menyhárd and A. Sulyok, Journal of Appl. Phys. 89/1 (2001) 804.

[2] G.Á. Sziki, A. Simon, Z. Szikszai, Zs. Kertész, E. Dobos, I. Uzonyi, article submitted to Nucl. Instr. and Meth B.

8.11 Refining the CO_2 absorption method for low level ^{14}C liquid scintillation counting in the ATOMKI

M. Molnár, É. Svingor, S. Nagy[a], *I. Svetlik*[b]

A new method of chemical sample preparation for liquid scintillation ^{14}C measurements was implemented in the Laboratory of Environmental Studies of the Institute of Nuclear Research of the Hungarian Academy of Sciences (ATOMKI).

The developed absorption method is quick, inexpensive and simple. In a special preparation line CO_2 samples are absorbed in CarboSorb absorbent. The developed line consists of a gas-bag CO_2 container (PG), a freezing finger for easier CO_2 transport, a fine- regulation valve (VG), a bubbler filled Hg for gas-flow control (Hg), a puffer bulb for initial pressure reduction (PB), and the vial containing CarboSorb (CS) (Figure 1.).

For the exact determination of the amount of the absorbed CO_2 gas two independent techniques were applied (direct weighing of vial and measuring of the amount of the rest CO_2 gas).

Several tests were executed with old borehole CO_2 gas (Linde Hungary Ltd. Répcelak, Hungary) without significant content of ^{14}C. This gas has been used as background gas in our gas proportional counter (GPC) system. Tests were also performed on samples of known ^{14}C activities between 29 and 7000 pMC, previously measured by GPC. The ^{14}C activities of all prepared samples were measured by liquid scintillation counter (LSC) including quenching parameter (tSIE).

The observed agreement between LSC and GPC data was really good in the case of several samples. We demonstrated the reproducibility of the sample preparation and the stability of the prepared counting mixture.

We have determined parameters for measurements in our TRI-CARB 3170 TR/SL liquid scintillation counter (LSC) including optimised ^{14}C window with counting efficiency (65.3 %) and the corresponding ^{14}C dating limit (31.200 yr BP). The combined uncertainty of the determination was about 2 % for recent carbon samples. Thus, the presented method is suitable for ^{14}C determination and dating of geological, hydrological, and environ-

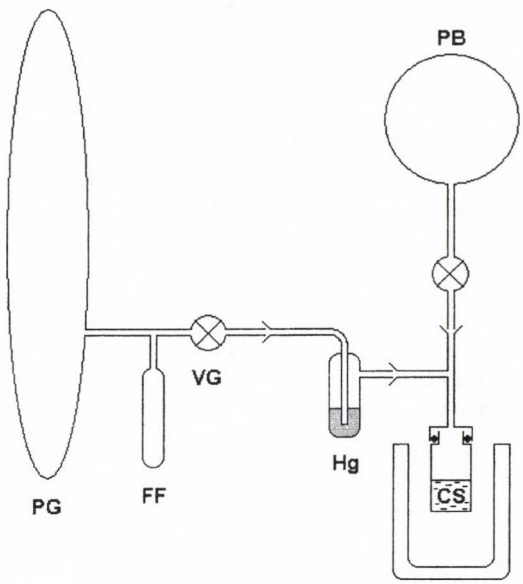

Figure 1. Schematics of CO_2 absorption line.

a) University of Debrecen, Egyetem tér 1, 4001 Debrecen, Hungary

b) Department of Radiation Dosimetry, Nuclear Physics Institute AS CR, Prague, Czech Republic

8.12 An arrangement for investigation of semiconductor detector response functions

T. Papp, G. Kalinka, I. Török

We have presented in many papers that the majority of the atomic physics parameters obtained in physics measurements based on x-ray detection occasionally contradict basic conservation rules, like parity, angular momentum and energy conservation. We have seen significant contradictions in analytical works, based on x-ray detection as well. We are specially worried using such a technique at air quality measurements, which become popular in recent years.

There are elaborated csalibration procedures for the x-ray detectors, however, the above observations indicate that either they are not sophisticated enough, or the system is changing its behavior in time. One of the approaches of describing the system is to assume all sorts of dead layers incomplete charge collection layers, and using Monte Carlo approaches to verify, the assumption. This approach has not considered the potentiality that the signal processing electronics could modify the spectrum.

To look for the details of such a possibility, we used our x-ray crystal diffraction spectrometer as an x-ray monochromator. A new Soller slit was developed to improve the resolution. Although we are aware of the limitations of an x-ray monochromator, as the Si(Li) and HPGe detectors are of high quality, and the peak width at the thousandth and ten thousandth might be better than the breadth of the quasi monochromatic peak from the monochromator at these levels. However, with differential measurements such issues can be overcome at a sufficient level.

We have studied several detector and electronics performances, and our basic assumption that it is improper to use the electronics as a black box with unit performance, was overwhelmingly verified. We have identified structures in the spectra related to electronics, observed significant signal identifying efficiency differences between various electronics, furthermore the event recognition capability was x-ray energy dependent.

The basis of the general neglect of such a potentiality from the detector efficiency calibration, remain a mystery to us.

8.13 Monte Carlo simulations of possible Ge arrays for the DESPEC setup at FAIR

A. Algora, A. Jungclaus[a], L. Caballero[b], B. Rubio[b] and J.L. Tain[b] for the DESPEC Collaboration

The experiment DESPEC is part of the low-energy branch project of the future installations at FAIR (GSI) and will be devoted to the study of the decay properties of exotic nuclei. The basic instrumentation for this experiment consists of an active catcher, a Ge array and neutron detectors. Presently the collaboration is considering two possible setups for the Ge array. One possibility is to use an array of stacks of planar Ge detectors specifically designed for DESPEC. The other alternative is to use standard segmented Ge detectors of EXOGAM [1] or TIGRESS [2] type. The Ge array will surround a focal plane of 24×8 cm^2. The R&D phase requires the realization of Monte Carlo simulations in order to determine the optimal setup for the future facility.

The "planar setup" consists on an array of 24 composite planar detectors (see Fig. 1). Each detector unit is formed by a stack of three planar Ge detectors with dimensions $72 \times 72 \times 22$ mm^3 with an active Ge volume of $68 \times 68 \times 22$ mm^3. The distance between the planars is 3 mm and the stack is encapsulated in an Al capsule of 1.5 mm thickness.

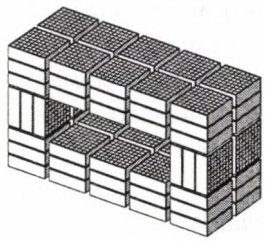

Figure 1. Schematic view of the planar setup.

The "CLOVER" setup is an array of 6 CLOVER detectors of the EXOGAM type. In this setup the detectors are positioned in an annular arrangement around the focal plane. Four CLOVER detectors are facing the longer side of the focal plane (two detectors on the top, two detectors on the bottom), while the other two detectors face the shorter sides of the focal plane.

The two described geometries have been implemented using the Monte Carlo code GEANT4 [3]. In this framework, we have studied the detection efficiency of the two setups either for point-like or extended monoenergetic sources. In Table 1. the results for the two setups are presented for centered point-like sources. The quoted peak efficiencies correspond to the sum of the individual detector efficiencies of each setup.

As part of our study, efficiencies have been also calculated for other possible geometrical arrangements with more detectors (8 CLOVER detectors), and for a focal plane of 8×8 cm^2. The possibility of an arrangement that optimizes the coupling to a neutron detector array has been also studied. The next step of our work will be the study of the performance of tracking algorithms for the different setups as well as their γ-imaging efficiency.

Table 1. Calculated efficiency (%) of the studied setups for point-like sources.

Energy	Planar array		Clover array	
(MeV)	Peak	Total	Peak	Total
0.10	48.4	53.7	36.4	46.3
0.25	34.5	57.4	30.7	46.2
0.50	21.0	55.6	23.5	43.6
1.00	13.3	50.3	18.0	40.7
2.00	8.9	44.5	12.9	36.6
5.00	4.1	39.6	7.1	32.8
10.00	1.8	36.7	4.0	28.7

Acknowledgments

A.A. acknowledges support from the MERG-CT-2004-506849 contract, and from the János Bolyai fellowship.

a) Univ. Autonoma de Madrid, Madrid, Spain

b) IFIC, CSIC-Univ. de Valencia, Valencia, Spain

[1] http://www.ganil.fr/exogam/

[2] H. C. Scraggs *et al.*, Nucl. Inst. and Meth. A543 (2005) 431

[3] S. Agostinelli *et al.*, Nucl. Inst. and Meth. A506 (2003) 250

8.14 Electrostatic electron spectrometer based on two cylinders without axial symmetry

D. Varga and K. Tőkési

During the last decades electrostatic analyzers were widely used in atomic and surface physics. This was due to their good focusing and dispersion properties, The cylindrical mirror analyzer (CMA) is one of the most advantageous electrostatic analyzers. Its second order focusing properties have been calculated by many authors. A modified, so called "box" type, CMA (ESA-13) is described in ref. [1].

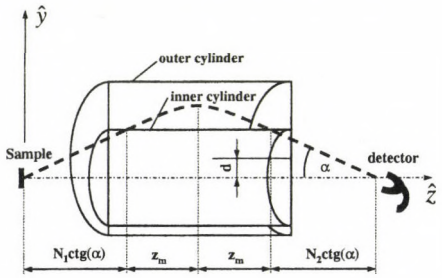

Figure 1. Schematic cross section of the calculated electrostatic analyzer with typical electron trajectory along the spectrometer axis z.

For CMA (ESA-13), the position of the electron source and focus are outside the analyzer which is desirable for practical reasons. The ends of the cylinders are closed with two coaxial discs, therefore the electrostatic field near the edge is distorted compared to the logarithmic field existing in the classical "infinite" cylindrical mirror analyzer. However, the "box" type distorted field cylindrical mirror analyzer geometry contains several limitations regarding the irradiation of the sample. Therefore, the construction of these analyzers was changed by replacing the endings of the analyzer with conically shaped electrodes [2] ensuring a better accessibility for excitation. But among the various experimental tasks many geometrical conditions arise that are different or that need different sizes compared with the previous ones. Therefore, in a practical point of view, it is extremely advantageous to have different variations of spectrometers. This allows us to choose the best solution for a given problem.

In this work, we present electron-optical properties of a mirror type electrostatic electron spectrometer consisting of two cylinders with eccentricity (see Fig1.), namely the Eccentric Cylindrical Mirror Analyzer (ECMA). The designed analyzer is a possible variation of CMA for measuring the energy distribution of electrons with high energy resolution or making an electron monocromator. It has been shown that the Eccentric Cylindrical Mirror Analyzer has second-order focusing properties with remarkable dispersion (see Fig2.) [3].

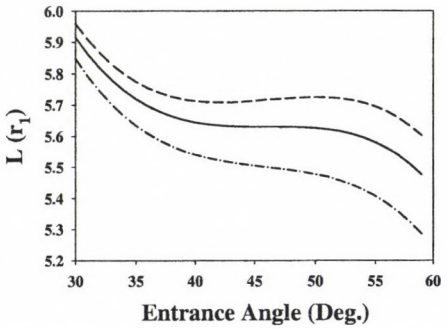

Figure 2. The focal length (L) as a function of the entrance angle of the electron trajectories with respect to the analyzer geometrical axis (point source - point focus). Dashed-dotted line: k=1.715, solid line: k=1.740, dashed line: k=1.780.

Acknowledgements

The work was supported by the Hungarian Scientific Research Foundation: OTKA No. T038016, and one of the authors (K.T.) is a grantee of the Bolyai János Scholarship.

[1] D. Varga, I. Kádár, Á. Kövér, L. Kövér, Gy. Mórik, Nucl. Instrum. Meth. 154 (1978) 474

[2] K. Tőkési, L. Kövér, and D. Varga, Nucl. Instr. and Meth. A 348 (1994) 173

[3] D. Varga, and K. Tőkési, Surf. Interface Anal. 2006 in press

8.15 Computer code for molecular dynamics simulations

I. Lévay and K. Tőkési

Molecular Dynamics (MD) simulation is a widely used technique for modeling complicated physical phenomena. In materials science, the trajectories of a number of interacting atoms (from 10^2 to 10^5 atoms) over a given time interval are calculated numerically. The technique allows us to model the complex dynamical behavior of materials, provided that the relevant spatial and temporal correlations can be contained within the finite size and time span of the simulation.

During the last few years, experimental and theoretical research activities have turned to the fusion research again. One of the interesting classes of these investigations is the study of material damage, surface modification, and plasma-wall interactions. Our special interest of this field is to simulate the He and/or Be atom motion in Be crystal. MD simulations has been quite successful in performing such calculations. Therefore we are developing a MD simulations code for PC computers. The computer code is written in C++ object-oriented programming language. The aim of the present work is twofold: a) to develop a fast computer code for the study of random walk of guest atoms in Be crystal, b) 3 dimensional (3D) visualization of the particles motion. In this case we will mimic the motion of the guest atoms in the crystal (diffusion-type motion), and the motion of atoms in the crystal-lattice (crystal deformation). As an example, Fig. 1 shows the Be crystal-lattice generated by our recently developed MD code. The regular Be atoms are indicated by green sphere. The blue sphere represents the selected atom. During the calculation the trajectory of the selected atom (blue in the Fig.1) can be analyzed. We have a few options to select the interaction potential among the particles. In the present version of our MD code the classical nonrelativistic equations of motions for a many-body system are solved numerically. The 3D potential distribution inside the crystal can be scanned as function of time. Further works are in progress to improve our code.

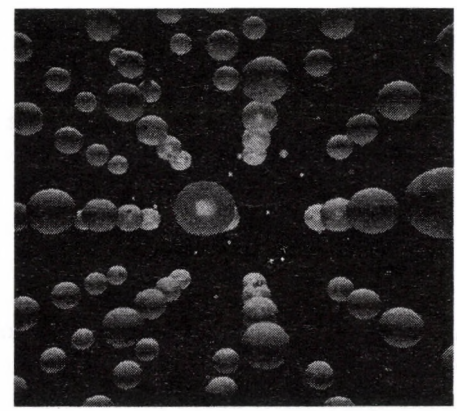

Figure 1. 3D visualization of the Be crystal. Green sphere: Be atom, red small sphere: electron, blue sphere: selected Be atom.

Acknowledgements

The work was supported by the Hungarian National Office for Research and Technology.

8.16 3D visualization of classical trajectories in ion-atom collisions

L. Budai, A. Pénzes, Á. Korda, J. Somodi, K. Tőkési

Collisions among energetic particles are fundamental processes of nature having importance in many different areas of research and technology. Therefore, the understanding of the detailed interactions between atomic particles is of continuing interest. The key point of the calculations is the proper description of the collisions. The classical trajectory Monte-Carlo (CTMC) method [1] is a good candidate for theoretical interpretations. It is a non-perturbative method. All interactions between the colliding partners can be taken into account exactly during the collision. However, we have to keep in mind that the CTMC method is a pure classical method and quantum-mechanical properties of the collisions cannot be reproduced with it. Nevertheless, the CTMC method is a very useful tool for the estimation of basic properties of various collision systems.

On the other hand, certain characteristic of the atomic processes can be demonstrated with the help of individual trajectory calculations. For this reason we developed a code for the three-dimensional (3D) visualization of the classical trajectories in ion-atom collisions. Details of the computer code can be found in Ref. [2]. As an example, Fig. 1. shows the classical trajectories in collision between 25 eV electron and hydrogen atom. The snapshots of the collision can be seen as follows: the incoming region (Fig. 1a), the core region (Fig. 1b), and the asymptotic region (Fig. 1c). A movie of the 3D motion can be seen at [3].

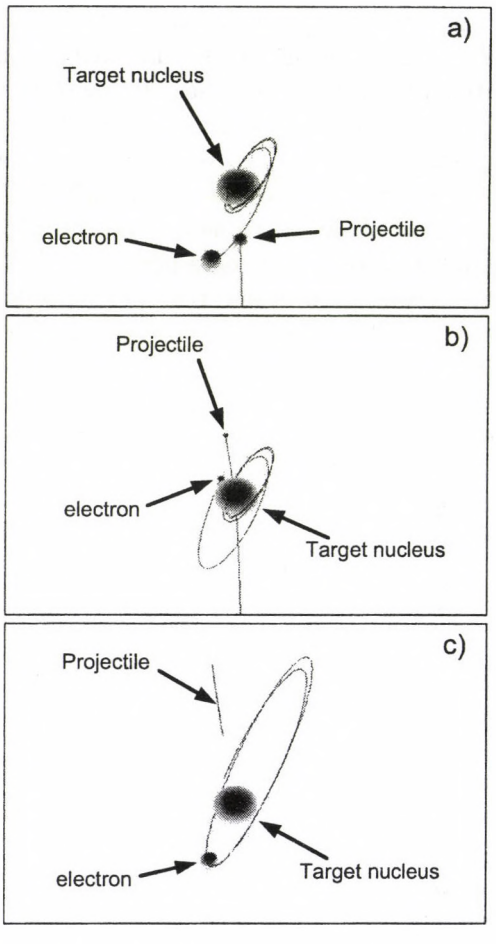

Figure 1. Typical classical trajectories for an excitation of the K-shell electron in the hydrogen atom by electron impact at 25 eV energy in the laboratory frame. a) the incoming region, b) the core region, c) the asymptotic region.

Acknowledgements

The work was supported by the grant "Bolyai" from the Hungarian Academy of Sciences and the UNIXLab association, Debrecen.

[1] K. Tőkési, G. Hock, Nucl. Instr. Meth. B **86** (1994) 201

[2] L. Budai, A. Pénzes, Á Korda, J. Somodi, K. Tőkési, to be published

[3] http://www.atomki.hu/ar2005/8_develop/test.avi

8.17 Advances in the development of the PIXEKLM-TPI software package

I. Uzonyi and Gy. Szabó

During the past decade great effort has been devoted to the developments of various local analytical methods which are capable to analyze small volumes of a sample (in the range of some μm^3) by high lateral and/or depth resolution. Among the Ion Beam Analytical (IBA) methods, Particle Induced X-Ray Fluorescence Emission (PIXE) analysis has been used for qualitative elemental imaging for a long time. Nevertheless, production of quantitative images is still a challenging and unresolved problem in general.

Ryan and his co-workers were the first who developed a software package (GeoPIXE) for on-line quantitative mapping which is capable to analyze especially thick samples [1]. Some years ago we also started to develop quantitative PIXE imaging software and suggested a different approach for the compensation of matrix effects and sample thickness [2]. It is based on the rapid matrix transform method called Dynamic Analysis which directly converts the spectrum vector (S) into the concentration vector (C) in terms of the matrix Γ [1]. We modified the earlier version of the PIXEKLM [3] program in order to calculate the Γ matrix for materials of any thickness. Furthermore, we have developed a windows-based program (True PIXE Imaging, TPI) which calculates elemental distributions on a pixel by pixel basis and creates so called elemental images from them in bit map form using colour bars.

The basic part of the new program package was published in 2005 [2]. During the past year much efforts has been devoted to develop various new options such as visualization of spectrum components in order to make the program more user-friendly and applicable. In the figure below the decomposed PIXE spectrum of an industrial material is visualized.

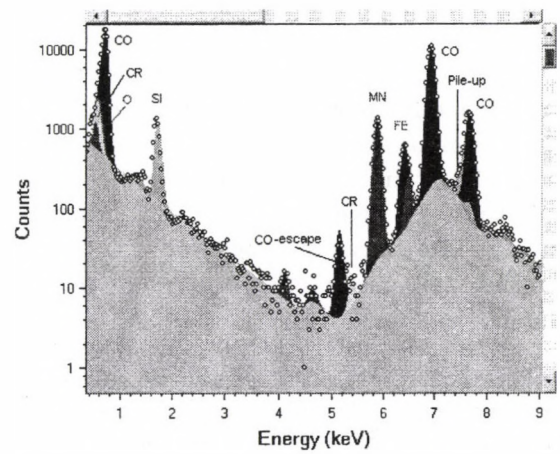

Figure 1. Decomposed PIXE spectrum of an industrial material.

[1] C.G. Ryan, D.N. Jamieson, Nucl. Instr. and Meth. B 77 (1993) 203.

[2] I. Uzonyi, Gy. Szabó, Nucl. Instr. and Meth. B 231 (2005) 156.

[3] Gy. Szabó, I. Borbély-Kiss, Nucl. Instr. and Meth. B 75 (1993) 123.

8.18 Development of the Stochastic Lung Model for Asthma

E. Dobos, I. Borbély-Kiss, Zs. Kertész, I. Balásházy[a)]

The Stochastic Lung Model [1] is a state-of-the-art tool for the investigation of the health impact of atmospheric aerosols. This model has already been tested and applied to calculate the deposition fractions of aerosols in different regions of the human respiratory tract. The health effects of inhaled aerosols may strongly depend on the distribution of deposition within the respiratory tract.

In the current study three Asthma Models have been incorporated into the Stochastic Lung Deposition Code. A common new feature of these models is that the breathing cycle may be asymmetric. It means that the inspiration time, the expiration time and the two breath hold times are independent. And the code can simulate the mucus blockage, too.

The main characteristics of the models are the followings:

a) ASTHMA MODEL I: One input bronchial asthma factor is applied for the whole tracheo-bronchial region. The code multiplies all tracheo-broncial diameters with this single value.

b) ASTHMA MODEL II: Bronchial asthma factors have to be given for each bronchial generation as input data (21 values). The program multiplies the diameter of bronchi with these factors.

c) ASTHMA MODEL III: Here, only the range of bronchial asthma factors are presented as input data and the code selects randomly the exact factors in pre-described airway generations. In this case the stochastic character appears in the Asthma Model, as well.

As an example, Figure 1 shows the deposition fractions in the tracheo-bronchial and acinar regions of the human lung in the case of healthy and asthmatic adults at sitting breathing conditions as a function of particle size computed by Asthma Model I where the bronchial asthma factor was 30%.

These models have been tested and compared for different types of asthma at various breathing conditions and in a wide range of particle sizes. The distribution of deposition in the characteristic regions of the respiratory tract have been computed and compared with healthy cases. Some conclusions are the followings:

1. In the tracheo-bronchial region the deposition probabilities increase compared to healthy case if the bronchial asthma factors increase.

2. In the acinar region at slight asthma there is no significant difference in acinar deposition (for example about 30% bronchial asthma factor).

3. In the acinar region at heavy asthma the deposition probabilities are much smaller than in healthy case (for example about 70% bronchial asthma factor).

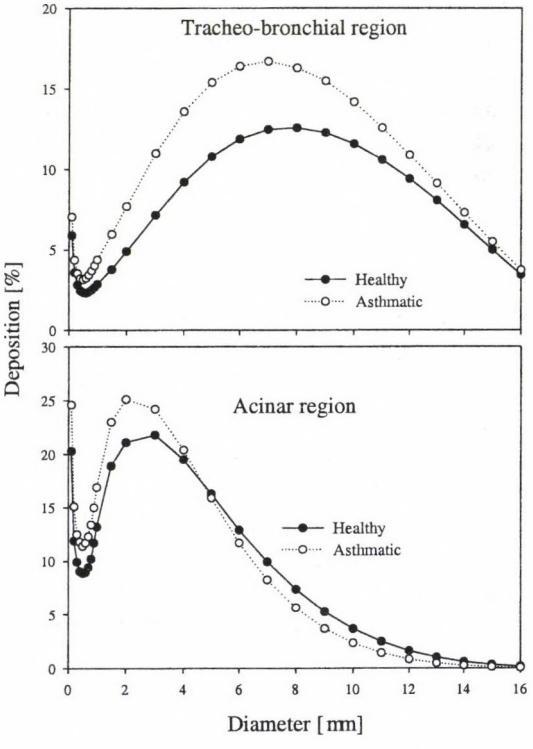

Figure 1. Deposition fractions of aerosols in the tracheo-bronchial and acinar regions of human lung in healthy and asthmatic patients

Acknowledgements

This work was supported by the National Research and Development Program (NRDP 3A/089/2004).

a) KFKI AEKI, Health Physics Department, Budapest, Hungary

[1] Koblinger L., Hofmann W., J. Aerosol Science, 21, 5 (1990) 661-674

8.19 A new method for alpha-particle detection in a classroom experiment

A. Simon, Z. Pintye, Z. Szillási[a)], P. Raics[a)], N. Béni[a)], J. Molnár

The World Year of Physics (WYP 2005) was a worldwide celebration of Physics and its importance in our everyday lives. In harmony with its aims, that is to raise the worldwide awareness of Physics and Physical Science, we introduced a novel lab work involving a new imaging and data evaluation method for alpha-particle detection, which can be easily implemented in a classroom environment [1]. The target group of the experiments is mainly secondary school students (age between 16-18 years).

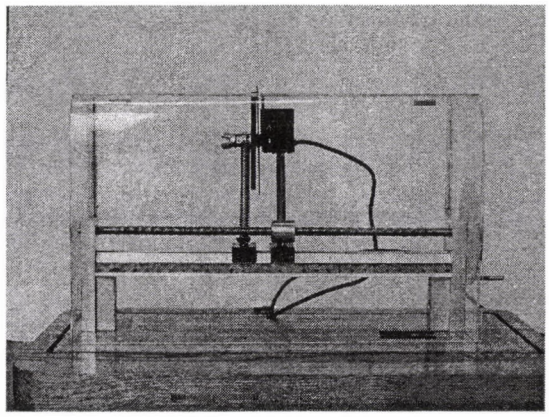

Figure 1. Photo of the experimental setup showing the alpha-source and absorber holder (left) facing to the CMOS sensor (right).

Our aim is to motivate students to develop a better understanding of Physics, allowing them to experience for themselves something of its fascination. In order to increase their attractiveness, the experiments include using a CMOS video image sensor with a video output. The covering glass window of the sensor must be carefully removed in order to make it sensitive for alpha rays. The sensor is connected to a computer where the images are recorded as a short video clip. The recorded video is played back by frames. The resulted frames are then merged together into one image. On this image the student can count the number of spots, where each spot corresponds to a hit of an alpha particle.

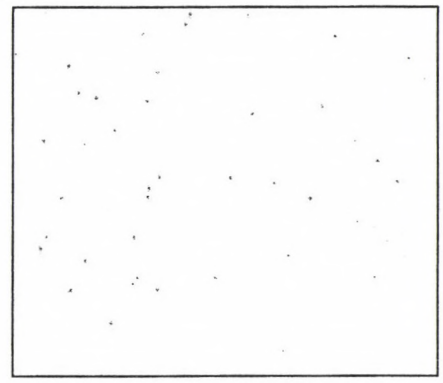

Figure 2. A superimposed video image. The dark spots indicate where a charged particle reached the sensitive volume of the sensor.

The experiment can also be visible on a TV screen even by a whole class, however the authors suggest implementing the following experiments as a practical work individually or in small groups. As students are familiar with modern information technology, we think that they will be highly motivated to make these experiments on their own.

Acknowledgements

The development of the above experimental setup was funded by ATOMKI and it was presented to the interactive science centre "Magic corner", Debrecen, Hungary at Christmas, 2005.

a) University of Debrecen, Egyetem tér 1, H-4032 Debrecen, Hungary

[1] A. Simon, J. Molnár, Z. Szillási, N. Béni, P. Raics: A new method for alpha-particle detection in a classroom experiment, Nuclear Physics News International 15 (2005) 50.

9.1 Hebdomadal Seminars

January 11

Recent progress on the invstigation of spontaneous formation of chirality in rotating nuclei
Takeshi Koike (Tohoku University, Sendai, Japan)

January 13

New ways in the study of structures
Gy. Faigel (Research Institute for Solid State Physics and Optics, Budapest)

February 24

State of affairs
M. Pálinkás, R. Lovas

March 17

Excitation and electron transport processes in solid materials following the creation of high energy Auger electrons
Z. Berényi

March 23

Prototype microstructures by proton beam micromachining
I. Rajta

March 24

Surface plasmons and their nonclassical statistics
N. Kroó (general secretary of HAS)

March 31

Study of atmospheric aerosols: results and plans
I. Borbély-Kiss

May 4

Electron gas secondary neutral mass spectrometry - fundamentals and applications
M. Kopnarski (University of Kaiserslautern)

May 12

Hectic activity and excitement at RHIC in Brookhaven
Gy. Fái (Eötvös Loránd University /ELTE/ and Kent State University (USA))

May 27

Nuclear superfluidity in neutron stars
N. Sandulescu (Bucharest, Orsay)

June 2

Cosequences of continental drift (tsunamies, earthquakes, volcanism)
Gy. Bárdossy (member of HAS)

June 9

Reports of young scientists
B. Király, I. Nándori, I. Rajta, G. Szíki, Z. Szikszai

June 29

Particle acceleration in laser plasma

I. Földes (Research Institute for Particle and Nuclear Physics /RMKI/, Budapest)

September 15

From Van de Graaff accelerators to Saharan dust-storms

Á.Z. Kiss, Gy. Gyürky, Zs. Kertész

September 20

Short presentment of the new book Nuclear Physics

T. Fényes

September 22

Machining of solid state surfaces and formation of thin layers with the help of lasers

Zs. Tóth, J.Budai (University of Szeged)

September 23

Electron emission from a magnetized Fe surface under impact of N^{6+} ions

B. Solleder (Technical University of Vienna)

October 13

Traceing the synthesis of elements by nuclear methods

Zs. Fülöp

October 27

Introduction of new colleagues in Atomki

G. Berek, Á. Elek, I. Iván, Z. Juhász, P. Salamon, B. Ujvári, I. Valastyán, T. Vértesi

November 3

Free electron lasers

B. Ujvári

November 9

Random interactions and 0^+-dominance

A. Arima (Japan Science Foundation)

December 8

Exotic nuclear effects close to the neutron drip line

Z. Elekes

December 13

Elemental analysis and surface topography by focused ion beams

A. Simon

9.2 List of Publications

The list of the Institute's publications can be found on-line at:

http://www.atomki.hu/p2/years/yea02005.htm

Author index